CHARLES UNIVERSITY IN PRAGUE, FACULTY OF SCIENCE

Institute of Hydrogeology, Engineering Geology and Applied Geophysics

Seismic Monitoring of Fluid Contacts from Horizontal Wells

MASTER THESIS

Eva Janska

Supervisor: Steen Agerlin Petersen, Ph.D.

Consultant: RNDr. Jan Vilhelm, CSc.

Praha, September 2009

Abstract

When producing oil from a thin layer with a gas cap, gas is generally unwanted since the reservoir looses pressure. The pressure loss might cause the fluid vertical migration and therefore a misplacement of the horizontal production well. This is the main reason why the oil production is held back when a gas breakthrough occurs. The well is chocked, or run on lower production rates, until the oil column is recovered, but it is not known how long this will take. If the gas-oil contact could be monitored over time, then the gas breakthrough could be better prevented by reducing production from a particular well branch or even by blinding a specific part of the branch.

The aim of this research is to test if monitoring of the gas-oil contact by a seismic acquisition inside the horizontal well is feasible. This could be done much cheaper, more often and with better repeatability than classical 4D seismic. The feasibility was investigated on 2D Troll subsurface models, using finite-difference acoustic modelling. Receivers are planned in the horizontal part of the production well and suggesting the best source position was one of objectives. The influence of variations in geological settings was also investigated.

The most accurate information about the gas-oil contact shape and its distance from the well is delivered by multiple sources in the horizontal part of the well. Since these multiple sources are rather difficult to install in reality, the sources placed at the sea bed and in the well junction are the most feasible. These two acquisition scenarios provide only a rough idea about the gas-oil contact shape and further modelling would be required to particularize the actual gas-oil contact position.

Contents

Appendix

Acknowledgements

On this place I would like to express my thanks to my supervisor Steen Agerlin Peterson who guided me whole way through this thesis project and my stay in Bergen. Moreover my acknowledgements belong to Guy Drijkoningen, Kristian Gjerding and Gerrit Toxepeus for their comments and suggestions, to Jan Vilhelm for his support and help with the arrangements for this thesis at Charles University in Prague, to Norunn Skjei for introducing me to the fluid substitution software and to Jan Thorbecke for executing elastic simulations of some of my models.

A special acknowledgement belongs to CREWES whose software was utilized for the thesis and to StatoilHydro for providing the base for the thesis evolvement.

Nomenclature

Some of three letter abbreviations (TLAs) became a part of the project (GOC, OWC, VSP,...), another may appear in adopted figures and graphs or are widely used in the related literature.

Table 1: **Frequently used shortcuts**

OWC	Oil-Water Contact
GOC	Gas-Oil Contact
Original GOC	The horizontal GOC before the production starts, but generally any GOC state preceding the drawdown GOC.
Drawdown GOC	GOC after certain time of production.
Differential seismogram	Difference between seismograms corresponding to original and drawdown GOC state for the same geological setting and source position.
FD	Finite Difference
VSP	Vertical Seismic Profiling
GOR	Gas-Oil Ratio
TWOP	Troll West Oil Province
TWGP	Troll West Gas Province

Table 2: **Substcripts**

o	Oil
w	Water
g	Gas

Chapter 1

Introduction

The Troll field is a giant gas field in the North Sea with a thin oil column of 4-27 m in the western part. The development of horizontal well technology transformed the Troll West also into a large oil reservoir with the oil production of 50 millions barrels per year. It is the target to enhance the oil production and recovery before the gas production from the Troll West starts. One of the reasons for this strategy is the pressure communication between Troll West and Troll East, which will eventually increase the production costs and finally stop the oil production with the unreachable oil left behind.

When producing oil from a thin oil leg with a gas cap, a gas breakthrough will normally occur after some months of production, due to a local drawdown of the gas-oil contact. The gas breakthrough depletes the reservoir pressure and changes the reservoir dynamics which might lead to miss-positioning of the horizontal producer within the thin oil column and hence increase the gas rates or water cut.

Drilling the horizontal wells at the oil-water contact in high-permeable sand, together with the optimal well completion, reduce the frequency of a gas breakthrough. Beside these fixed precautions, managing the production of each well branch separately on a daily basis is a powerful mechanism to prevent the gas breakthrough, especially if the gas-oil contact position would be known up to date.

There is confidence that monitoring the gas-oil contact by seismic devices fixed in the production well could deliver precise information in a short time and for a reasonable price.

Therefore the aim of this feasibility study is to investigate seismic responses for several source characteristic and positions and estimate the serviceability in Troll conditions. Since investigation is done by acoustic modelling all the geological models are represented only by the formation velocity.

There are generally two ways how to gain information about the gas-oil contact by seismic acquisition in a horizontal well: The first is by recording reflections from the gas-oil contact during a single seismic acquisition. The second is by observing a change in the velocity field in time due to oil production by repeating the acquisition with the same source and receiver position and by comparing recorded seismograms.

Schlumberger (2005) presents an attempt of interpreting the gas-oil contact from borehole acoustic acquisition, but it is not a common practice. The advantage of fixing seismic devices to the well itself is in obtaining additional information about changes in the reservoir, which is going to be utilized.

The feasibility of the gas-oil contact monitoring by seismic acquisition in horizontal production well was examined in two phases: both simulating the acoustic wave field spreading in two-dimensional models representing the gas-oil contact before and after a certain time of production. The variations in recorded seismograms caused by the gas-oil contact drawdown were examined. The goal is to determine the gas-oil contact shape and its distance from the production well.

In the first testing stage a computational process was adopted to check if the monitoring would be possible in highly idealized version of the Troll environment. Since the feasibility was proved, the second stage focuses on investigating the effect of the model complexity. A very detailed near-to-realistic velocity model of the Troll reservoir is employed for these tests. This model also covers the process of permeability-dependant fluid substitution and allows implementation of different fluid transient zones.

The receivers are meant to be placed on the production screens; the position of source(s) was the topic of the investigation. Although the best observation of the gas-oil contact is obtained with the multiple sources along the horizontal well, due to the cost issue, it is the source in the well junction and at the sea bed which might be the first implemented in the practice. These two single-source acquisition scenarios also provide a significant indication of the gas-oil contact shape. The impact of qualitative changes in geological features was inspected and the gas-oil contact indications stay observable for all alterations.

The thesis contribution can be seen in:

- Proving the feasibility of the gas-oil contact monitoring by a seismic acquisition in horizontal production wells.
- Evaluating the source positions for the gas-oil contact monitoring.
- Suggesting basic data inversion for the gas-oil contact parameters.
- Compiling a software for creating precise synthetic seismograms, which might be used for interpretation of the data.

On the other hand, beyond the scope of this thesis is to apply or develop an advanced interpretation and inversion techniques and to resolve technical limitations and implementations of acquisition scenarios.

Chapter 2

Troll field

The seismic acquisition inside horizontal production wells could be a generally applicable method for the GOC monitoring. This case study then focuses on its possible implementation in the Troll reservoir. Therefore this chapter introduces the Troll field and briefly describes the origin and recent state of the reservoir, emphasising the impact on the GOC shape and monitoring.

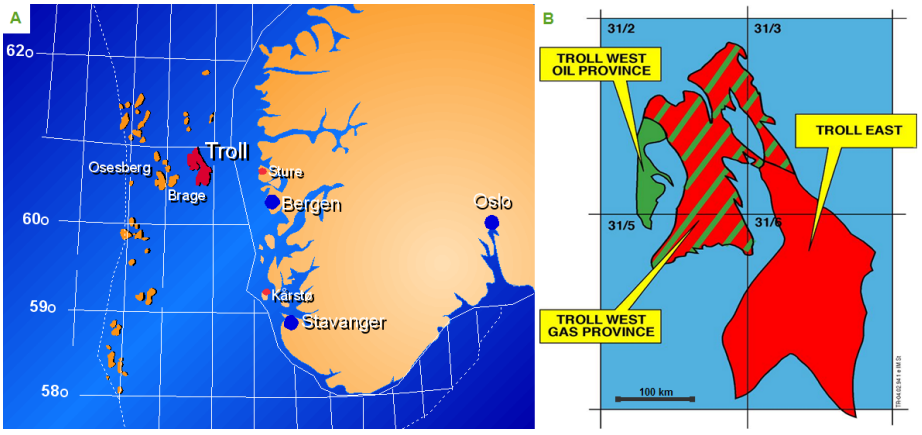

Figure 2.1: **Troll field location and main parts.**

The Troll field was discovered in 1979 and it is one of the largest gas fields in the world. Due to the horizontal well technology it became also an important oil reservoir. The field is situated in the Norwegian North Sea in area with the water depth of more then 300 m; geographical position is pointed in Figure 2.1A. The reservoir comprises of two main structures following faults of the Viking Graben: Troll East and Troll West, as it is illustrated in Figure 2.1B. The Troll West is then divided into Oil and Gas Province. Whole reservoir is characterized by a thick column of gas and a thin rim of oil, which is exploitable in the western part. The common reservoir depth is about 1550 m below the sea level. The regional oil and gas column thicknesses are demonstrated in the seismic cross-section (see Figure 2.2). Our target region lies in the Troll West Gas Province therefore further description concerns mainly this area. More about the Troll

field can be found in Mikkelsen et al. (2005) and in the almanac about The Norwegian petroleum sector (2008).

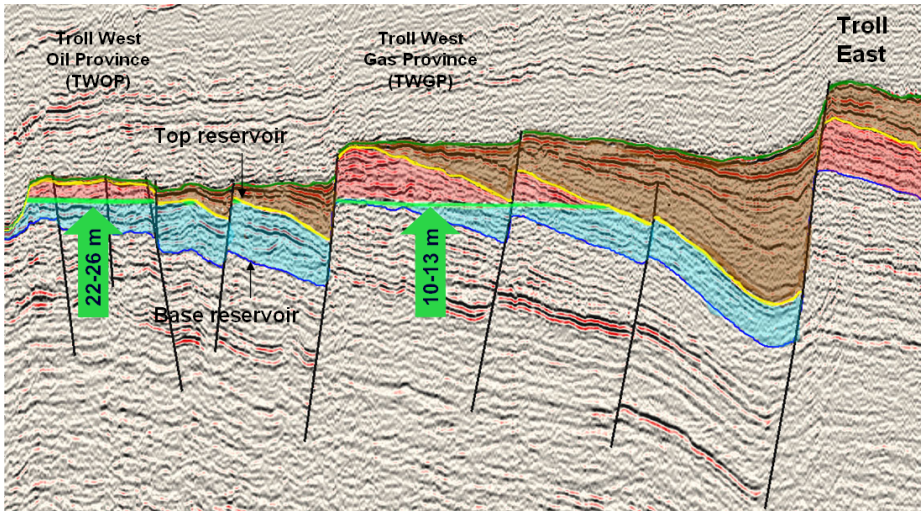

Figure 2.2: **Troll seismic cross-section**, courtesy to StatoilHydro Troll subsurface team.

2.1 Reservoir Geology

The Troll West reservoir was formed on the north-western part of the Horda Platform during the Late Jurassic rifting and it occupies two fault block related to the Viking Graben. The reservoir comprises of tree main sequences bounded by large sea level changes and it is slightly tilted (0-2%) towards East. Two sequences belong to the Sognefjord Formation (159-152 Ma), the third and the top most one is a part of the Draupne Formation (152-140 Ma). More about the North Sea geological evolution can be found in Ziegler (1975) and Dreyer at al. (2005).

The reservoir consists of numerous coarsing-up sequences of siltstones and sandstones stacked up to 100 to 170 m thickness. The sediments were deposited over 8 Ma years during several sea level cycles and they are related to the system evolution from spit to tide-dominant deltaic one. Beside the large mass of clean sandstone (c-sand) and siltstone (m-sand) the reservoir contains also calcite-cemented zones; lithological types are closer introduced in the subsections below.

The Troll West reservoir stratigraphical scheme is displayed in Figure 2.3. A layer name (for example 4Cc) refers about the origin of the layer: Number (1-6) assigns it to one of six main flooding surfaces, capital letter (A to D) to a minor sea level cycle (system track) and the low-case letter (m or c) refers bout the type of sand. The same nomenclature is used in this section.

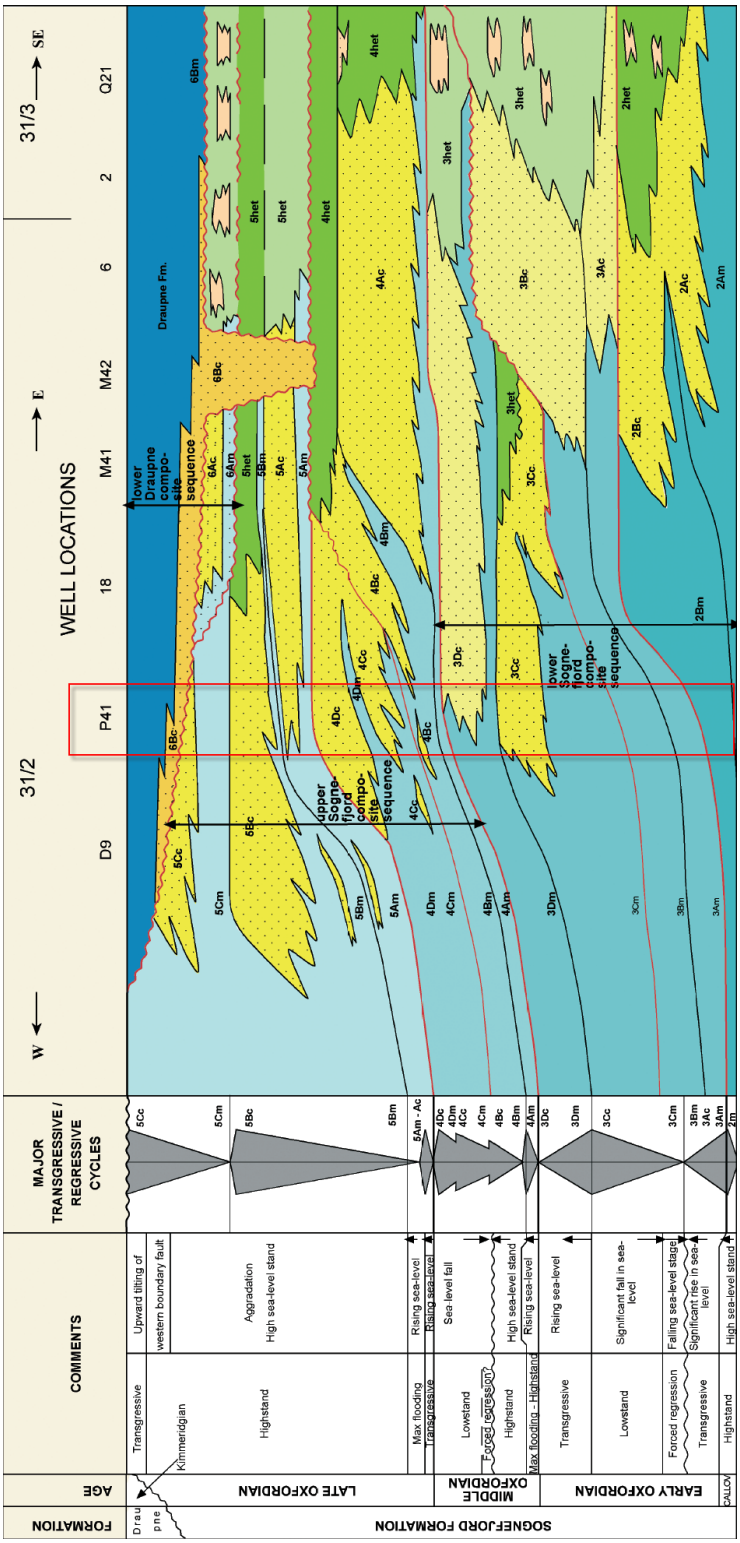

Figure 2.3: **Troll West stratigraphical scheme,** Dreyer et al. (2005). V shaped cross-section from the Western boundary of the Troll West reservoir to its middle-North and to the East boundary. Red box marks the well on display.

2.1.1 Clean Sand (C-sand)

The c-sand is mostly unconsolidated coarse-grained sandstone reflecting a high-energy environment of upper shoreface and foreshore. The c-sand occurrence is limited and its thickness varies from place to place.

In cores, the c-sand layer are recognized as light massive layer without a visible internal structure, see Figure 2.4 a and c. Occasionally there are laminations of fine dark sediment which can be caused by a short time sea level rise or a storm. The lower boundary of a c-layer is not always easy to define due to its transient characteristic. On the other hand the top of layer is mostly sharp.

The c-sand is the target reservoir formation due to its extremely high permeability (1-30 D).

2.1.2 Micaceous Sand (M-sand)

The m-sand is consolidated micaceous siltstone corresponding to approximately 100 m water depth, consistent in thickness in whole occurrence. A high content of mica is reflected in the gamma ray and drastically affects it permeability. In the well logs, the m-sand is defined by gamma ray higher then 68 APA.

In cores, the m-sand is usually recognized as a fine, gray layer with laminations, see Figure 2.4 b, d and f. Very often there is a lot of shells present in m-sand. This is explained by the low permeability (10-500 mD) of the m-sand which prevented the fossils leaching. The lower boundary of an m-sand layer is usually sharp and refers about a flooding event.

2.1.3 Calcite-Cemented Zones

The calcite-cemented zones are rigid low permeable features of various shape and size. They are not reflected in the surface seismic but they are identified by tough drilling and as extremely high velocity layers in the sonic logs (up to 6 500 m/s).

These calcite-cemented zones are post-depositional features. There are two reduction environments causing the calcite precipitation below sea bed and they might be identified according to the calcite isotope composition:

- Bacterial sulphide reduction zone ($\delta^{13}C = 1 - 2.5\%$) - 0.1 to 10 m depth below sea bed, depending on permeability.
- Sulphide reduction zone ($\delta^{13}C = 3 - 6\%$) - down to approx. 1500 m depth.

Several demonstrations of calcite-cemented zones can be encountered in cores (see Figure 2.5): calcite nodules, concretions and thin layers, mainly in the c-sand. They have irregular interface (but sharp boundary) and different sizes from nodules of few centimetres to layers of 1 m height.

2.1.4 P-41 Core

The GOC monitoring feasibility is conducted on a 2D velocity model representing a reservoir cross-section along the well K-13, which is in the same region as the well P-41, whose core was examined. The purpose of a personal examination of the core from our target region was to learn more about the calcite layers and to get a closer idea about the environment are we dealing with.

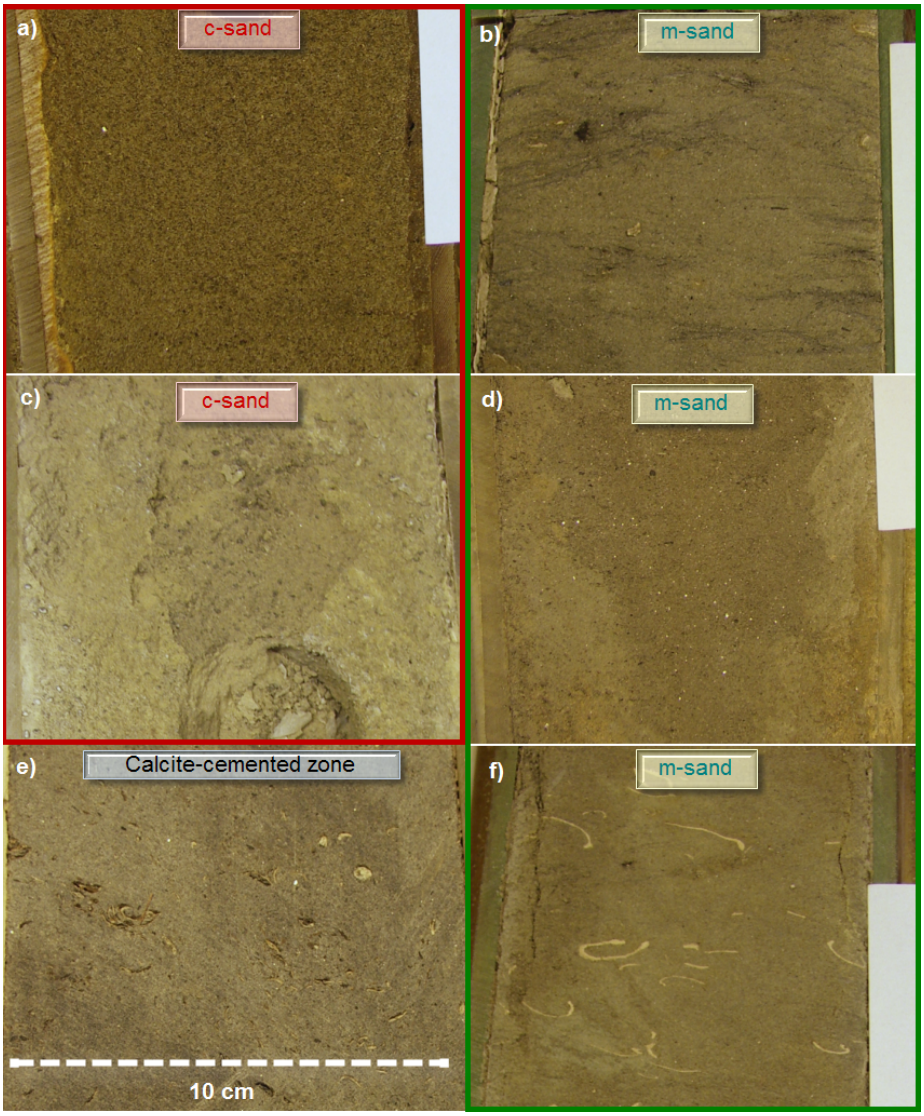

Figure 2.4: **Lithologic types in Troll reservoir .** The red rectangle bounds the c-sand (figures a & c), green rectangle m-sand (figures b, d & f) and calcite-cemented zone in e. The core segment is 10.5 cm wide, the photos taken at 25.3.2009.

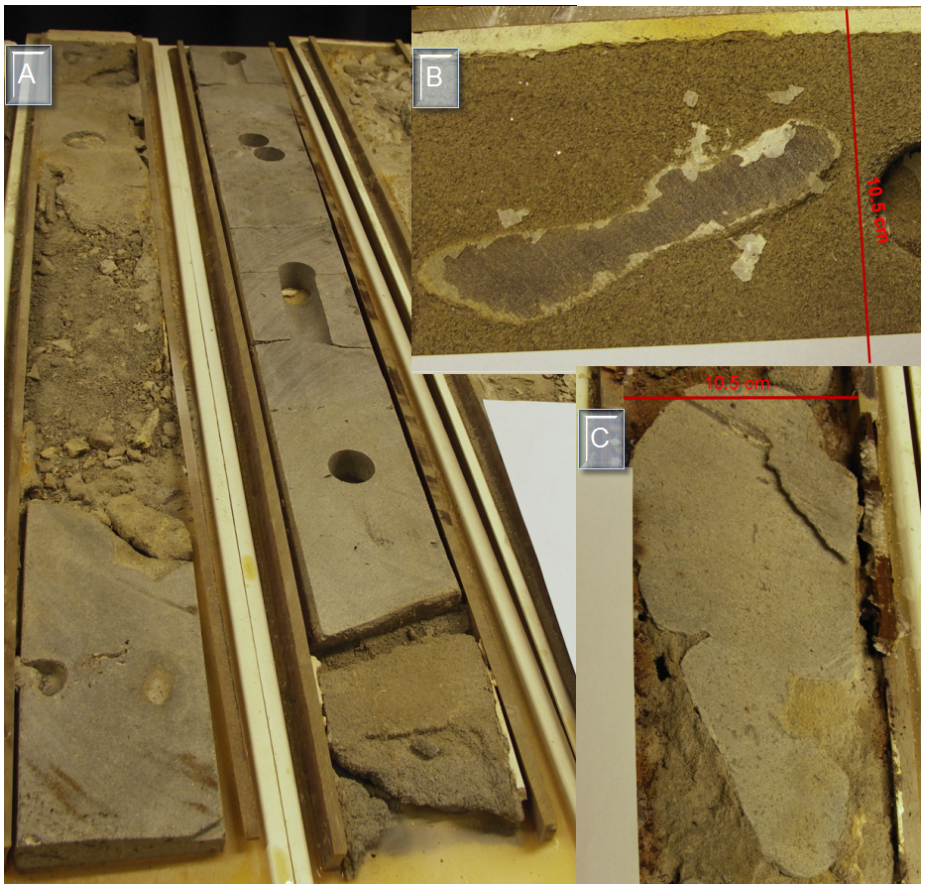

Figure 2.5: **Calcite-cemented zones.** A - calcite-cemented layer; B - little limestone nodule; C - concretion. The bright material around the calcite is a residual of glue. The core segment is 1 m long and 10.5 cm wide, the photos taken at 25.3.2009.

Calcite-cemented zones: It is their high velocity and acoustic impedance contrast to the sandstones which makes them of high importance for our subsurface seismic acquisition. For the gas-oil contact monitoring are significant mainly the high reflective layers above the GOC.

In our near-to-realistic subsurface Troll model, there are two calcite-cemented layers above the GOC, in 4Cc, represented as 0.5-1 m thick continuous layers with a smooth surface. The question is: Are these calcite-cemented layers present in the P-41 in a state that would confirm or disprove their continuity or smoothness?

In P-41, there are two calcite-cemented zones present in the 4Cc: the first one was 3 m from the layers top and the second one 7 m lower at the layers bottom. The first was 25 cm thick and occupied whole core. The second calcite occurrence is more symbolic so it cannot be really considered as a layer.

Generally, the calcite-cemented zones of various shape and size were encountered in the P-41 core; see photos in Figure 2.5. The boundary between

these limestone features and surrounding is absolutely sharp, tilted and can be frequently cracked. Vertical fractures in the calcite-cemented layers and few nodules lined up horizontally indicate discontinuity of possibly large zone.

Internal StatoilHydro studies (personal communication Arve Lonoy) show that the most of the limestone features comes from the bacterial sulphide reduction zone. This origin enhances the probability of a regional character of calcite cemented zones in the Troll reservoir.

Consequently, the calcite-cemented layers in our subsurface model might be in reality present along their whole declared length, but their continuity is rather disputable. Moreover the calcite-cemented layers are not expected to have flat surface, but they might be massive and continuous with curved boundary in the ideal case or just discontinuous line of nodules causing a lot of dispersion in the least favourite case.

Other observations: The interpreted layer boundaries follow both rock type and genesis, but it is common to encounter thin layers of m-sand in a thick layer of interpreted c-sand and opposite. Moreover, there is a close relation between c-sand and m-sand in limiting cases, as demonstrates the selection of sand types displayed in Figure 2.4, especially then c and d. These might have an impact on the precision of the fluid substitution simulation, as described in the section 4.2.2.

Even after 12 years of storage, the gas, oil and water zone can be recognized in the core by the sand colour and characteristic garage smell of oil. The GOC was within the m-sand 4Dm so the Troll favourable 5 cm transient zone was not really observable (Figure 2.6). The transient zones are discussed in the following section 2.1.5.

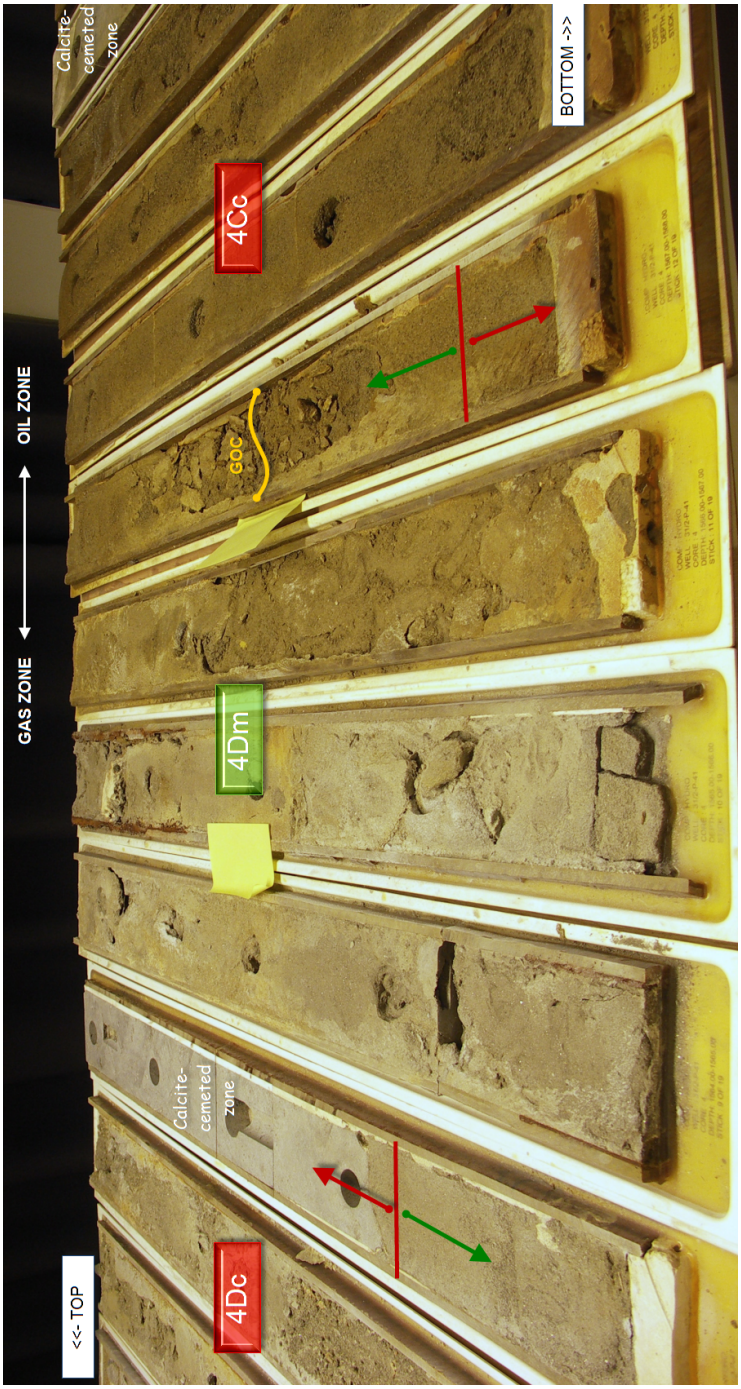

Figure 2.6: **P-41 well core segments** displaying the GOC within m-sand layer 4Dm. Layer 4Cc is oil bearing, 4Dm and 4Dc contained gas. The core segment is 1 m long and 10.5 cm wide, the photo taken at 25.3.2009.

2.1.5 Gas-Oil Contact (GOC)

Generally, the production is proven along whole horizontal well by 4D seismic. It is also known that there is a pressure loss along the well. Therefore the most of production tends to be coming from the heel part of the well. Inflow Control Device in the production part of screen is used to stabilize the gas-oil contact drawdown along the horizontal well and therefore to reduce the high risk of gas breakthrough in the heel of the well. The resulting GOC drawdown is then an unknown function of the formation permeability and pressure drawdown in the well.

The other unknown is the transient zone between oil and gas zone. In Troll West reservoir well cores, a sharp boundary is observed - the oil zone turns into gas zone within 5 cm. But this sharp transition was created within a different time scale than we are experiencing during the production. It is known that after production there is always a certain irreducible residual oil. To make it more problematic, the amount of residual oil can be also a function of distance from the GOC and of the sand type. And it can have also a patchy distribution. Therefore several types of transient zones are modelled and discussed in the section 8.1.

Figure 2.7A shows the relation between gas saturation and P-wave velocity in the formation. It is calculated using Gassmann equation (4.1) and mass parameter values common in the reservoir body, as presented in Table 2.1.5. It assumes 6% of irreducible water saturation. Notice that it has a minimum. The same parameters are used in Figure 2.7B which shows the linear relationship between the gas saturation and formation density.

Table 2.1: **Mechanical properties in the Troll subsurface model.**
K - bulk modulus [GPa], ρ - density [g/cm^3], μ - shear modulus[GPa], Φ - porosity [100%], $\alpha = 1 - K_{dry}/K_{matrix}$ - Biot parameter [-].
Fluid properties are constant; the other values are an average from the oil and gas part of the reservoir body.

K_{matrix}	37	Φ	0.29
K_{dry}	7.5	μ	4.5
$\rightarrow \alpha$	0.79	ρ_{dry}	1.89
K_w	2.7081	ρ_w	1.019
K_o	1.113	ρ_o	0.798
K_g	0.239	ρ_g	0.1175

Because even a little gas saturation has a large effect on the seismic velocities, the GOC contact can be defined as no-gas line. The relation between the gas saturation and a formation velocity shows that inverting seismic velocities for the gas content is not possible without a pre-interpretation and constraining assumptions. On the other hand, if the seismic data were inverted to the change in the formation density, the gas saturation determination would be possible due to linear relationship between the formation density and the gas saturation (Figure 2.7B).

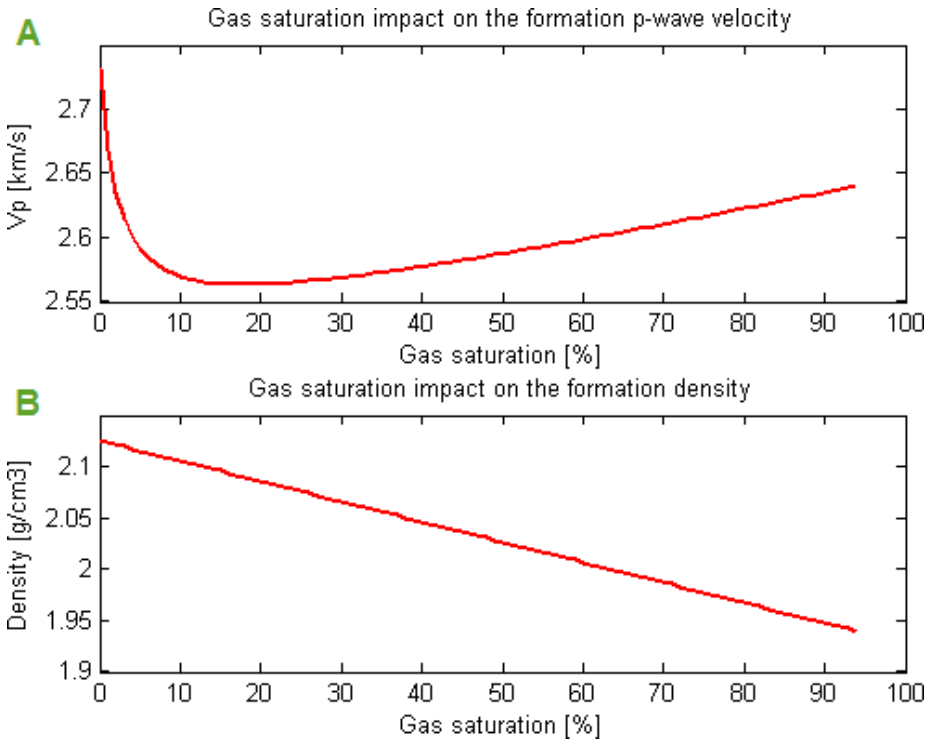

Figure 2.7: **Gas saturation vs. rock density and p-wave velocity.** (A) Relation between gas saturation and P-wave velocity and (B) between gas saturation and formation density, based on Gassmann equation (4.1). Mass parameter, as presented in the table 2.1.5. 6% of irreducible water saturation.

The reservoir monitoring on Troll is already done by 4D seismic and gravimetry. None of these methods provides such a resolution of the GOC to enable preventing the gas breakthrough.

4D seismic is a modern and frequently used method of reservoir monitoring. A modelling of the seismic response shows the data interpretation also in the range of gas saturation in the oil zone.

The GOC monitoring by vertical seismic profiling (VSP) in Troll is addressed in Elde et al. (1992). There it is considered a horizontal-incidence wave for which the source and receivers positions should be fixed in order to obtain reliable results.

2.2 Production Wells on Troll West

Because of the thin oil column, the economical oil production from the Troll West is possible only by multi-lateral wells. A typical well has three horizontal branches (single in average exceeding 2 km).

The production is handled by a subsea system of templates[1] and pipelines. Up to six wells are drilled from each subsea template and then connected to the platform by two subsea production lines. System of two production lines enables to test the production of a single well or, in case of branch control, also of a single well branch.

The production interval of a well is drilled along the oil-water contact or even slightly above, preferably in high-permeable sands. This setting lowers the risk of a gas breakthrough and enhances the oil output, however the water cut is high. It remains that water is less unwanted fluid than gas. More about the well placement strategy can be found in Madsen & Abtahi (2005).

Figure 2.8 shows a scheme of the multi-lateral production horizontal well completion used in Troll West. Generally the lower completion arranges the oil depletion from the reservoir and the upper completion carries the fluid inside tubing up.

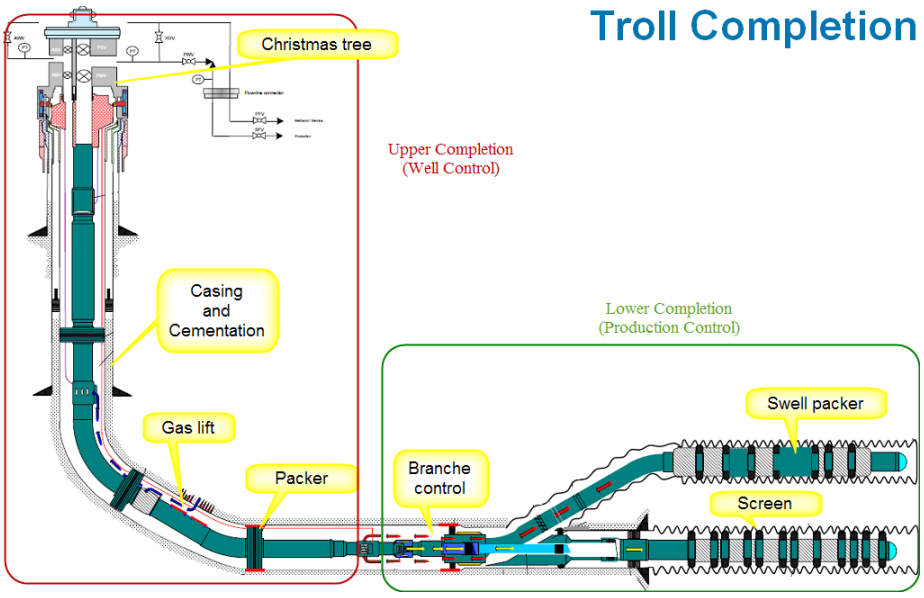

Figure 2.8: **Multi-lateral production horizontal well.** Courtesy to Statoil-Hydro Troll subsurface team.

Metal screens (Figure 2.9) are the main lower completion part in the horizontal production branch in Troll reservoir. Their role is to prevent the collapse of the borehole and to block the reservoir sand from coming into the tubing. The screens are fixed by packers and tided by gravel to the borehole wall. The-

[1] A subsea template is a large tubular steel structure accommodating a number of wellheads and christmas trees. It is also a base for the well drilling.

oretically is possible to blind an unwanted part of well between two packers, usually only during the well completion.

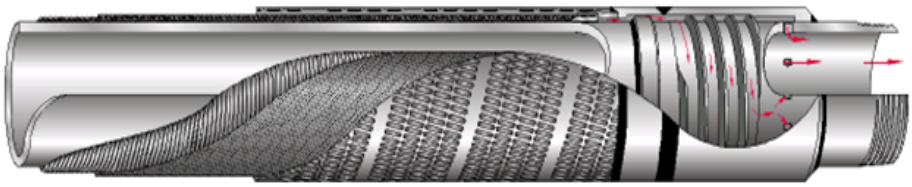

Figure 2.9: **Screen** is a system of metal perforated sheets preventing the reservoir sand coming inside the tubing.

The upper completion consists mainly of tubing attached to the wall of cemented and cased well. In the reservoir part there is a gas lift to reduce the oil density and a branch control enabling to cut back or shut the production from each of the well branches.

If the GOC is monitored then the branch where a gas breakthrough occurs (or is going to occur) could be identified and chocked. This would prevent loosing production from the other branches.

Chapter 3

Acquisition Scenarios

A consequent goal of this thesis is to figure out what is the optimal source and receiver geometry to monitor the gas-oil contact. Therefore this short chapter is going to introduce the considered source and receiver settings with their main features and limitations.

The seismic tools are supposed to be permanently attached to the production well or to the sea bed and controlled from the production platform. This setting should enable a frequent testing of the GOC position without additional operational costs. Fixing the tools location then provides the best compatibility of data from repeated acquisition.

Situating the acquisition close to the GOC restricts the size of target area and enhances the possibility of a precise GOC monitoring. A relatively small area of interest brings the possibility of employing the finite difference method for the feasibility investigation and of using sources with higher frequencies.

Since the idea of the GOC monitoring by seismic acquisition in a horizontal production well is new, the instruments are not developed yet, but many can be employed from the sonic or VSP acquisition tools.

To simulate a 'line source' several sources are triggered during the simulations. It is not expected to shoot the sources at once in reality but due to the wave superposition principal, an effect of the multiple (line) sources would be simulated by adding receiver records from single shot gathers.

Shooting the sources in a time sequence can create a tilted or even vertical plane wave. The implementation in reality would be equivalent to the multiple sources simulation but with shifting the time zero of the single shot gathers. The time shift would take in consideration the velocity field, actual source position and required shape of the head wave. Since no exploitation had been seen behind these managed plane waves they were not included in the tests.

3.1 Receiver Position

Screens in horizontal production wells are the best place for placing receivers because it is close to the GOC, especially in case of an impeding gas breakthrough. Therefore, for all testing of the GOC monitoring the receivers are going to be within whole horizontal production part of a well, as denoted in Figure 3.1B. Receiver spacing in the basic models is fixed to 1 m (which simulates the probable implementation in the reality but causes a spatial aliasing for higher frequencies), in near-to-realistic Troll model follows modelling requirements (but maximum 1 m), but in reality further technical constraints could be encountered. The receivers might be triaxial accelerators due to their small size. If the screens are oriented during instalation, then the incidence wave angle could be determined for high frequencies by placing the receivers around the screen diameter, for example as shown in Figure 3.1A.

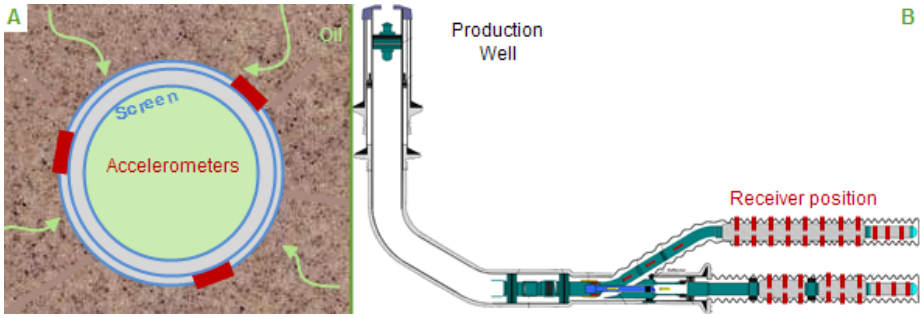

Figure 3.1: **Sketch of the receivers position** in the horizontal production well. A - one receiver position, cross-section perpendicular to the screen. B - receivers position in a multilateral horizontal production well.

3.2 Source Position

The source position can be either on the sea bed or in the well. In the subsurface, a source can be placed in the horizontal part of the production well or close to the well junction (at the well heel). It is also considered placing the source right above the horizontal well in the gas layer, but this possibility is nowadays just theoretical. Following source positions are pointed in the tests on GOC monitoring:

Source in heel of horizontal well (Figure 3.2A) preferably just above the OWC. A heel of a well is a place where the vertical well turns into horizontal and it is usually the place of a well junction. This might be up to 150 m from the start of production interval. Placing the source in the well heel means to place it between the production pipe and the cased well wall in the region of well junction. This setting may allow transmitting a large amount of seismic energy without endangering the well construction. It is also one of the most potential source positions in the first application of this method, because it is relatively easy to implement. Since receivers might be up to few kilometres away from the source, it is probable to use low frequency source.
The heel source position has the advantage in using one source for several well branches with receivers and disadvantage in the loss of some information due to the distance between sources and receivers. In models this source can be found on a side of the receiver chain.

Source in centre of horizontal well (Figure 3.2B). This source is supposed to be attached to the production screen in the middle of the receiver line. There are questions about costs for developing such a source and about the amount of energy that could be transmitted without a negative impact on the production.
This source position has some similarities in recorded seismograms with the heel case. The difference is that the source would be closer to receivers and the target area of the GOC drawdown. In models the source is placed in the middle of the receiver line.

Multiple sources in horizontal well (Figure 3.2C). A sequence of sources attached to the production screen. There is an additional question about operating multiple sources.
This source positioning allows various modulations of the head wave shape. For the modelling the sources are placed along the receiver line.

Single source in gas zone (Figure 3.2D). Placing a source in the gas zone is now a purely theoretical possibility. It is not believed in this stage that somebody would drill a well just for placing a source.
In models this source is below the ceiling and above the centre of receiver line.

Multiple sources in gas zone (Figure 3.2E). Even more theoretical position than the previous.
The sources in model are in a horizontal line below the reservoir ceiling.

Source at Surface: VSP (Figure 3.2F). It stands for the source placed at the sea floor close to the well head or far in the direction away from receivers. This source should be easy to place and operate. It is expected to attach the source to the sea floor. The source frequency is the same as for the marine or surface seismic. This VSP configuration is expected to create a vertical wave front propagating along the receiver line.
The subsurface model is extended to Earths surface and the source is placed 300 m below the free surface (the sea bed) and on the edge of the model, far from the beginning of the receiver line.

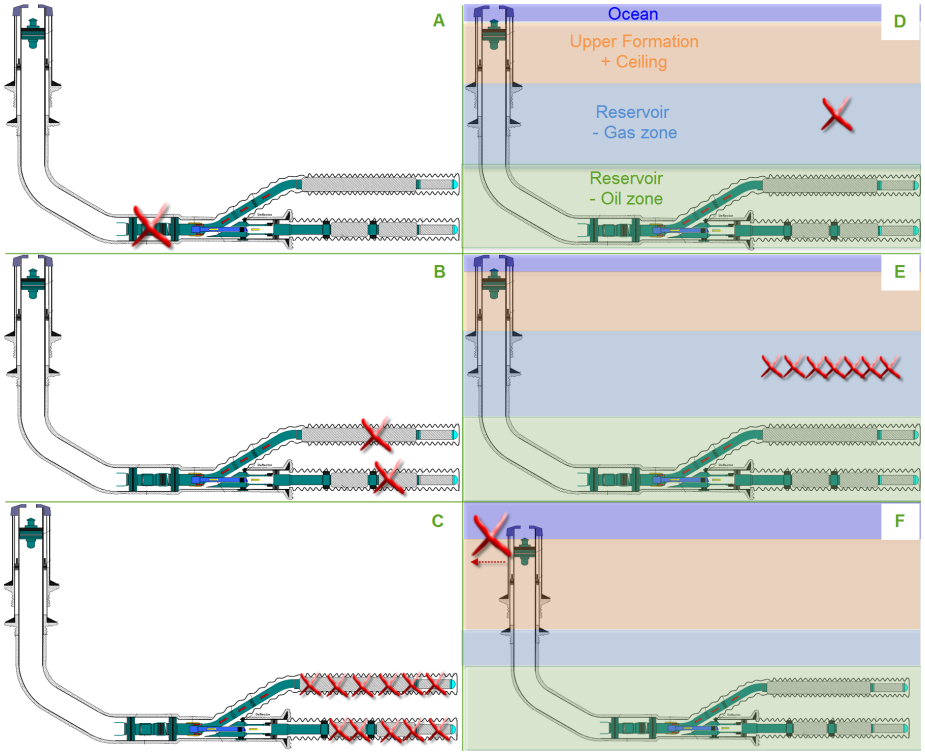

Figure 3.2: **Sketch of assumed source positions.** Red cross - single source position. Multiple sources - number of crosses does not reflect actual number of assumed sources. Colour variation in Figures D, E and F sketches the geology, as noted on D.
A - Heel of horizontal well; B - Centre of horizontal well; C - Multiple sources in horizontal well; D - Single source in the gas zone; E - Multiple sources in the gas zone; F - source position for the VSP acquisition, red arrow stands for possible source shift in the direction.

3.3 Source Frequency

The second question regarding seismic sources is the source frequency and a shape of the source wavelet in the time domain.

The source signature in time domain is approximated by Ricker wavelet. Figure 3.3A shows the source wavelet dominant frequency of 1000 Hz as it is applied for creating synthetic seismograms reflecting both the basic and the near-to-realistic Troll models. It is this wavelet frequency which is used to present the most of the data in chapter 6. It also points why the time zero on seismograms does not correspond to the maximum peak, as it would be in ideal case, but is shifted (2.08 ms for 1000 Hz source). Figure 3.3 B shows the frequency characteristic of the same wavelet.

The source is characterized by its central frequency. The frequency range for the subsurface acquisition lies between frequencies used by surface seismic and acoustic logging, therefore the wellbore source central frequencies are tested from 100 to 10 000 Hz. Moreover each source position can have its own preferred ones. The tests are performed for central frequency of 100, 500, 1 000, 5 000 and 10 000 Hz.

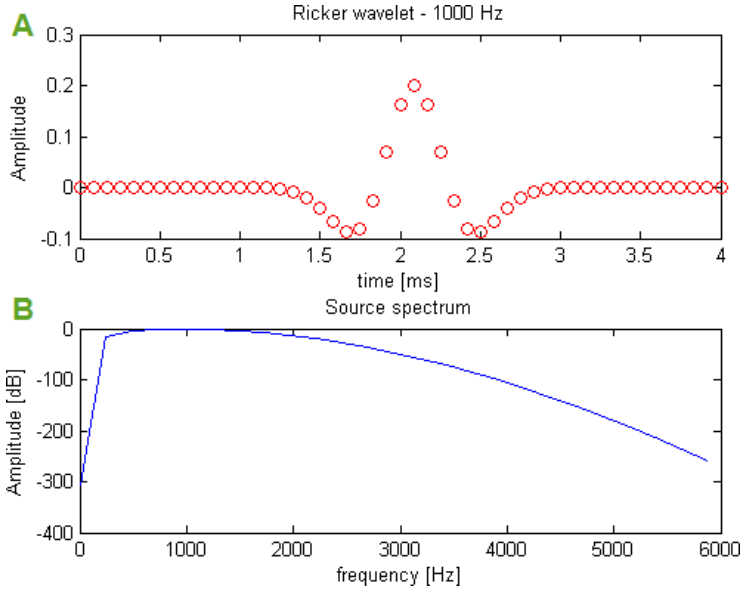

Figure 3.3: **Ricker wavelet 1000 Hz.** A - source wavelet in time domain. B - frequency characteristic of the same wavelet.

Although the source at the sea floor includes also high frequencies, the wave reaching receivers contains only low frequencies. To simulate this ground filtering effect, the dominant frequency of the sea bed source in the VSP simulations is 50 Hz.

Chapter 4

Scenarios for Velocity Models

The possibility of the GOC monitoring is tested on two 2D model families, both representing the Troll quasi-horizontal geology in terms of P-wave velocity:

1. Basic model comprises homogeneous layers.
2. Detailed near-to-realistic model of a Troll West reservoir.

The basic model family was used in a preliminary testing stage to identify the main features exploitable in the GOC monitoring feasibility study. As well some general observations and conclusions regarding the optimal source position were made during this stage. The model development towards a more realistic one then enables simulating the impact of the geology structure on the GOC monitoring.

Each subsurface model is demonstrated by two P-wave velocity models denoting the GOC in its original and drawdown state. This model sequence representing an evolution of the reservoir during the oil production is the essence of the GOC monitoring feasibility investigation. As long as it is not the topic of an inspection, the OWC is kept constant.

The drawdown GOC shape in models is usually an irregular cone (see Figure 4.1B), which does not represent the expected reality credibly, but enables the GOC to be recognisable on differential seismograms. In case of the near-to-realistic model the GOC line represents initial conditions for the fluid substitution, so the final GOC shape is slightly different.

Since the area of interest is close above the horizontal wellbore, the velocity models of subsurface are restricted to maximum 100 m in the vertical direction. The horizontal dimension is usually 200 m and the initial grid size 25 cm. This size limitation is used only for models with sources in the subsurface. The VSP configuration requires the models extension to the surface and further from the receiver line, so the resulting model size is in a range of kilometres.

The difference between basic and near-to-realistic models is not just in the complexity of displayed geology but also in the velocity changes related to the oil production. In basic models the velocity decreases by 150 or 300 m/s, in the advanced models the velocity changes varies within the drained region in range from +20 to -120 m/s, dependant on the permeability.

4.1 Basic Models

Basic models represent Troll in terms of homogeneous velocity layers and a sharp boundary between oil and gas invaded zone. This can be also understood as homogenous sandstone reservoir, where the velocity changes are driven only by the fluid in pores. A velocity profile A used by Elde et al. (1992) for a VSP simulation in the Troll area was adopted, but some adjustments according to real data were done.

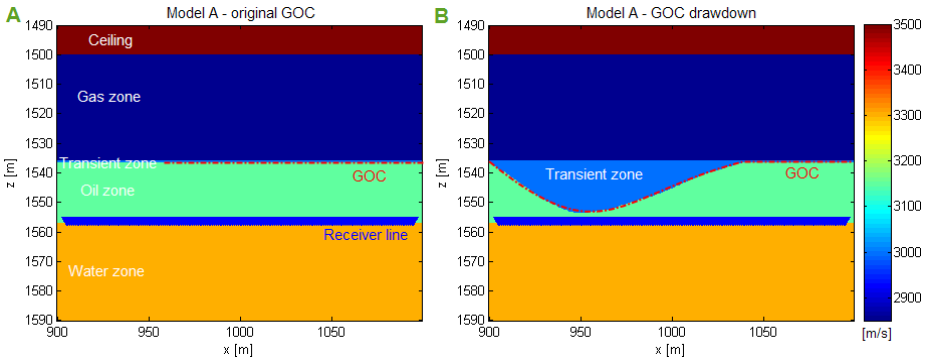

Figure 4.1: **Basic velocity model A** in the original (left figure A) and the drawdown state (right figure B).

Model A (see also Figure 4.1) has the same depth and horizontal range as the near-to-realistic Troll model: x: 900-1100 m, z: 1490-1590 m. The original GOC model A, described from the bottom, comprises of approximately 33 m water (3300 m/s), 20 m oil (3150 m/s), 0.5 m transient zone (3000 m/s) and 36 m gas zone (2850 m/s) covered by 10 m of the reservoir ceiling (3500 m/s). The GOC drawdown horizontal extent is 900 to 1040 m with a maximum drawdown of 17 m at x = 950 m. The irregular shape of the GOC drawdown denotes unbalanced effect of the oil production.

This basic velocity model was created by the user within MATLAB. The model with the original GOC comprises of overlying polygons given by a user drawn line and lower corners of the velocity model. These polygons are then filled consecutively with a constant velocity according to a velocity vector. The velocity model with the drawdown GOC is a copy of the original case but user gets the opportunity to shift the line defining the free gas surface (the lower boundary of the transient zone).

4.2 Near-to-Realistic Troll Model

The subsurface near-to-realistic Troll model is located along the well K-13 and it represents the reservoir in the Troll West Gas Province not too far away from the well P-41. A part of it in terms of slowness presented in Figure 4.2. The horizontal part of the production well K-13 is situated slightly above the original oil-water contact, mostly in the c-sand.

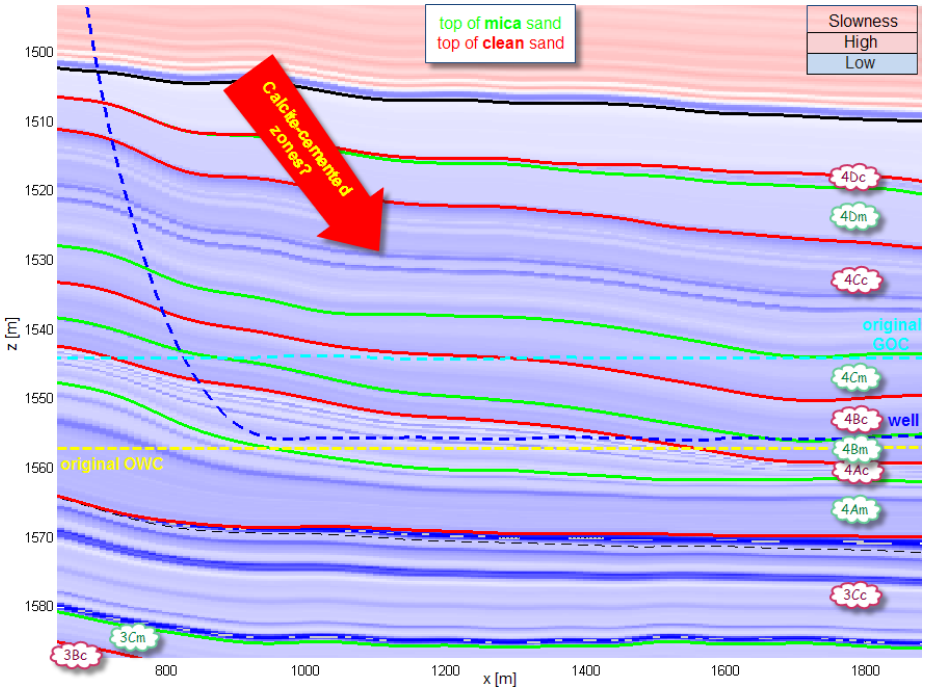

Figure 4.2: **Stratigraphy and detailed near-to-realistic Troll model** along the well K-13. Beware of the non-proportional scale. The black line follows the reservoir ceiling. The model initially created in by Norunn Skjei from StatoilHydro and it is utilized also in Ona et al (2006).

The high velocity (low slowness) layers are the calcite-cemented zones. In this original model, they are smooth and continuous in the whole model which does not have to be necessarily the case in reality as was mentioned in the section 2.1.3. Note that in the model, most of the calcite-cemented layers are situated below the well and that these layers have higher velocities than the one above. Taking into account the different horizontal and vertical scale in Figure 4.2, it is clearly visible that the reservoir sand layers are nearly horizontal and with generally constant thickness.

Data for the physical model are coming from well logs recorded in the region near the target well K-13 and from the seismic acquisition. In this particular case, the velocity related properties are recalculated to the dry rock ones using the Gassmann equation. This modification might be the reason for the decrease in the velocity of the calcite-cemented layers above the GOC, if a high sand porosity was assumed also for them. The purpose of this modification is

enabling the calculation of the rock characteristic for different fluid boundaries by the fluid substitution and re-applying the Gassmann relation. The essence and possibilities within building this kind of velocity models are discussed in subsections below.

Although the whole model of the Troll cross-section covers an area of 3 500 m in horizontal direction and 1 250 – 1 750 m in depth, mainly a part of the model of x: 900 – 1 100 m, z: 1 490 – 1 590 m is accommodated in this feasibility study. The shape of the GOC drawdown in the whole near-to-realistic model is of the same type as in the basic case, but the extent is larger. That is why there is visible only an increase of the GOC drawdown with offset in this 200x100 m model. The maximal grid size of this smaller (200x100 m) model is 25 cm.

Figure 4.3 shows this 200x100 m velocity cross-section with corresponding velocity changes due to the oil production, which highlights the shape of the GOC drawdown. The profile of the residual oil after the oil production is a function of the distance between the original and drawdown GOC and of the type of sand. The predefined GOC drawdown shape and the type of the transient zone between the oil and gas zone is unchanged during all investigations on this velocity field as long as it is not said opposite.

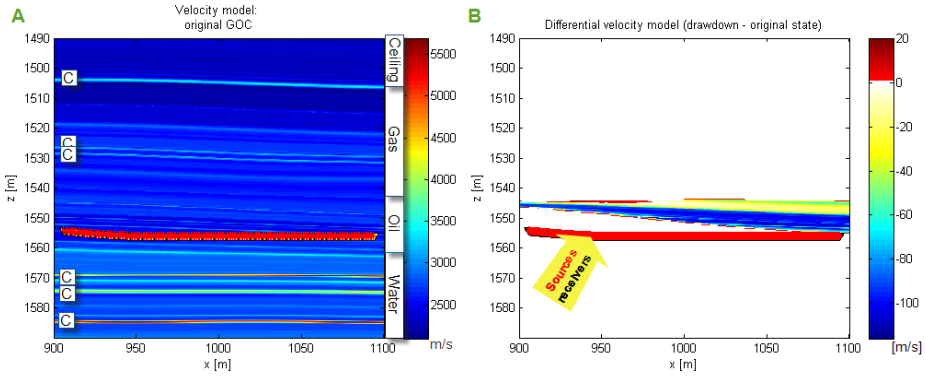

Figure 4.3: **Velocity model of Troll reservoir** (A) and the velocity changes due to oil production (B). Red asterisks (seems like a red line) - sources. Black triangles with yellow filling - receivers mainly covered by sources. Subfigure A - fluid zones denote the state before the oil production. 'C' shows the calcite layers.

Beside this 200x100 m velocity model a larger part of the near-to-realistic model (x: 900 – 1 900 m, z: 1 450 – 1 600 m) is used to investigate further possibilities of the source in the heel of the horizontal well. Settings and the GOC shape mentioned above applies also for this larger model, only the grid size is two times larger.

4.2.1 Compound DDr(x)

Compound DDr(x) is a software toolkit for simulating a seismic gather reflecting a complex physical model of a subsurface. Compound stands for the complex and composite, DDr(x) for dual-dimensionality (2D & 3D), recursive and ex-

perimental modelling. An introduction to the software principles can be found in Petersen (1999 & 2008).

The substance of a quick seismogram construction in Compound DDr(x) is in convolving the physical model of a subsurface with a resolution function simulating the migrated response; described by Toxopeus et al. (2003). The subsurface model is created by assigning physical properties from logs to layers honouring geological processes. The Compound model of a subsurface is a set of rectangular grids, each reflecting one of required log properties, such as P-wave slowness, S-wave slowness, density, gamma ray, (neutron) porosity, ...

Since the Compound seismic resolution function is constructed for the surface/marine seismic, only the model construction was employed during this GOC monitoring study to define the GOC shapes and to modify the appearance of the calcite-cemented zones. The initial near-to-realistic model was created in Compound by N. Skjei from StatoilHydro.

4.2.2 Fluid Saturation Field & Gassmann Equation

Norunn Skjei from StatoilHydro has designed software to calculate rock properties reflecting changes in the fluid contacts in the Troll reservoir. The calculation is carried out by managing a complex saturation field and then applying the Gassmann equation to calculate corresponding saturated rock properties. The software is for StatoilHydro internal purposes, but an insight can be found in Ona et al. (2006). The calculation principle is schematically represented in Figure 4.4 and is going to be briefly introduced in this subsection.

The essence is in calculating permeability (k) from porosity (Φ) and normalized gamma ray (GRN) according to the equation below.

$$\log(k) = c_1 \log(k_{KZI}) + c_2; \qquad k_{KZI} = k_{KZI}(\Phi,\ GRN)$$

The speciality is that the permeability is calculated separately for c and m-sand, which is provided by different constants c_1 and c_2. Porosity and normalized gamma are in a form of grids coming from the Compound, constants are set inside the programme.

Oil, gas and water saturation calculations accommodate the underlying equation for water saturation (S_w):

$$S_w = a\left[\sqrt{\frac{k}{\Phi}}\Delta z\right]^b,$$

where a and b change according to the sand layer type and the Δz reflects vertical distance to the OWC. The fluid substitution is carried out as a sequence of saturation corrections in all possible flushed zones. Complete fluid substitution is driven by the OWC and GOC lines of the original and drawdown state and by assigned original and irreducible saturations in flushed zones. Here, the original state reflects the state before production, with sharp transient between fluids. Although the script enables various parameters describing the reservoir behaviour with respect to the fluid substitution, only the basic setting was used during our investigation.

The bulk modulus of the saturated rock (K_{sat}) is calculated using the Gassmann equation below. The derivation of the equation is described in Carcione (2007).

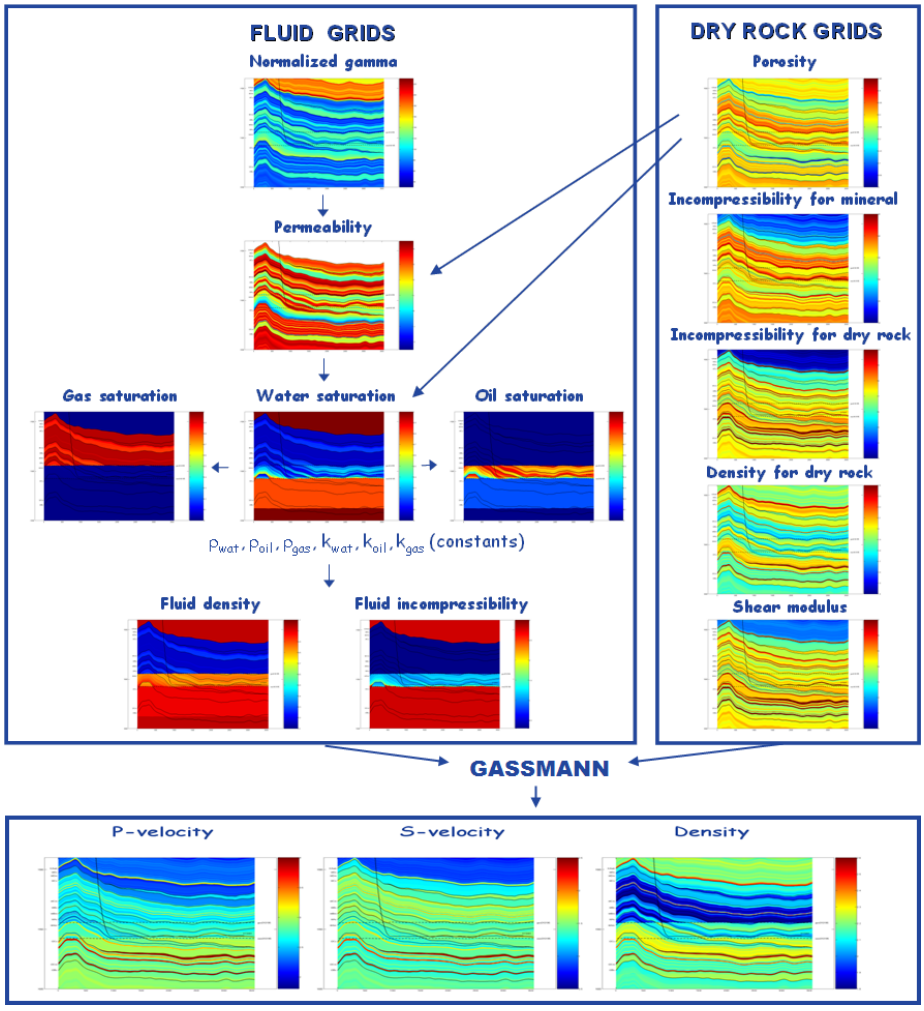

Figure 4.4: **Calculation of saturated rock properties.** Displayed model is identical to the near-to-realistic Troll model used for the GOC monitoring feasibility study. Input grids are from Compound. Courtesy to StatoilHydro Research Centre. Related case study in Petersen at al. (2003).

$$K_{sat} = K_{dry} + \frac{1 - \left(\frac{K_{dry}}{K_{matrix}}\right)^2}{\frac{\Phi}{K_f} + \frac{1-\Phi}{K_{matrix}} - \frac{K_{dry}}{K^2_{matrix}}}, \tag{4.1}$$

Overall fluid bulk modulus (K_f) is given as the weighted harmonic mean of the fluid (oil, gas and water) bulk modulus, where the weight is given by fluids saturation. K_{matrix} is bulk modulus of the solid phase, K_{dry} of the dry rock; grids with both these bulk modulus available from Compound. To get an idea about the parameter values used for the simulations see Table 2.1.5.

Finally, the primary and secondary wave velocity (v_p and v_s) is given by classical relations:

$$v_p = \sqrt{\frac{K_{sat} + \frac{4}{3}\mu}{\rho_b}} \qquad v_s = \sqrt{\frac{\mu}{\rho_b}},$$

where the bulk density (ρ_b) is a sum of dry rock density (ρ_{dry}) and a proportional part of fluid density: $\rho_b = \rho_{dry} + \Phi\rho_f$. The overall fluid density (ρ_f) is determined as the weighted arithmetic mean of the fluid densities. Shear modulus (μ) is constant.

4.3 VSP Velocity Models

Since our VSP configuration requires the source to be placed on the sea floor away from the receiver line, the velocity models described in the sections above are extended to the sea surface by a sequence of horizontal layers of velocities increasing with depth. Similar to for basic and near-to-realistic model is the model extension of 3 500 m in horizontal and 1650 m in the vertical direction, grid spacing of 2 m, water depth of about 300 m and the source position at the sea bed and 10 m away from the model boundary. Note that the GOC shape is not very smooth because it has to follow the assignment to the grid. The grid spacing is large because of the velocity model size and memory demanded for the acoustic modelling.

4.3.1 Basic Model with Overburden

The VSP velocity model covers the structure of model A. With respect to the origin of these basic models, the corresponding VSP model had to be created separately. Therefore there are some discrepancies in depths of individual horizons and in the shape of the GOC between the model A and basic VSP velocity model. It also means that the extending layers are homogeneous. The size of the velocity model corresponds to the Troll one and therefore there is also given an extra high velocity layer added below the ones represented by model A. The resulting velocity model for the original and GOC drawdown state is shown in Figure 4.5.

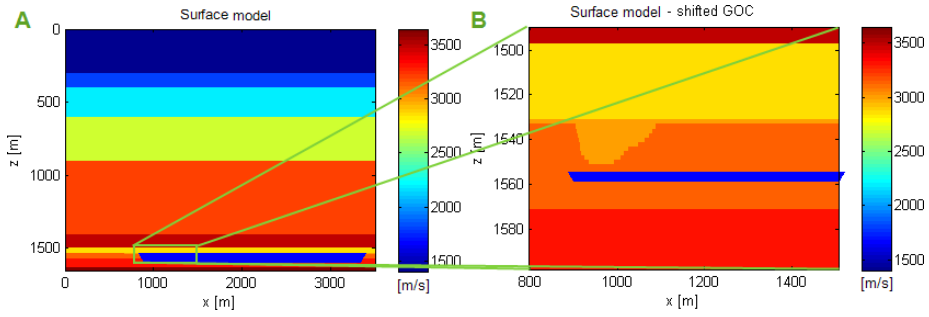

Figure 4.5: **VSP basic velocity model.** A - model in the original size. B - zoom on the drained zone in GOC drawdown state. Blue triangles (line) denote the receiver positions.

4.3.2 Near-to-Realistic Troll Model with Overburden

The VSP configuration of the near-to-realistic Troll model is represented by complete 3.5 km long Troll Compound model and above lying set of layers. The velocity in the overburden layers is not constant but linearly increases with the depth except for the sea water layer. The resulting model is shown in Figure 4.6.

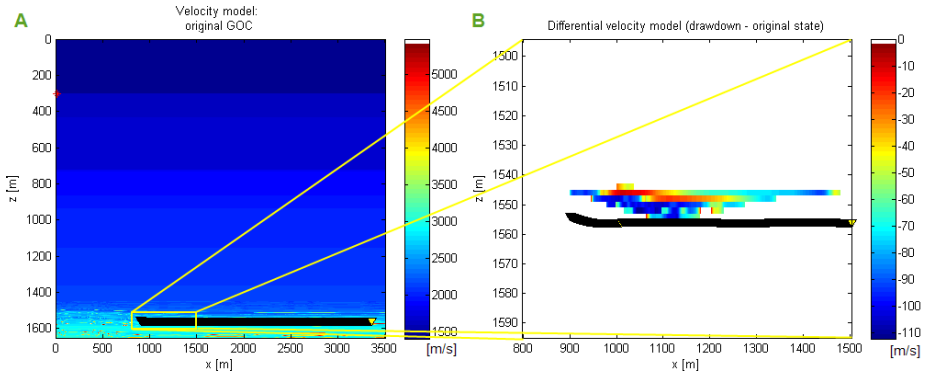

Figure 4.6: **VSP near-to-realistic Troll velocity model.** A - velocity model in the original size. B - change in velocities due to the GOC drawdown; zoom on drained zone. Receivers - black triangles with yellow filling (connected into black line) and the source by a red asterisk at [10, 300].

Chapter 5

Finite Difference Approximation of Acoustic Wave Field

The GOC monitoring feasibility study is carried out by acoustic wave field simulation with 2D velocity models. The models were discussed in the previous chapter; here the approach to the wave field modelling will be introduced. Special attention is going to be paid to model parameter restrictions applied to our investigation.

The forward evaluation of the acoustic field is handled by adapted MATLAB programs by CREWES. These scripts provide tools for source specification, time-stepping a wavefield, seismogram creation and making wavefield movies within a 2D medium. Absorbing boundary conditions are implemented. Only a little was changed on these scripts, namely the way seismogram is convoluted with the wavelet and the part catching snapshots to create a wave propagation movie.

A forward evaluation of the acoustic wave field is based on the theory summarized below; more the information on the application of the CREWES software can be found in Margrave (2003). An acoustic wave in 2D space ($\psi(x, z, t)$) is described as:

$$\nabla^2\psi(x,z,t) = \frac{\partial^2\psi(x,z,t)}{\partial x^2} + \frac{\partial^2\psi(x,z,t)}{\partial y^2} = \frac{1}{v^2(x,z)}\frac{\partial^2\psi(x,z,t)}{\partial t^2}.$$

Following second-order finite difference approximation of the second time derivative of the wave fields is applied:

$$\frac{\partial^2\psi(x,z,t)}{\partial t^2} \approx \frac{\psi(x,z,t+\Delta t) - 2\psi(x,z,t) + \psi(x,z,t-\Delta t)}{\Delta t^2},$$

which leads to the subsequent relation for the acoustic wave field in the future time $t + \Delta t$ employing the wave field at actual t and earlier time $t - \Delta t$. This relation is then used for calculating the wave field propagation:

$$\psi(x,z,t+\Delta t) = \nabla^2\psi(x,z,t)\Delta t^2 v^2(x,z) - 2\psi(x,z,t) + \psi(x,z,t-\Delta t) \quad (5.1)$$

The second-order spatial derivatives in the Laplacian (∇^2) are approximated by fourth-order finite difference operator:

$$\begin{aligned}
&\nabla^2\psi(x,y,t) = \\
&\frac{1}{12\Delta x^2}\Big[-\psi(x+2\Delta x,z,t)+16\psi(x+\Delta x,z,t)-30\psi(x,z,t)+ \\
&\qquad +16\psi(x-\Delta x,z,t)-\psi(x-2\Delta x,z,t)\Big]+ \\
&\frac{1}{12\Delta z^2}\Big[-\psi(x,z+2\Delta z,t)+16\psi(x,z+\Delta z,t)-30\psi(x,z,t)+ \\
&\qquad +16\psi(x,z-\Delta z,t)-\psi(x,z-2\Delta z,t)\Big],
\end{aligned}$$

which provides more precise results than second-order FD operator.

Absorbing boundaries are handled according to Clayton & Engquist (1977) and their effect is supported by enlarging the input wavefield matrix with extra rows and columns of zeros.

5.1 Constraints on Modelling

The forward evaluation of an acoustic wave field using the finite difference approximation is a powerful, memory consuming process and it can introduce several artefacts if used in an improper way. This section introduces the limitations and sums them up in a manner that allows creating undisturbed synthetic seismograms.

The modelling parameters can be divided into two parts: Parameters which are defined by the acquisition setting and parameters which are a topic of the examination and adjustment.

Predefined parameters are receiver line, velocity field and source position and characteristic. The receiver line defines possible positions of the receivers but does not say the exact receiver position. The velocity field frame is set by the basic or near-to-realistic Troll velocity model and can be characterized by the minimum and maximum velocity (v_{min} and v_{max}). The source position is given by x and z coordinates but in reality it will be assigned to the nearest grid position in the velocity model.

The source wavelet is the Ricker wavelet defined by a dominant frequency (f_{dom}). Because most of the modelling parameters are depending on the maximum frequency (f_{max}), the relation between central and maximum frequency was examined in the expected frequency range. Figure 5.1 shows that the most extreme relation is: $f_{max} \sim 6f_{dom}$.

Consequent parameters are velocity grid spacing (Δx), velocity model size, distance between receivers (Δrec), maximal recording time ($t_{1/2max}$), time sampling for computation (Δt_{step}) and for display in seismograms (Δt). All these parameters have a predefined value, which is a topic of tests. All of them are depending on the velocity extremes and maximum frequency of the source. Aspects influencing these parameters are briefly described in subsections below. Beside them there are another general rules: $\Delta t_{step} \leq \Delta t$ and $\Delta rec \geq \Delta x$.

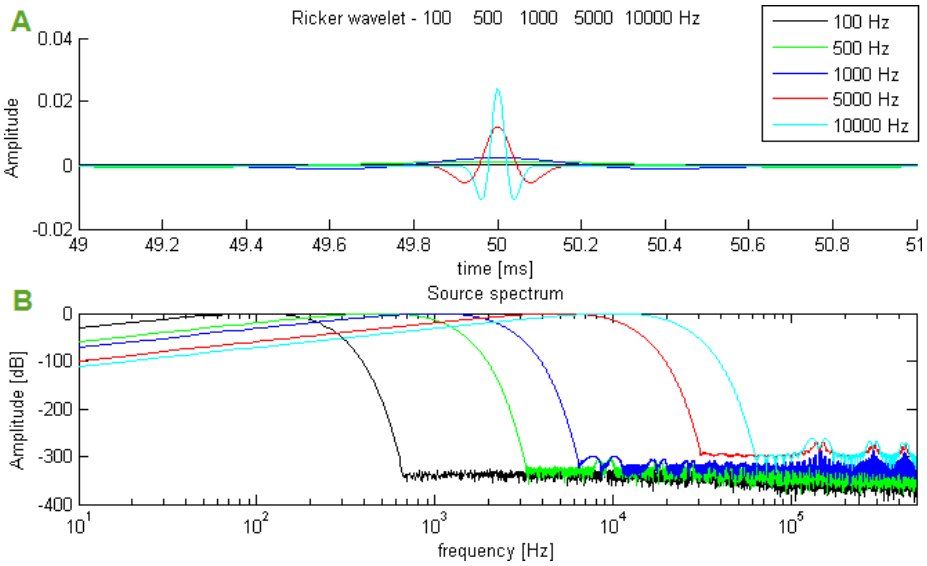

Figure 5.1: **Source characteristic.** A - source wavelets in time domain; B - their frequency content. Amplitude of the source spectrum (A_3) at $3f_{dom}$ is 10^5x smaller than for the central frequency (A_0); at $6f_{dom}$ the ratio (A_0/A_6) is 10^{25}. Note that a time shift of 50 ms in the maximum of wavelets is not the same as during simulations.

5.1.1 Aliasing

Aliasing causes signal distortion and wave indefiniteness due to an insufficient sampling of a continuous signal. To avoid the aliasing effect the sampling must be done with at least two times higher frequency then is the highest frequency in the signal:

$$f_{sampling} \geq 2f_{max}$$

This condition stands for both the time and spatial sampling, therefore:

$$\Delta t \leq \frac{1}{2f_{max}} \qquad \& \qquad \Delta rec \leq \frac{v_{min}}{2f_{max}}$$

Avoiding the aliasing in the spatial domain may not be possible in reality for higher frequencies, so it might be worthwhile to see the effect on the GOC monitoring. Therefore FD modeling with the basic model is executed with fixed 1 m distance between receivers.

5.1.2 Grid Dispersion

Grid dispersion is due to false / inaccurate finite difference estimation of second-order derivatives. It generates false long durations of oscillations and artificially slows down the signal, mostly of the shorter wavelength. To avoid the grid dispersion an oversampling is required: 5-10 samples per a minimum wavelength:

$$\Delta x < \frac{\lambda_{min}}{5(10)} = \frac{v_{min}}{5(10) f_{max}}$$

A comparison with the anti-aliasing criteria for receiver spacing leads to a relation between the maximum grid and receiver spacing:

$$\Delta rec_{max} = 2.5(5)\Delta x_{max}$$

Figure 5.2 shows the extensive constraint that the grid dispersion brings to the high frequency sources: the grid size for 10 kHz source wavelet should be smaller then 6 mm, which creates enormous matrices if the original velocity model size (200x100 m) stays.

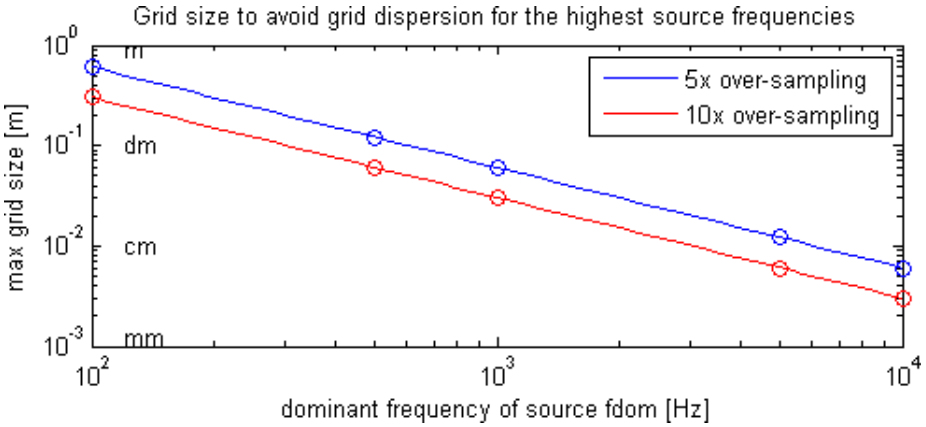

Figure 5.2: **Grid size to avoid grid dispersion effect.** The chart is calculated assuming $fmax \sim 6 f_{dom}$. Minimum velocity in the Troll near-to-realistic model is 1812.5 m/s. The model original grid size is 25 cm, therefore the model must be resampled only for source dominant frequencies of 5 and 10 kHz.

Because problems with the computational memory were encountered during the forward evaluation it was decided to eliminate the grid dispersion effect only for $fmax = 3 f_{dom}$, since also this ratio should cover most of the frequency range. This eliminates the most of the distortion but disables to look closely on the wavelet shape at further distances from the source.

5.1.3 4^{th} order Laplacian

According to equation 5.1, the future wave field is depending on the previous wavefields and on the amplification factor $\Delta t_{step}^2 v^2 \Delta x^{-2}$ (the grid spacing is similar for x and z dimension), which might cause the amplitude grow in time. Lines at al. (1999) shows the condition for stability as:

$$\frac{v_{max}\Delta t_{step}}{\Delta x} \leq \sqrt{\frac{3}{8}}$$
$$\Rightarrow \quad \Delta t_{step} \leq \sqrt{\frac{3}{8}}\frac{\Delta x}{v_{max}}$$

Although it may looks like the time stepping of the wavefield is constant through all our modelling, the grid size is constrained by the grid dispersion, which brings the frequency dependency also to the Δt_{step}, as shown in Figure 5.3. Note that the high frequencies require special - denser time sampling than the initial value of 1 ms.

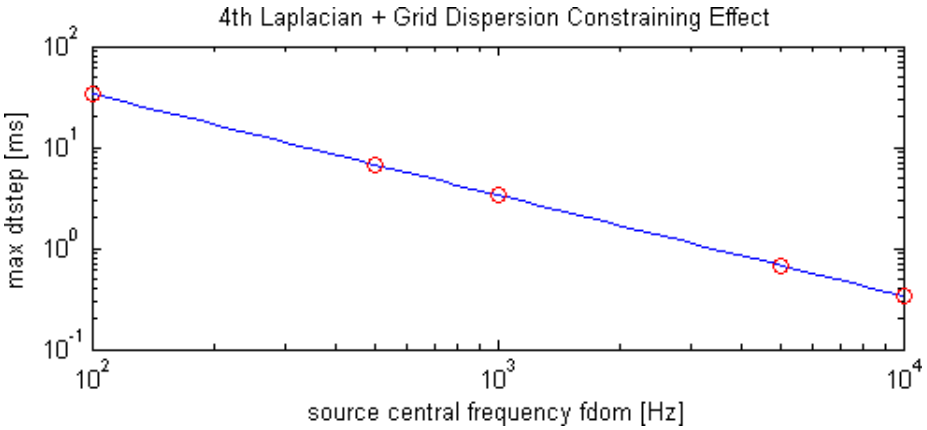

Figure 5.3: **Time stepping of the wave field** is limited by the finite difference wave field approximation and by the grid dispersion. Initial value of the time step for the wave spreading is 1 ms.

5.1.4 Wave Attenuation

While the seismic signal is spreading it is attenuated due to several aspects which are not incorporated in the finite difference simulation. For near-to-realistic models, the attenuation frequency dependant effect is going to be simulated by constraining the recording time and therefore also the velocity model size in purpose to avoid interpreting unrealistic data. The frequency attenuation is given by:

$$\|A_t(f)\| = \|A_0(f)\| * \exp(-\pi f t/Q),$$

where $\|A_t\|$ stands for absolute value of the wave amplitude in time t and Q is quality factor ($Q = 120$ in the Troll reservoir; value received from the Troll operation department in StatoilHydro). It is the aim to find the time t_{max} for which the signal amplitude is on the same level as the noise. The signal to noise ratio (S/N) in term of the ratio between the initial amplitude and common noise level (smallest recognizable amplitude) is uncertain, but S/N=100 should cover also the unpleasant conditions. This leads to the maximum one way travel time (t_{max}) of the main frequency wave component, which is also transferred to the maximum height of the velocity model (H_{max}) assuming the sources and receivers in the middle of the model and average velocity of 2694.8 m/s. Maximum recording time ($t_{1/2max}$) is then defined as half of the maximum one way travel time:

$$\begin{aligned} t_{max} &= -\frac{Q \ln\left(\frac{\|A_t(f)\|}{\|A_0(f)\|} = \frac{N}{S}\right)}{\pi f_{dom}} \\ \xrightarrow{\text{S/N=100;Q=120}} \quad & t_{1/2max}[s] \sim \frac{88}{f_{dom}} \\ \xrightarrow{v_{average}=2694.8m/s} \quad & H_{max}[m] \sim \frac{4.74 * 10^5}{f_{dom}} \end{aligned}$$

Once more the initial setting of the recording time (60 ms) and model height (100 m) are not appropriate for sources with frequencies higher 1000 Hz. For the maximum considered central frequency of 10 kHz the recording time is less than 9 ms and model height less than 50 m.

Chapter 6

Optimal Acquisition Geometries & Parameters

What is the optimal acquisition geometry? Assuming receivers along the horizontal part of the production well, the optimal acquisition covers the source position and frequency which provides the most accurate information about the GOC shape and its distance from the well. Delivering these two unknowns about the GOC would enable to control the production in the way preventing a gas breakthrough.

While searching information about the GOC we are looking mainly at the difference between seismograms reflecting the reservoir before and after a certain time of the oil production. The subtraction of these seismograms is called a differential seismogram and provides a look-and-see type of information about the production effect. The signal in differential seismograms is reflecting the time delay in seismic waves travelling through the oil depleted zone. It might be said that the differential seismograms roughly substitute a time-consuming picking of relevant seismic events, especially for lower source frequencies. Further, it enables to observe easily the delay in a wave arriving to receivers at the same time as a wave without a time delay. Generally, the thicker is the differential signal along the time axis, the larger GOC drawdown was experienced by the recorded wave.

Consequently the evaluation of target source positions is based on the differential seismograms for the basic and near-to-realistic Troll model. The basic differential seismograms, together with original seismograms, help to understand the origin of the differential signal. The Troll differential seismograms then show how the complex geology affects the GOC indications. The GOC monitoring possibilities are described separately for each of the source positions in sections below.

There are slightly different scripts for calculation of the synthetic seismograms for the basic and near-to-realistic Troll case. As a result of settings, the receiver spacing in the basic case is fixed to 1 m, but for the Troll case it follows the anti-aliasing conditions. Moreover the recording time is longer for basic models.

The seismograms, whose differential seismogram was adopted for the major result presentation, can be found in the appendix A. For the near-to-realistic

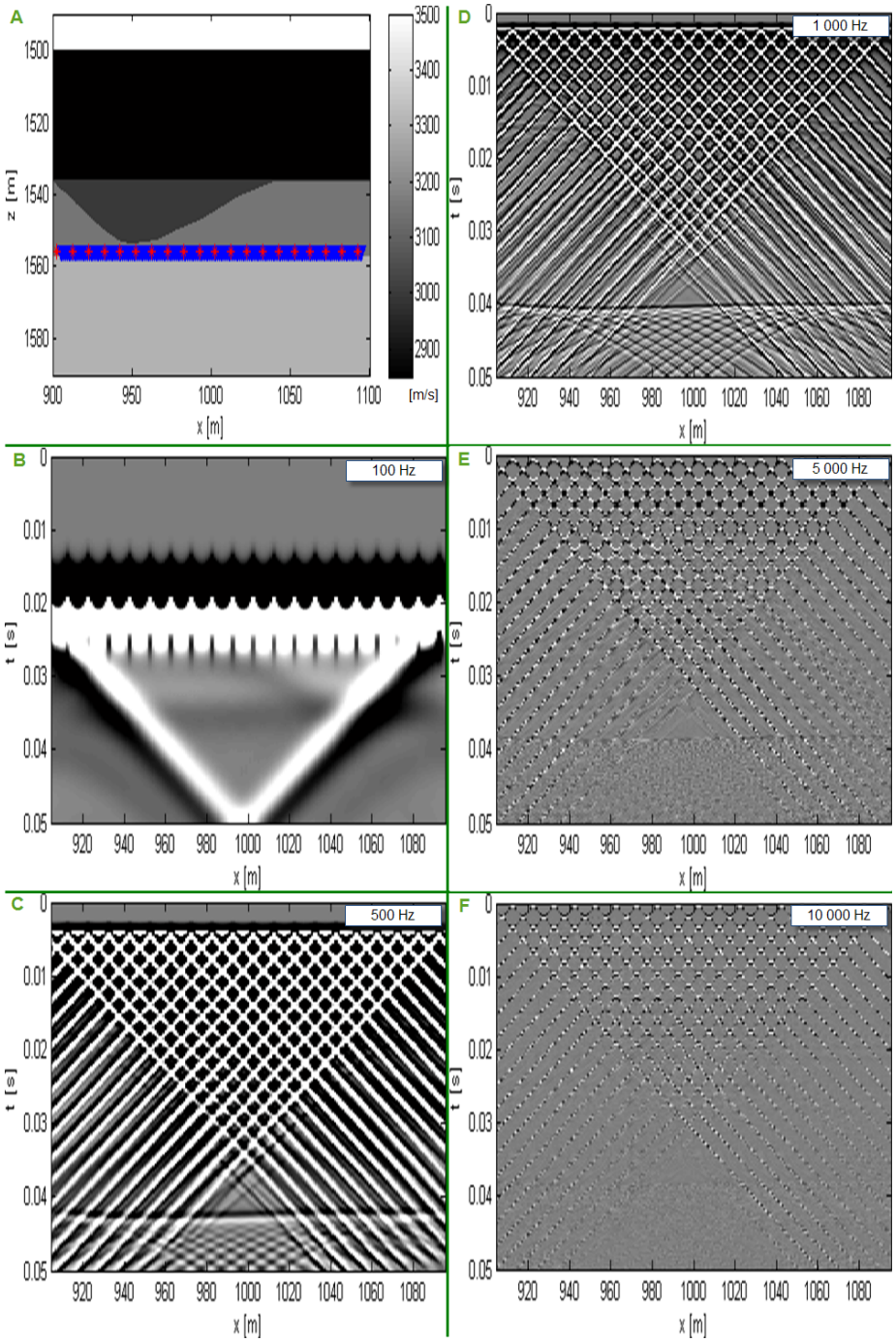

Figure 6.1: **Model and seismograms for various central frequencies of the line (multiple) source in the well.** A - basic velocity model in the drawdown state, with source (red star) and receiver (blue triangle). The rest of sub-figures - seismograms reflecting the GOC drawdown model A; the label denotes the central frequency used for the simulation. The colour scale of the differential seismograms: -0.001 to 0.001.

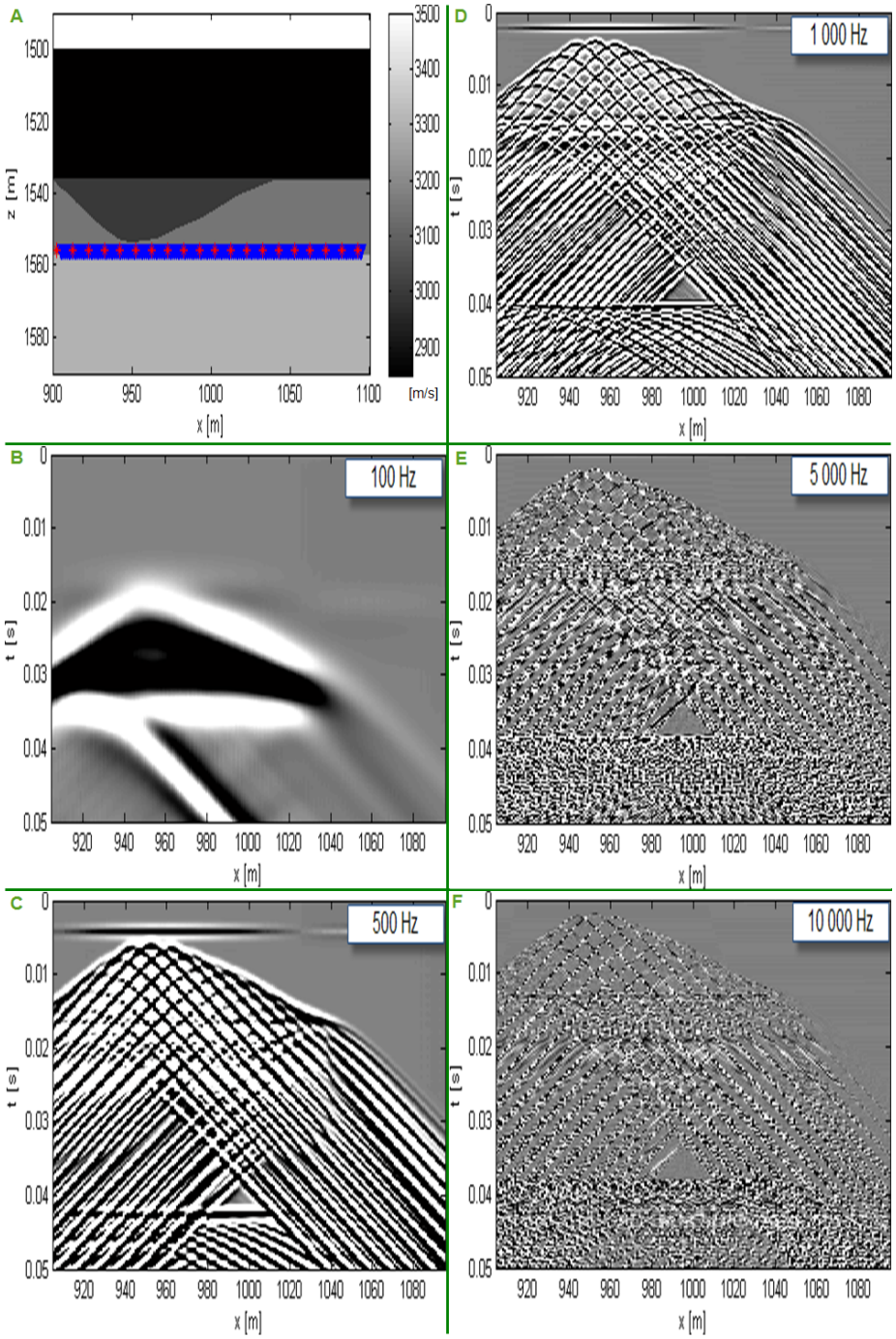

Figure 6.2: **Model and differential seismograms for various central frequencies of the line (multiple) source in the well.** A - basic velocity model with source (red star) and receiver (blue triangle). The rest of sub-figures - differential seismograms representing corresponding acquisition setting on A; the label denotes the central frequency used for the simulation. The colour scale of the differential seismograms: -0.0001 to 0.0001 (10x more highlighted then the seismograms of the GOC drawdown).

case only the synthetic seismogram reflecting the GOC drawdown is displayed because, due to the model complexity, a difference is not visible from the seismogram of the original GOC without a very detailed zoom.

Optimal source dominant frequency: All models and receiver positions were tested with sources of dominant frequency 100, 500, 1 000, 5 000 and 10 000 Hz. To represent the frequency effect seismograms for the GOC drawdown (Figure 6.1) and differential seismograms (Figure 6.2) are displayed for the line (multiple) source in the horizontal well of all these central frequencies. Many diagonal events are present for all source frequencies but for the 100 Hz one, as a result of the source spreading. All of the differential seismograms show something what could be called the direct observation of the GOC, which means that the differential seismogram highlights a weak reflection of the plane wave on the GOC. Since the source and receiver spreading is fixed in the basic model, according to assumed possibilities in reality, you can see the aliasing in the spatial domain for 5 000 and 10 000 Hz source (Figure 6.1 E and F, Figure 6.2 E and F). A horizontal event at early times on the differential seismograms in Figure 6.2 C and D is a calculation artefact[1].

1 000 Hz source was chosen as the most appropriate one for evaluating the different acquisition geometries because of its high resolution, the good readability of events and sufficient penetration of seismic energy. Note that this source introduces a time shift of time zero of 2.08 ms (see Figure 3.3) and that time picking should be at the maximum of the wavelet. The exception is for the VSP simulation in the section 6.6, where the source dominant frequency is 50 Hz and therefore the time shift of wavelet maximum is 41 ms.

Comments on the data for the acquisition setup evaluation. The data for each acquisition scenario are presented in a consistent manner. Further, for some scenarios, also other models are presented with relevant results or wave field snapshots. Since it is not the goal of this thesis to develop or apply an advanced time lapsed seismic data interpretation, only basic interpretation ideas are discussed in relevant cases.

For the presentation of the main result, the differential seismograms for the subsurface scenarios are calculated for the source central frequency of 1000 Hz. Since the velocity models are fixed, the time sampling and receiver spacing do not change with the acquisition scenarios, only the source position varies. That is why axes and colour scales of velocity models and differential seismograms can be kept constant for the subsurface scenarios. General structure, scales and axis limits utilized in the presentation of the main result are shown in Figure 6.3. The only exception is in the colour scale of the differential seismogram reflecting basic model for the multiple sources in the gas zone and for the VSP scenarios results.

[1] This artefact is due to the way FD CREWES software convolves the synthetic seismograms for a peak source with the source wavelet. It was removed for simulations with the near-to-realistic model.

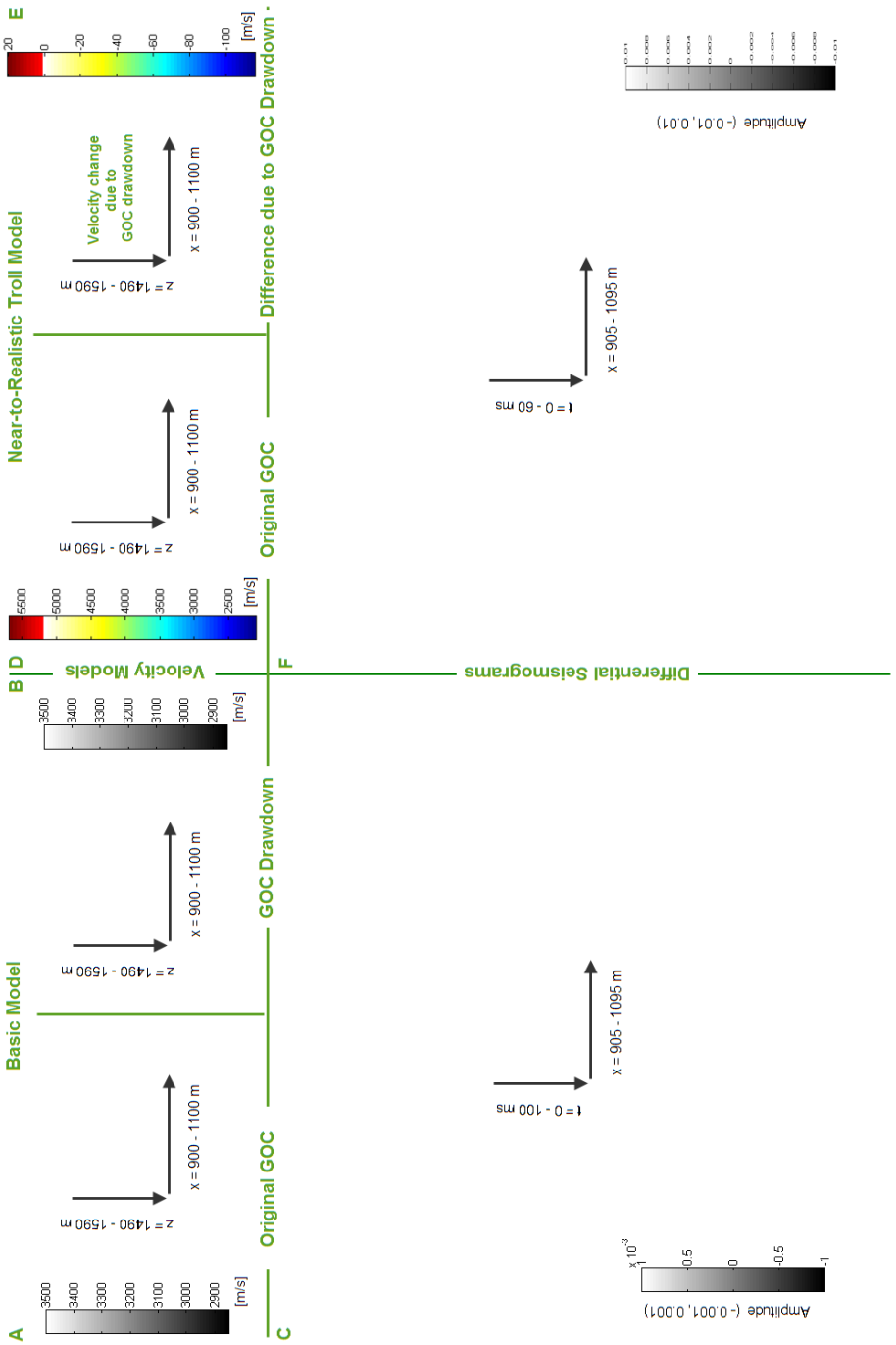

Figure 6.3: **Layout and scales of result presentation** in this chapter and for 1000 Hz source. Green signs along green lines describe the content of the subfigure. A, B, C refer about the basic model; D, E, F about the near-to-realistic Troll one.

6.1 Source in Heel of Horizontal Well

In Figure 6.4, models with the acquisition setting and differential seismograms for this case are shown.

Looking at the differential seismogram for the basic model in Figure 6.4C you can see three events carrying information about the change in the velocity field. The earliest ($t_0 = 0.013$ s) comes due to energy reflection on the lowered GOC. The second event ($t_0 = 0.015$ s) in time is due to the delay in a reflection from the gas zone. You might realize that the width of this event increases with offset before it joins the first event. The latest recorded time delay ($t_0 = 0.04$ s) is in the reflection from the ceiling. Here the width increase with offset is observable along whole receiver line, although at the larger offsets it might be because a weak multiple reflection is joining the third event. Figure A.1 in the appendix A.1 should help better understanding the observations.

The differential seismogram reflecting the near-to-realistic Troll model is more complex but the main difference from the basic situation is that here the reflection from the GOC after the production is not visible. The amplified segment in Figure 6.4F highlights the time delay in several reflections, where the lowest two (at time 22 and 23 ms) come from the calcite-cemented layers at depth about 1530 m. It is also apparent from Figure 6.4F, that the most differential signal for further offsets is coming from several joined, indistinguishable reflections (within the direct wave on original seismograms). The snapshots for a point peak source displayed in Figure 6.5 show the horizontal direct wave reaching far offsets at 61 ms, energy concentration in the oil layer and waves carrying information about the GOC. Figure A.2 in the appendix A.1 shows synthetic seismograms for drawdown GOC of near-to-realistic Troll model and should help better understanding the observations.

The advantage of the heel source setting is that one source provides two types of the GOC related time delay: in single reflections and hidden in joined reflections. Inversion methods generally allow converting the time delay in a reflection into the slowness field. The joined reflections might then carry information about the GOC shape.

The disadvantage of the heel setting is that the information about the GOC is spread along a large distance and that the strongest signal on the differential seismogram is merged and therefore the inversion into the GOC shape might be uncertain. The GOC-information based on reflections might not be reachable in reality due to a large distance between the source and the first receiver.

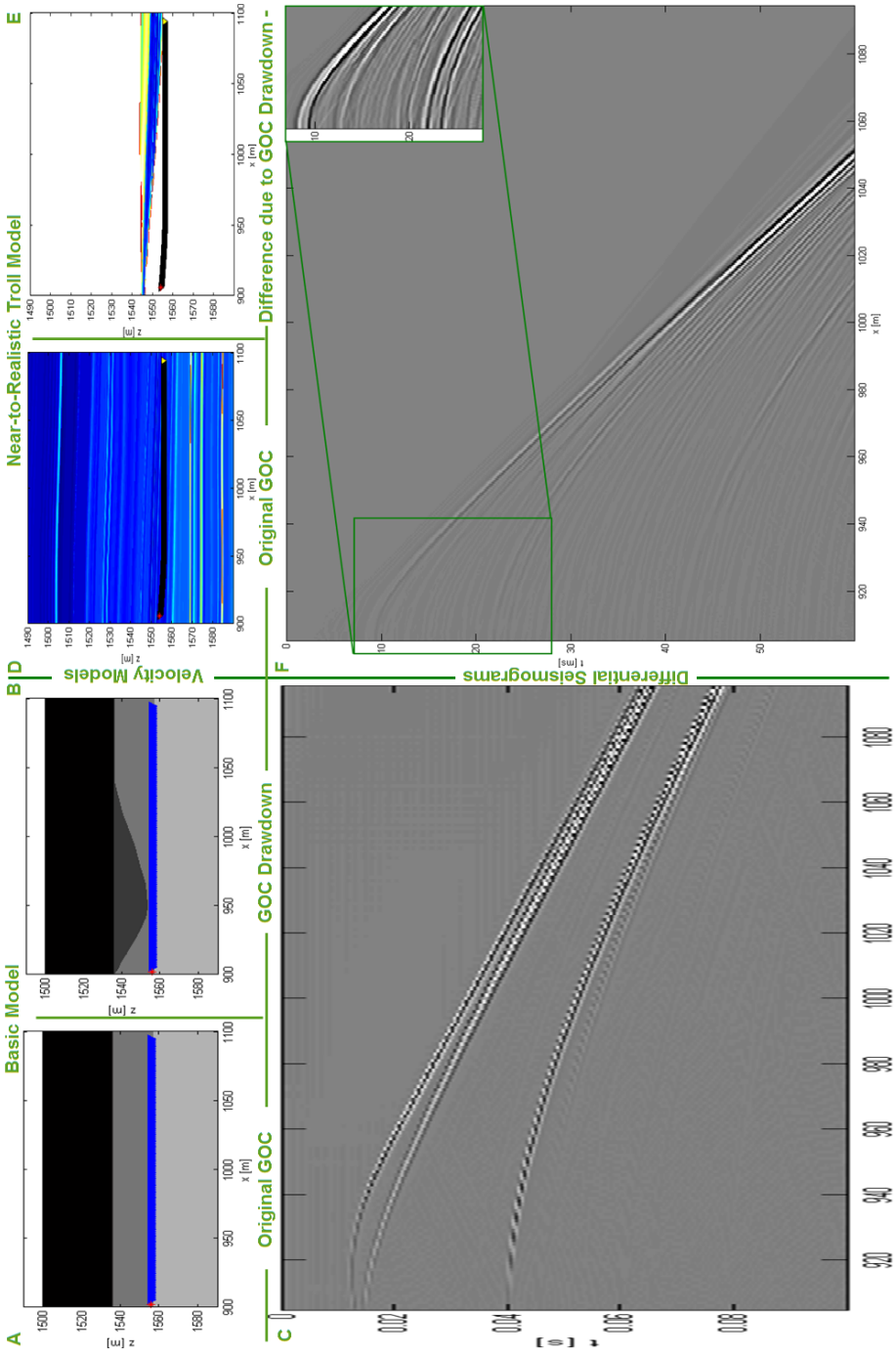

Figure 6.4: **Heel source acquisition setting and differential seismograms.** A, B - blue triangles (joined into a blue line) are receivers, red star source position. D, E - black triangles with yellow fill (joined into a black line) are receivers, red star is source. E - velocity changes due to the GOC drawdown, highlights the shape of the GOC drawdown. Relevant seismograms can be found in the appendix A.1.

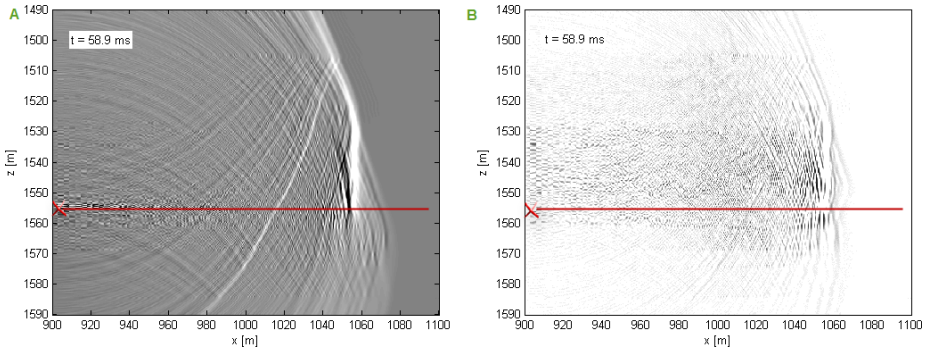

Figure 6.5: **Snapshots of the wave field created by the heel source in the near-to-realistic model.** A - wave field reflecting the original GOC state. B - difference in the wave fields in the original and drawdown GOC state at the same recording time t as B. Red line - approximate receiver line position, red cross - source. The snapshots show the field of a point peak source.

6.1.1 100 Hz Source and Larger Model Simulation

In case of the heel source position, a single source is supposed to deliver information about the GOC also from a great distance. Therefore a low frequency (100 Hz) source and a larger velocity model are adopted for further tests of this acquisition setting. The advantage of a low frequency source would be a better readability of the wave front. The larger model then enables an examination of the GOC-information smearing and therefore provides more reasonable base for the heel data interpretation.

In Figure 6.6, models with the acquisition setting and differential seismogram for this case are shown.

The differential seismogram in Figure 6.6C shows a smooth variation of the differential signal in the position of the direct wave along the offset. Position of the maximum drawdown does not correspond with the maximum time shift and receivers. Further a differential signal is observed also by receivers above which the GOC drawdown does not occur. Both can be explained by the reflection origin of the differential data.

A reflection from the first of two calcite-cemented layers at the depth of 1530 m would be expected at the first receiver at $t = 40.1$ ms. Even if the amplitudes of the differential seismogram are strongly highlighted (Figure 6.6D) there is very little reflection visible at that time (the minimum layer resolution for 100 Hz is more than 6 m, thickness of calcite layers is about 1 m). Therefore a negative feature of the heel source with lower frequencies is the loss of the information about the GOC from reflections.

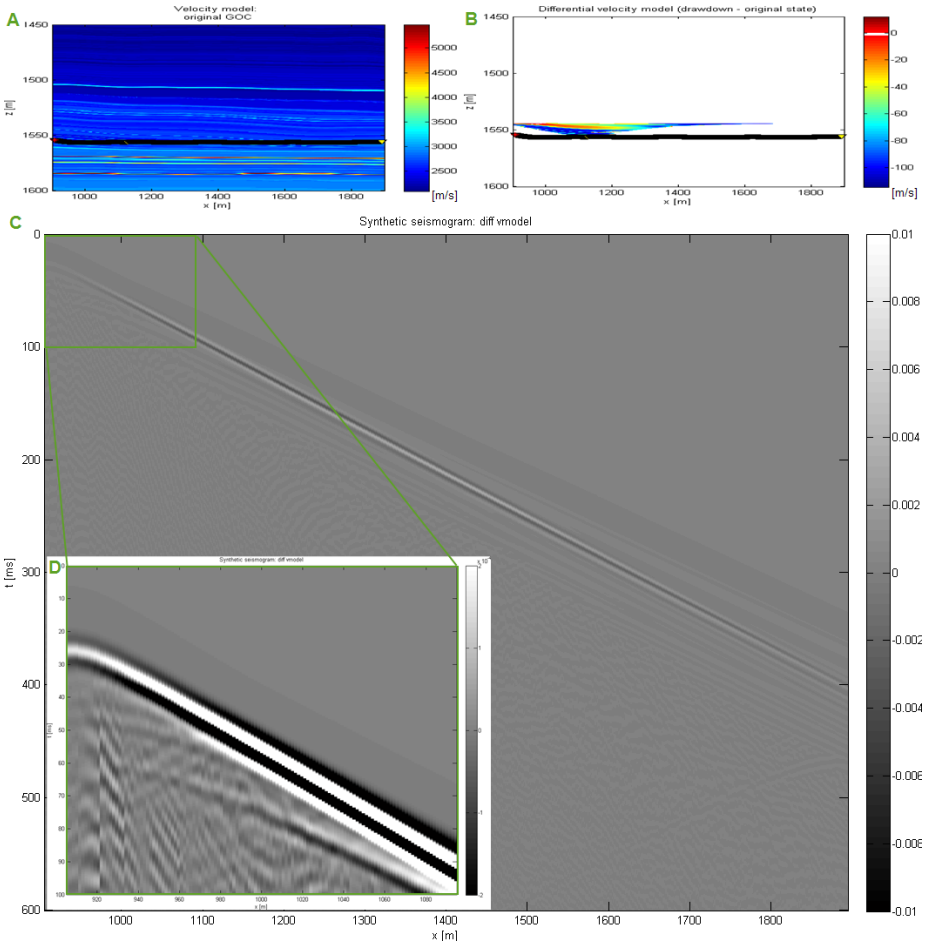

Figure 6.6: **100 Hz heel source large model and differential seismogram for 100 Hz source.** A, B - black triangles with yellow fill (joined into a black line) are receivers, red star is source. A - original velocity model, grid size is 0.5 m. B - velocity changes due to the GOC drawdown, highlights the shape of the GOC drawdown. C - differential seismogram. D - zoom with 50-times amplified amplitude. Relevant seismogram can be found in the appendix A.1.1.

6.2 Source in Centre of Horizontal Well

In Figure 6.7, models with the acquisition setting and differential seismograms for this case are shown.

The seismic response of the basic model has the same character as for the heel source with a difference that the signal provides information from both sides of the source. On the differential seismogram in Figure 6.7C you can see the reflection from the GOC gasping and the time delay in reflections from gas layer and ceiling. Moreover it highlights the smearing of the information about the GOC hidden in joined reflections over a large distance. Specifically, even if the GOC gasping on the basic model (Figure 6.7B) disappears shortly after the source, the signal on the differential seismogram stays along the whole receiver line.

The differential seismogram reflecting the time changes in the near-to-realistic Troll model (Figure 6.7F) shows more complete reflection hyperbolas than for the heel source because the receivers are closer to the source from both sides. This might not be a true in reality because of the tube waves. Reflections from two target calcite-cementer layers are observable along the whole profile.

Central source position provides the same type of double information about the GOC as the heel source, but from both sides of the source, which is its main advantage. The disadvantages stay the same as for heel source, plus the uncertainty about the data quality due to the tube waves.

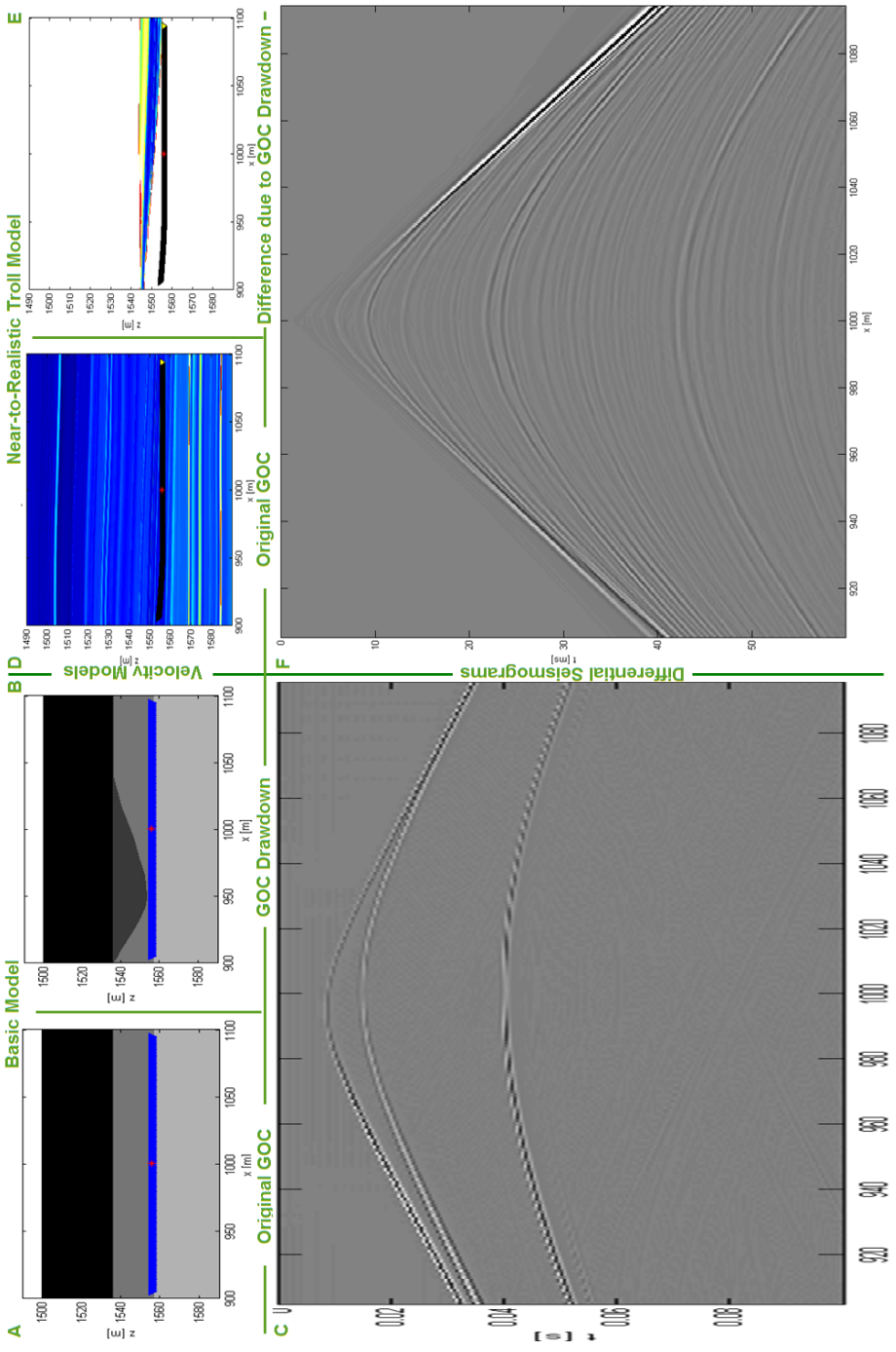

Figure 6.7: **Acquisition setting and differential seismograms for 1000 Hz source in the centre of horizontal well.** A, B - blue triangles (joined into a blue line) are receivers, red star source position. D, E - black triangles with yellow fill (joined into a black line) are receivers, red star is source. E - velocity changes due to the GOC drawdown, highlights the shape of the GOC drawdown. Relevant seismograms can be found in the appendix A.2.

6.3 Multiple Sources in Horizontal Well

In Figure 6.8, the models with the acquisition setting and differential seismograms for this case are shown.

The multiple source simulation in the basic case was executed with the source separation of 10 m (red asterisks on Figures 6.8 A and B), which simulates the possible implementation in reality. As you can see in Figure 6.8C, it causes a great number of linear events on the differential seismogram. These events are present also on the synthetic seismograms (Figures A.6 A and B in appendix A.3) . Closer look would clarify that only the event originating in source positions are linear but the others are hyperbolic. It also explains the origin of these events: the direct wave is not a line but has a bumpy shape. These events are not observable for the source with central frequency of 100 Hz (see Figure 6.2B). They could be limited by a filtering in the f-k domain and by migration.

There are only two strong nearly linear events visible in the differential seismogram for the near-to-realistic Troll case (Figure 6.8F). Since here the source spacing is equal to the receiver spacing (0.54 m), the resulting wave behaves like a consistent plane wave limited in the horizontal direction. It is the limitation which causes that the signal from extreme sources is not completely incorporated in the plane wave and therefore produces an additional seismic response as a single source (you might like to compare the left diagonal/hyperbolic events in Figure 6.8F with the heel source signal at Figure 6.4F).

Returning to the basic case differential seismogram, there are two GOC indications, if neglecting the events described above. The most obvious one is the GOC shape feature, which is coming from weak wave reflections on the GOC. The differential seismogram just highlights what is partially hidden in the strong direct waves. The second GOC indication is the delay in reflection from the gas zone or ceiling. It is more visible on the ceiling reflection that the width of the reflection delay on the differential seismogram is reflecting the amount of the GOC drawdown. Figure 6.2 shows that this direct GOC indication is present for all considered frequencies.

Although the situation on the near-to-realistic Troll model is more complex and the GOC shape is not highlighted on the velocity model by such a strong contrast as for the basic situation, there are still occurring reflections on the GOC which are uncovered by the seismogram subtraction. This direct GOC observation in Figure 6.4F refers about the distance from the well to the GOC. The delay in reflections from nearly horizontal high-reflective horizons carries also information about the GOC which might be also easy to invert for the GOC shape, but indentifying the distance from the well might be problematic.

The main positive feature of this multiple sources along receiver line is the direct indication of the GOC shape on the differential seismogram. Another advantage of this source position is that the information is doubled by the delay in reflection from strong reflectors and that the information about GOC is localized along the receiver line.

There are some uncertainty about the direct observation of the GOC because in this modelling there is not implemented the effect of the borehole itself and therefore the tube waves might affect the recording in a way covering the weak reflection form the GOC.

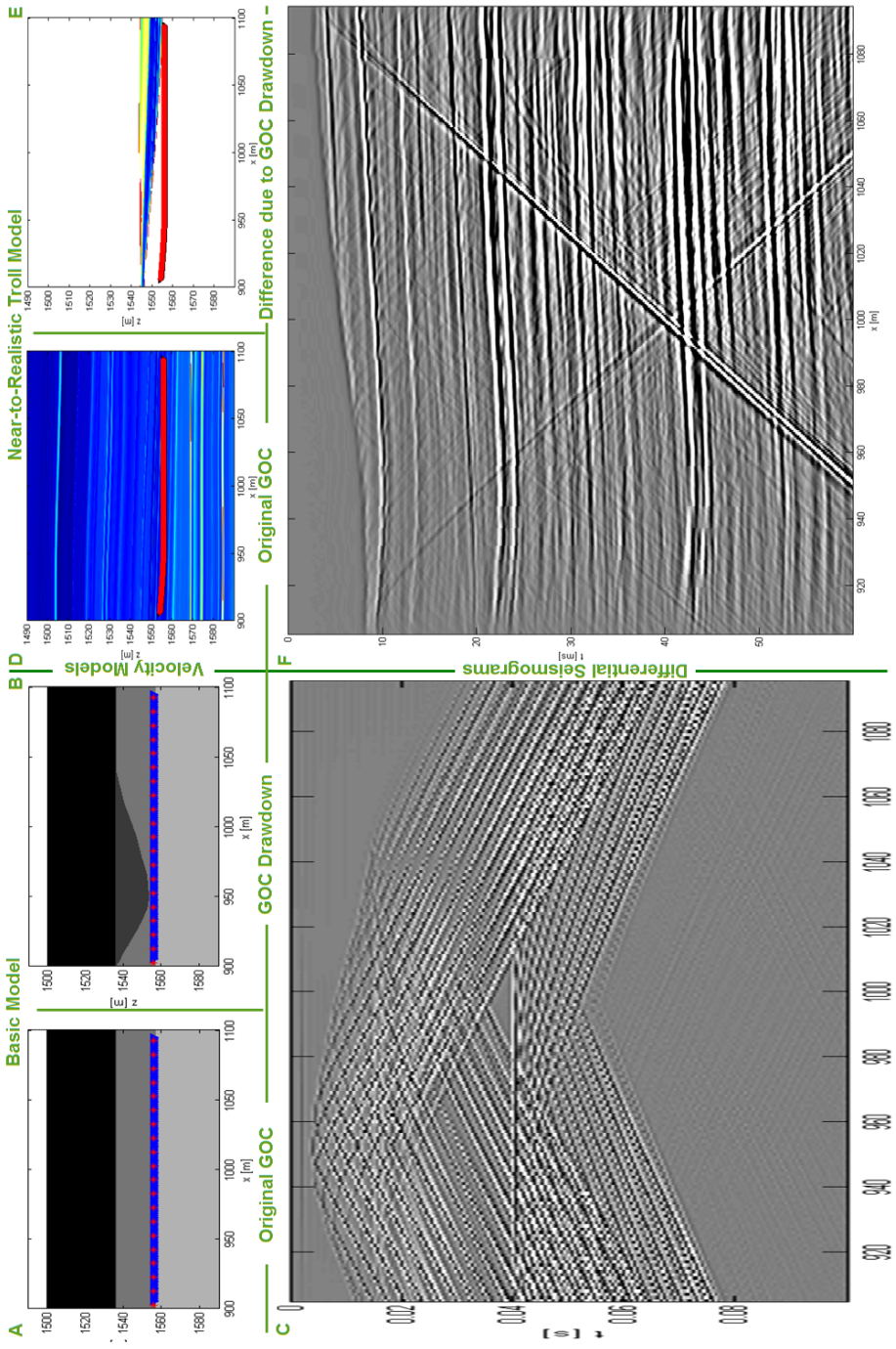

Figure 6.8: **Multiple 1000 Hz sources acquisition setting and differential seismograms.** A, B - blue triangles (joined into a blue line) are receivers, red stars source positions. D, E - black triangles with yellow fill (joined into a black line) are receivers, red stars sources (joined in a red line, overlying the receivers). E - velocity changes due to the GOC drawdown, highlights the shape of the GOC drawdown.Relevant seismograms can be found in the appendix A.3.

6.4 Single Source in Gas Zone

In Figure 6.9, models with the acquisition setting and differential seismograms for this case are shown.

The differential seismogram for the basic model in Figure 6.9C shows two major events. The first hyperbola (t_0 = 17.5 ms) is due to the delay in the direct wave from the source. The width in time of this hyperbola reflects the amount of the GOC drawdown, but the information is strongly spread along the profile. On the other hand, the second hyperbola (t_0 = 25.1 ms) is coming from the wave reflected on the ceiling and appears to focus the information better in the space.

There is a great amount of events on the differential seismogram (Figure 6.9F) reflecting the near-to-realistic Troll situation. It is due to the wave bouncing from calcite layers below and above the GOC and there is also one reflection hyperbola (with the peak at 29 ms) from the calcite cemented layer above the source. The overall characteristic is that the reflection width in time on the differential seismogram reflects somehow the amount of the GOC drawdown, but the direct wave is the most readable.

The advantage of this theoretical setting is that the time shift in the direct wave recorded by a receiver corresponds to the velocity changes on the (more-or-less) line between the source and the receiver. If an assumption is made about the gas saturation profile in the transient zone this should allow an easy data inversion for the GOC shape. Another advantage of placing source in a different well above the production well would be in avoiding the negative impact of the tube waves in the well with receivers.

The disadvantage of this setting is spreading the information about the GOC along the profile and that the original GOC position should be known for the inversion. Also the approximation of the ray path by a line would introduce an error.

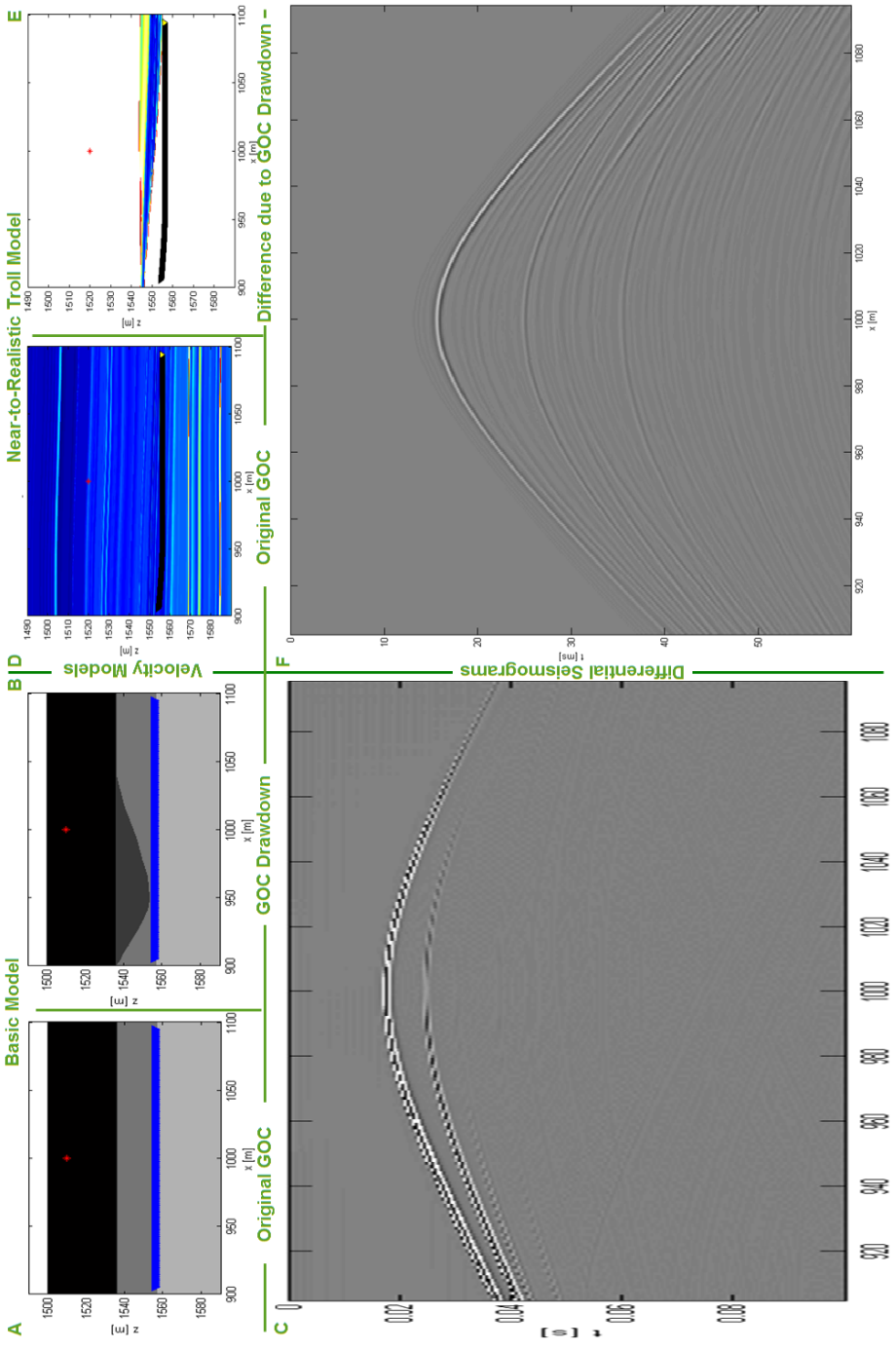

Figure 6.9: **1000 Hz source in gas zone acquisition setting and differential seismograms.** A, B - blue triangles (joined into a blue line) are receivers, red star source position. D, E - black triangles with yellow fill (joined into a black line) are receivers, red star is source. E - velocity changes due to the GOC drawdown, highlights the shape of the GOC drawdown. Relevant seismograms can be found in the appendix A.4.

6.5 Multiple Sources in Gas Zone

In Figure 6.10, models with the acquisition setting and differential seismograms for this case are shown.

Nearly diagonal but hyperbolic events are present on seismograms reflecting the base state (figures A.10A and B) due to the large source spreading of 10 m, which could be considered as a realistic one. These events are therefore also on the differential seismogram in Figure 6.10C. It is obvious that even applying just the normal-move-out correction on the single shot gather before creating the seismogram would bring significant data-quality improvement. This data improvement would then enable to see also the arrival of the wave reflected by the ceiling (now present, but completely hidden in the hyperbolic events) and better observation and interpretation of the time shift variation along the profile - reflecting the amount of the GOC drawdown.

In the differential seismogram (Figure 6.10F) for the near-to-realistic Troll situation, a general increase in the signal is observable for the right part of the model where the larger GOC drawdown occurs. Alike as for the single shot in the gas zone there are many arrivals carrying information about the GOC due to the wave bouncing between calcite-cemented layers.

This is the most theoretical situation and its advantage would be that beside the possibility of easily inverting the time delay into the GOC drawdown, it provides the look and see information about the GOC drawdown extension, which might be easily inverted to the GOC shape with the right positioning in place.

The disadvantage would be then in the ambiguousness of the distance of the GOC from the receiver line - production well.

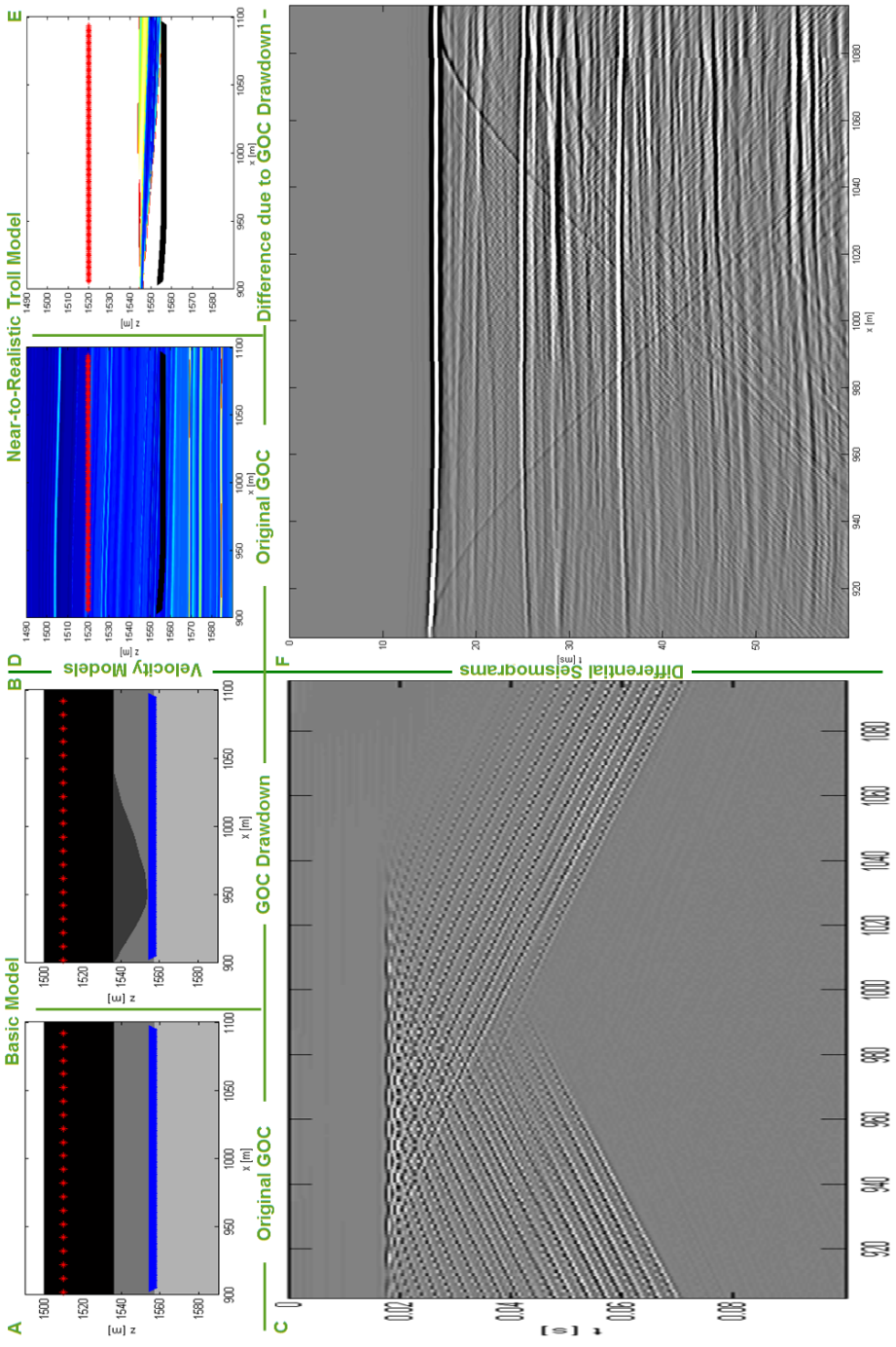

Figure 6.10: **Multiple 1000 Hz sources in gas zone differential seismograms.** The colour scale in Figure C is atypical: -0.01 to 0.01. A, B - blue triangles (joined into a blue line) are receivers, red stars source positions. D, E - black triangles with yellow fill (joined into a black line) are receivers, red stars (joined into a red line) are sources. E - velocity changes due to the GOC drawdown, highlights the shape of the GOC drawdown. Relevant seismograms can be found in the appendix A.5.

6.6 Source at Surface: VSP

In Figure 6.12, the models with the acquisition setting and differential seismograms for this case are shown.

There are two major events on the differential seismogram (Figure 6.12C) reflecting the GOC drawdown on the basic VSP model. The first is associated with the direct wave, the second with the wave reflection from the sea surface. The wave is arriving at the beginning of the receiver line with a declined front (as denoted on the wave field snapshot in Figure 6.11A), but further on the wave head is perpendicular. It causes spreading of the information about the GOC along the whole profile of about 2.5 km, but the strongest signal is recorded by receivers from 920 to 1075 m (see the zoom in Figure 6.12C) which corresponds to the GOC drawdown area. The angle of wave incidence along the receiver line is influenced by the over and under lying velocity structure as well as by the source distance from receivers. Original seismograms can be found in Figure A.12 A and B in appendix A.6. Figure 6.11A shows the snapshot of the wave field at time corresponding to the time t = 1.04 s on the differential seismogram.

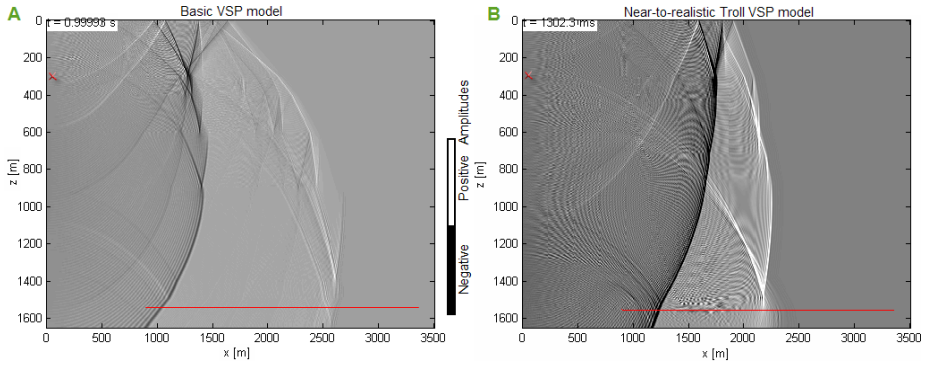

Figure 6.11: **Wave field along the receiver line in VSP models** for peak point source. A - wave field in the basic overburden model (t = 1.04 s on seismograms). B - wave field in the near-to-realistic overburden Troll (t = 1.34 s on seismograms). Red cross - source position, red line - receivers position.

The situation in near-to-realistic Troll model is of the same kind as in the basic one: two major events associated with the direct wave and the wave reflected from the sea surface, only the wave head along is more perpendicular to the receiver line (see the wave field snapshot in Figure 6.11B). Maximum signal on the differential seismogram is approximately between 950 and 1750 m (Figure 6.12F), but the GOC drawdown occurs no further than 1500 m.

It is positive that the area of the GOC drawdown can be approximately identified on the differential seismograms, but it might be disputable how precise is this information to enable preventing the gas breakthrough.

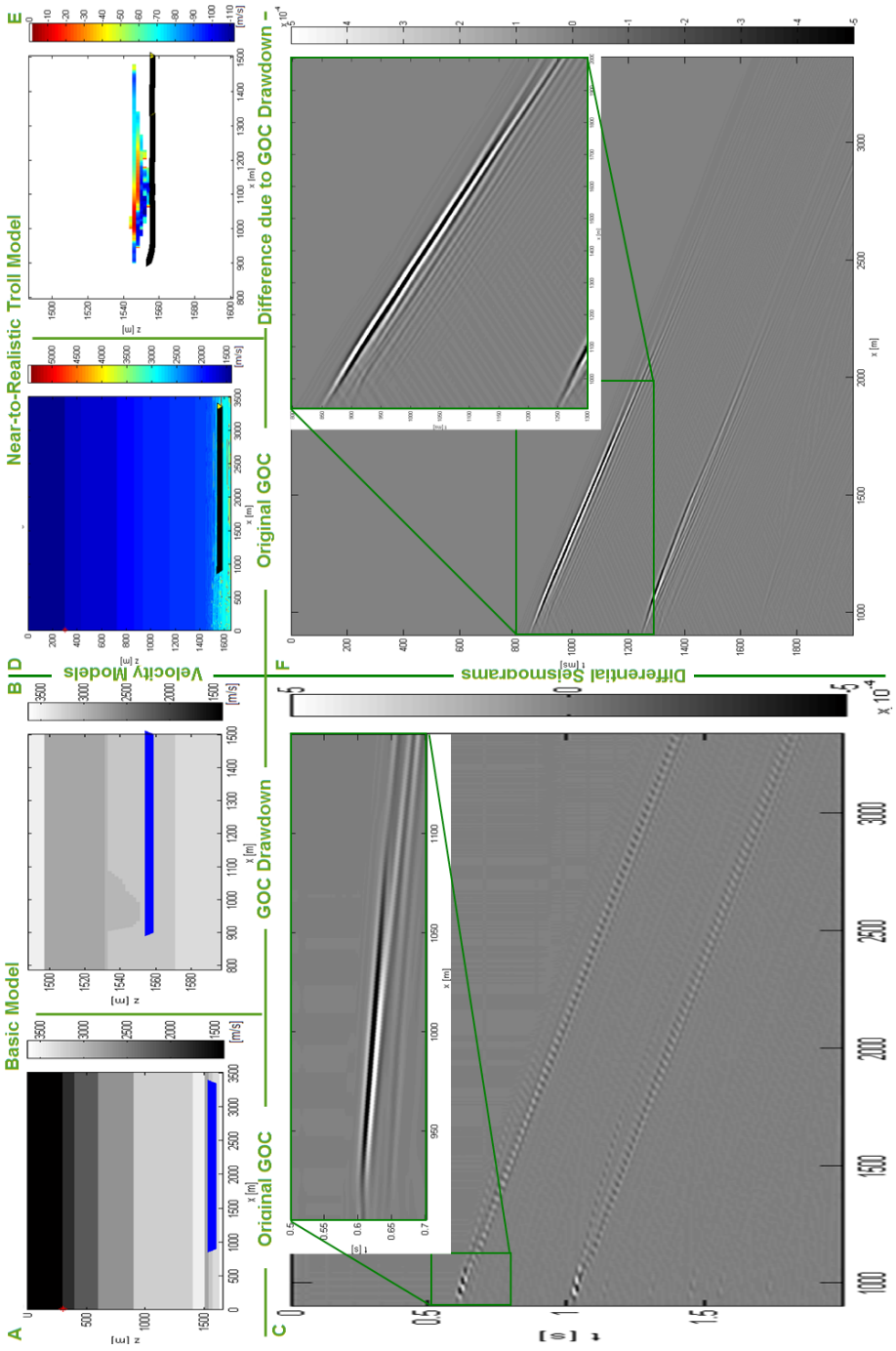

Figure 6.12: **VSP acquisition setting and differential seismograms.** Source with central frequency of 50 Hz (shift of time zero to t = 41 ms). A, B - blue triangles (joined into a blue line) are receivers, red star source position. B - zoom on the GOC drawdown state of basic model. D, E - black triangles with yellow fill (joined into a black line) are receivers, red star is source. E - zoom on the velocity changes due to the GOC drawdown, highlights the shape of the GOC drawdown. Relevant seismograms, can be found in the appendix A.6.

6.7 Most Favourite Acquisition Geometries

The time delay due to oil production represented by the differential seismogram was examined in the sections above for six source position scenarios. Below the acquisition scenarios are presented in order according to their convenience: at the top the one who delivers the most detailed information about the GOC, at the bottom the one with the most disputable relation between recorded time delays and the GOC. This source evaluation is based only on the simulations, it does not reflect expected complications in reality.

Multiple sources in horizontal well: Direct observation of the GOC and time delay in single horizons reflections - the first reflecting the actual GOC position, the second the amount of the GOC drawdown, but both defining the GOC position alone whole receiver line.

Multiple sources in gas zone: Direct relation between the GOC drawdown and the time delay in direct and reflected wave. Defines the GOC drawdown along whole receiver line; the original GOC position required for interpretation.

Single source in gas zone: Time delay in direct and reflected wave - first might be easily inverted toe the GOC shape is the velocity model and the original GOC is known. The direct wave provides information only about a part of the GOC above the receiver line.

Source in centre of horizontal well: Time delay is carried by a single reflection from above the GOC and by (multiple) reflections joining the direct wave. The first is significant for smaller offsets and can be converted into the GOC, the second is dominant for further offsets and lower frequencies and its relation with the GOC is complicated. Information about the GOC spread along large distance.

Source in heel of horizontal well: Time delay has the same origin as for the source in the centre of the well, but most of the GOC would have to be interpreted from the reflection hidden in the direct wave. A general relation between the GOC drawdown and the time delay hidden in the direct wave is observed.

Source at Surface: VSP Time delay carried mostly by the direct wave and wave reflected for the sea surface. Relation between the overall time delay and the GOC might be complicated but there is some, although spread along the profile.

Chapter 7

Suggestions for GOC Interpretation

In this chapter we are going to look at the possibility of a basic interpretation of the GOC. It is based mainly on differential seismograms for the multiple sources in horizontal production well and sources at the well heel and at the sea bed. Therefore, first of all, a relation between differential energy (E_d) of a receiver x and time shift of wavelets (Δt_{shift}) is examined for wavelets of dominant frequency 1000, 100 and 50 Hz. $A_d(t)$ stands for the differential amplitude at time t on the receiver x.

$$E_d(x) = \sum A_d^2(t, x)$$

Figure 7.1 shows the relation between differential energy and time shift for 1000 Hz. The differential energy E_d is proportional to the time shift Δt_{shift} up to 0.43 ms for 1000 Hz, 4.3 ms for 100 Hz and 8.6 ms for 50 Hz; all corresponding to $\lambda/4$. For a larger time shift the differential energy significantly decreases. Therefore before interpreting the GOC from a differential seismogram the validity of proportional relation between E_d and Δt_{shift} should be checked.

The interpretation is tested on the near-to-realistic Troll velocity models utilized in the previous chapter. These models were calculated with a complex transient zone between oil and gas invaded zone: Linear decrease in the residual oil saturation is different for c-sand (from 80 to 10%) and m-sand (from 70 to 40%). A rough estimate of the average residual oil is 50% (44% gas saturation) which, according to relation between gas saturation and P-wave velocity (Figure 2.7A), corresponds to a slowness change (Δs) of $2.05 * 10^{-5}$ s/m. The interest is in slowness because only for slowness there is linear relation between the distance (d) the wave travels through drained zone and the time delay (Δt_{shift}) it gains:

$$d = \frac{\Delta t_{shift}}{\Delta s}$$

According to this estimate of the slowness change, the proportional relation between the differential energy and the time shift exists for waves which travelled through drained zone for maximum of 21, 210 or 420 m (for 1000, 100 or 50 Hz).

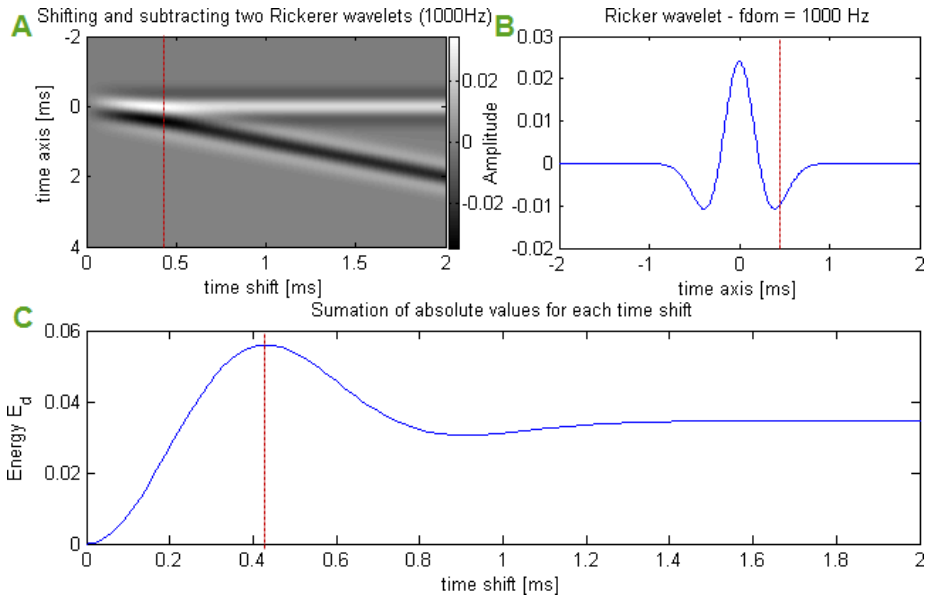

Figure 7.1: **Relation between wavelet shift and differential energy.** A - difference of two 1000 Hz Ricker wavelets (on subfigure B) sliding across each other. Red vertical line – critical time shift $\Delta t_{shift} = 0.43$ ms ($\lambda/4$).

7.1 Multiple Sources in Horizontal Well

These multiple sources represent the zero-offset gather for a large set of receivers and sources within a horizontal well. As mentioned, two types of the GOC indication are observable in the differential seismogram:

1. Direct observation, caused by a weak reflection on the GOC itself.
2. Delay in the horizon reflection dues to lower velocities in the drained area.

The direct observation time $t_{DireObs}$ brings the information about the two travel time between the GOC and the receiver line, which is easily convertible to the GOC distance above the well $h(x)$:

$$h(x) = \frac{t_{DireObs}(x) - t_0}{2} v_{average}(x)$$

Comparison between the initial and interpreted GOC, adopting average velocity in the oil layer and automatic first break picking, is shown in Figure 7.2B. It is mostly because of setting the right t_0 that there is a very small systematic shift between interpreted and original GOC.

The time delay $\Delta t_{shift}(x)$ *in horizon reflections* carries the information about the oil drained zone thickness $d(x)$ above a receiver x. The recorded time shift corresponds to the two-way travel time through this drained zone, therefore for 1000 Hz source, the maximum 10.5 m of the GOC drawdown can be interpreted from the differential seismogram

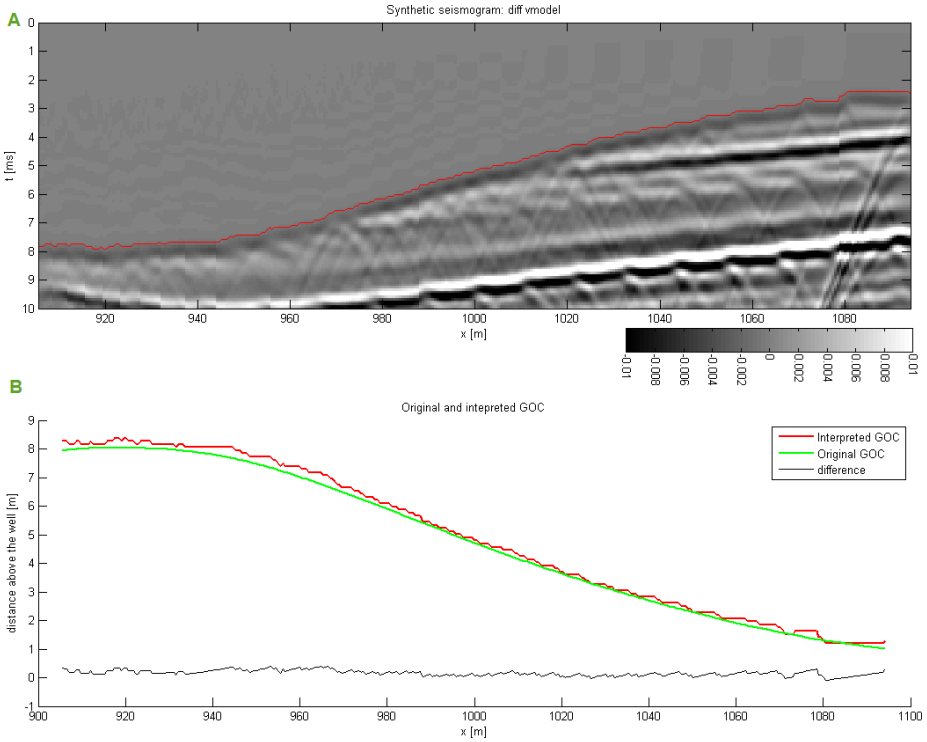

Figure 7.2: Multiple 1000 Hz sources in horizontal well: **GOC interpretation from the 'direct observation' feature.** A - red line - first breaks ($t_{DireObs}(x)$) by automatic picking. B - Black line - difference between interpreted and original GOC.

Although the condition of maximum 10.5 m drawdown is fulfilled in this acquisition setting, the differential energy of whole seismogram (Figure 7.3) or just a horizon (Figure 7.4) shows significant decrease at further offsets, where the largest GOC drawdown occurs. The reason might be in a too rough estimation of the slowness change due to oil production.

In spite of it, there is a correlation between the differential energy and the GOC shape for lower GOC drawdown. It is believed that an improvement of the seismogram quality (eliminating effect of the edge sources, diffraction hyperbolas) would improve the level of the correlation. Oscillations of the differential energy of a single horizon are due to diffraction hyperbolas intersecting the reflection.

For larger GOC drawdown the time delay $\Delta t(x)$ might be derived as a correlation between a horizon reflection on seismograms for the original and drawdown GOC. The horizon correlation might be a problem if its reflection coincides with another. Second options would be to pick these horizons and distract the time delay directly from the picks. The advantage of these GOC interpretations is its independency on the time zero estimation.

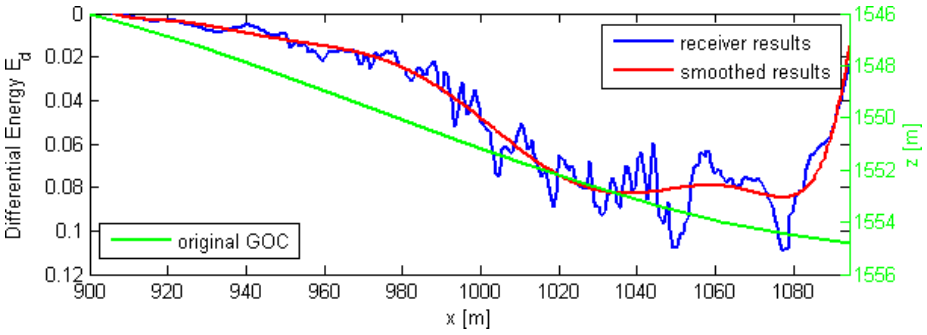

Figure 7.3: Multiple 1000 Hz sources in horizontal well: **Differential energy of whole seismogram - correlation with the GOC**

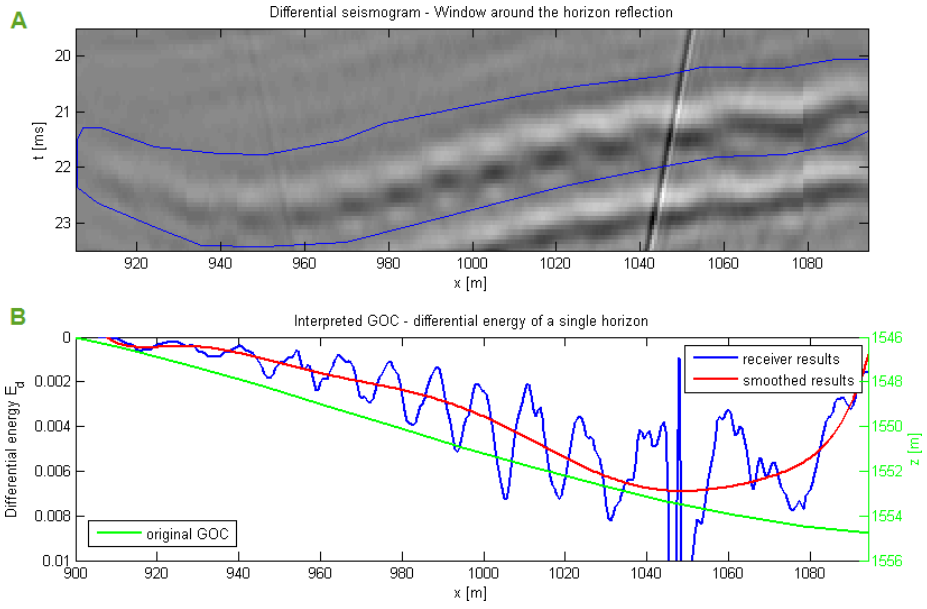

Figure 7.4: Multiple 1000 Hz sources in horizontal well: **Differential energy of one differentia horizon** A - Differential seismogram zoomed on the differential reflection from the calcite-cemented layer at 1529 m depth. B - blue line differential energy in the blue window on A.

7.2 Source in Heel of Horizontal Well

Looking at the differential seismogram for the 1000 Hz source in the heel of the horizontal well, it can be said that this high frequency source can carry information about the GOC in reflections from calcite-cemented layers up to 100 m from the source position. Unfortunately these reflections are not present for lower frequencies and the distance between the well heel and the beginning of the receiver line might be up to 150 m. Therefore there is a question if it is possible to derive the GOC shape and distance from the well from the time shift in reflections hidden in the direct wave. Tests in this section are conducted on the (differential) seismograms for the 100 Hz source in the larger velocity model (Figure 6.6).

There are generally two ways the interpretation might go, but only the first option is examined here:

1. from the differential seismogram itself
2. by comparing measured (differential) seismograms with synthetic seismograms for different GOC stages

The time delay is obtained by (multiple) reflections of different strengths and from various horizons. A very rough approximation would say that the time delay is related to the oil drained column right in the middle between source and the receiver. This approximation is reasonable for a simple shape of the GOC with one maximum.

The differential energy for 100 Hz source is proportional to the time shift for waves travelling through the drained zone for up to 210 m, but a single reflection from the top of the drained region recorded at the furthest offsets experience about 400 m of the drawdown area. But the wave reflected on calcite layers at 1530 m depth experiences only 90 m. Since there is not a strong reflector at the position of the original GOC we might expect that the maximum time delay will be related to reflectors further from the GOC.

Figure 7.5B displays the original GOC shape with the differential energy E_d assigned to the centre of the source and corresponding receiver and there is a significant shape coincidence. The differential energy highlights the maximum drawdown but for a lower GOC drawdown E_d is zero. On the other hand, the square root of the differential energy (*root* E_d, Figure 7.5C) respects more the low GOC drawdown.

If the GOC drawdown was constant along the well then the head wave spreading would be gaining a time delay linearly and the slope of the time delay change with offset would be proportional to the thickness of the GOC drawdown. Therefore the derivative of the smoothed time delay (represented by the differential energy) might be reflecting the GOC shape. Figure 7.6 shows that there is little correlation with the GOC shape and the position of the maximum derivative does not corresponds to the place of maximum drawdown.

The same data examination was done on a model with narrower drained zone and there the derivative shows better correlation with the GOC shape, especially for the more drained part, but the maximum of derivative is also shifted towards lower offset. Correlation of the root of differential energy variation and the GOC shape shows even more similarities with the GOC shape.

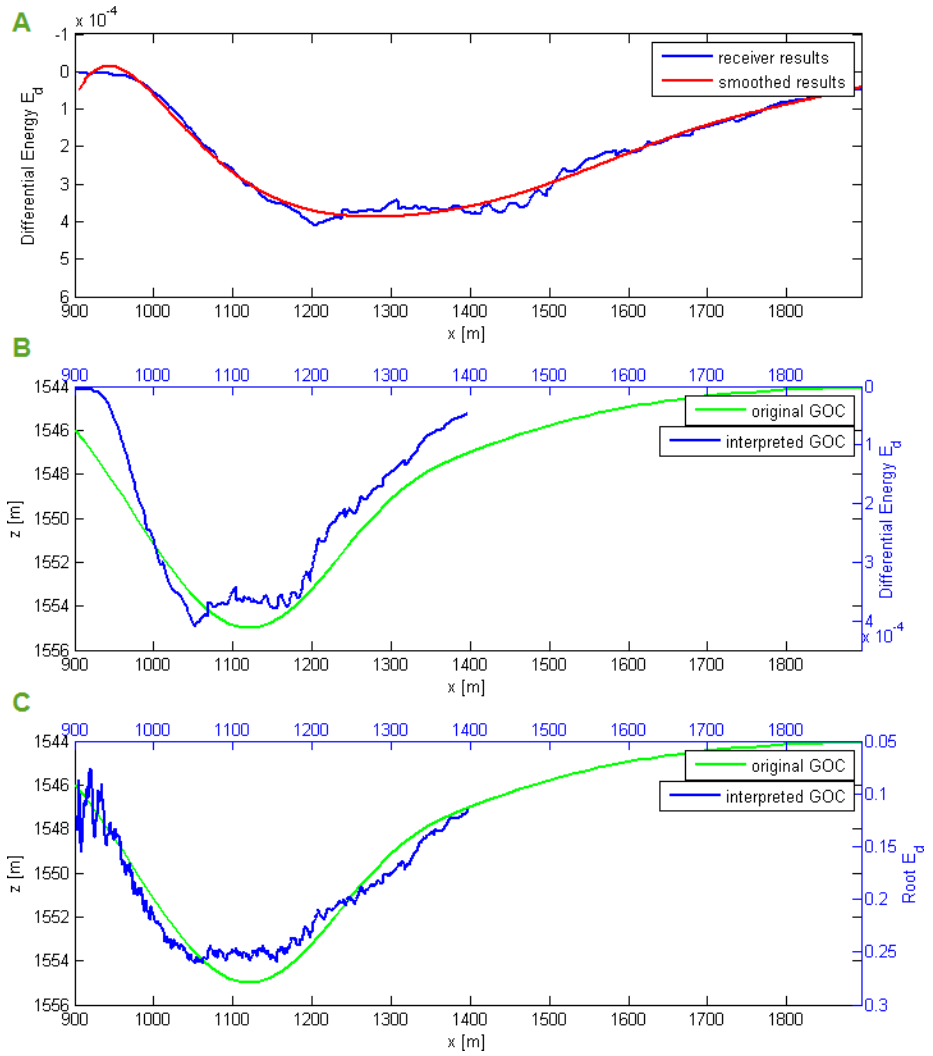

Figure 7.5: Source at the well heel: **Differential energy** corresponding to the differential seismogram in Figure 6.6C. A - E_d variation along profile; B -E_d assigned to the middle point between source and receiver; C - square root of differential energy assigned to the middle point between source and receiver.

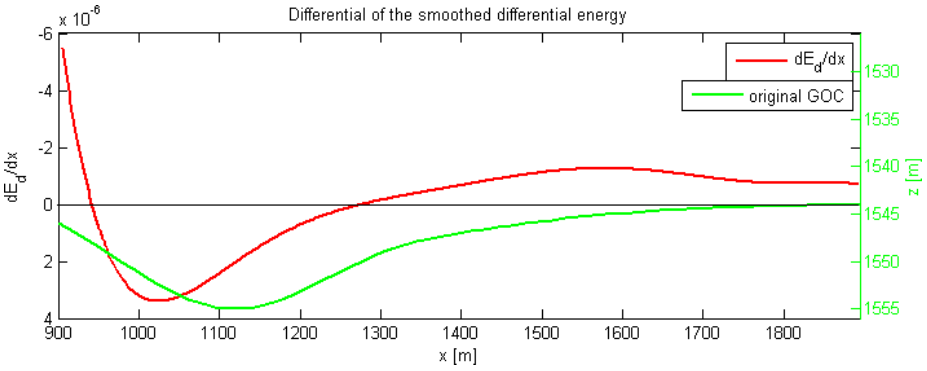

Figure 7.6: Source at the well heel: **Derivative of differential energy.** E_d smoothed - red line in Figure 7.5A.

The qualitative GOC shape approximation from the differential energy variation along the profile could be an initial GOC shape for creating the velocity models for comparing the measured data with synthetic seismograms. A calibration of the differential energy to drainage would be necessary.

7.2.1 Original Seismograms Analysis

The differential seismogram carries the information about the GOC, but what else does? Three different approaches were taken to look at the seismograms for 100 Hz heel source in the larger near-to-realistic Troll model. Two GOC shapes were adopted for these tests: the one utilized in cases mentioned above (Figure 7.7D) and the second of the same type but of a lower drawdown (Figure 7.7E).

Is there a relation between the change in the apparent velocity along the receiver line and the GOC drawdown? The apparent velocity in the original GOC case ($v_{app}^{orig}(x_{n+1/2})$) can be defined as a ratio of the receiver distance and the time shift in recorded signal maxima between two receivers:

$$v_{app}^{orig}(x_{n+1/2}) = \frac{|x_{n+1} - x_n|}{t_{max}(x_{n+1}) - t_{max}(x_n)}$$

The time shift in maxima is determined by cross-correlation between records of neighbouring receivers. The apparent velocity change between the GOC original and drawdown state ($\Delta v = v_{app}^{orig}(x_{n+1/2}) - v_{app}^{draw}(x_{n+1/2})$) is denoted in Figure 7.7A .

The arrival time of the direct wave changes due to the oil production. How does a derivative of this time change vary along the profile? The difference in the direct wave arrival to a receiver might be derived by cross-correlating the traces. The maximum time shift in our models is 1.4 ms[1]. The resulting time delay for larger GOC drawdown and the derivative of the time delay along the profile also for the lower drawdown are shown in Figure 7.7B.

[1]It shows that the for 100 Hz heel source the assumption about proportional relation between the differential energy and the time shift was rightful.

Further, the variation of the difference in the recorded time between neighbouring receivers was examined. Receiver record of neighbouring receivers was subtracted and derivative of the root of differential energy was calculated. Results are presented in Figure 7.7C.

The analysis of all these seismograms represent, in a way, changes in the apparent velocity due to the oil production. That is why they all show the same type of behaviour. Because of the complex wave behaviour it is not easy to determine the origin of these variations, but it can be said that in a region of hardly any GOC drawdown there the difference in the apparent velocity is nearly zero. It is also positive to observe that the amplitude of the apparent velocity change shows dependency on the amount of drained oil for all data analysis. The apparent velocity variation shows that between 1400 and 1500 m, there the head wave was travelling faster for the oil drained case.

It is a question how these variation in the apparent velocity reflects the GOC shape or even the residual oil profile in the drained zone. For that purpose, the same data analysis was applied on a changed geology (the half-space below the well was interchanged by a homogeneous block). The apparent velocity variation shows about half of the main oscillations and the major extreme is shifted towards further offsets. The apparent velocity decrease was present also here.

This leads to the conclusion that the variation in the apparent velocity along the receiver line strongly reflects the geology, but the amplitude of the variations is related to the oil drained amount.

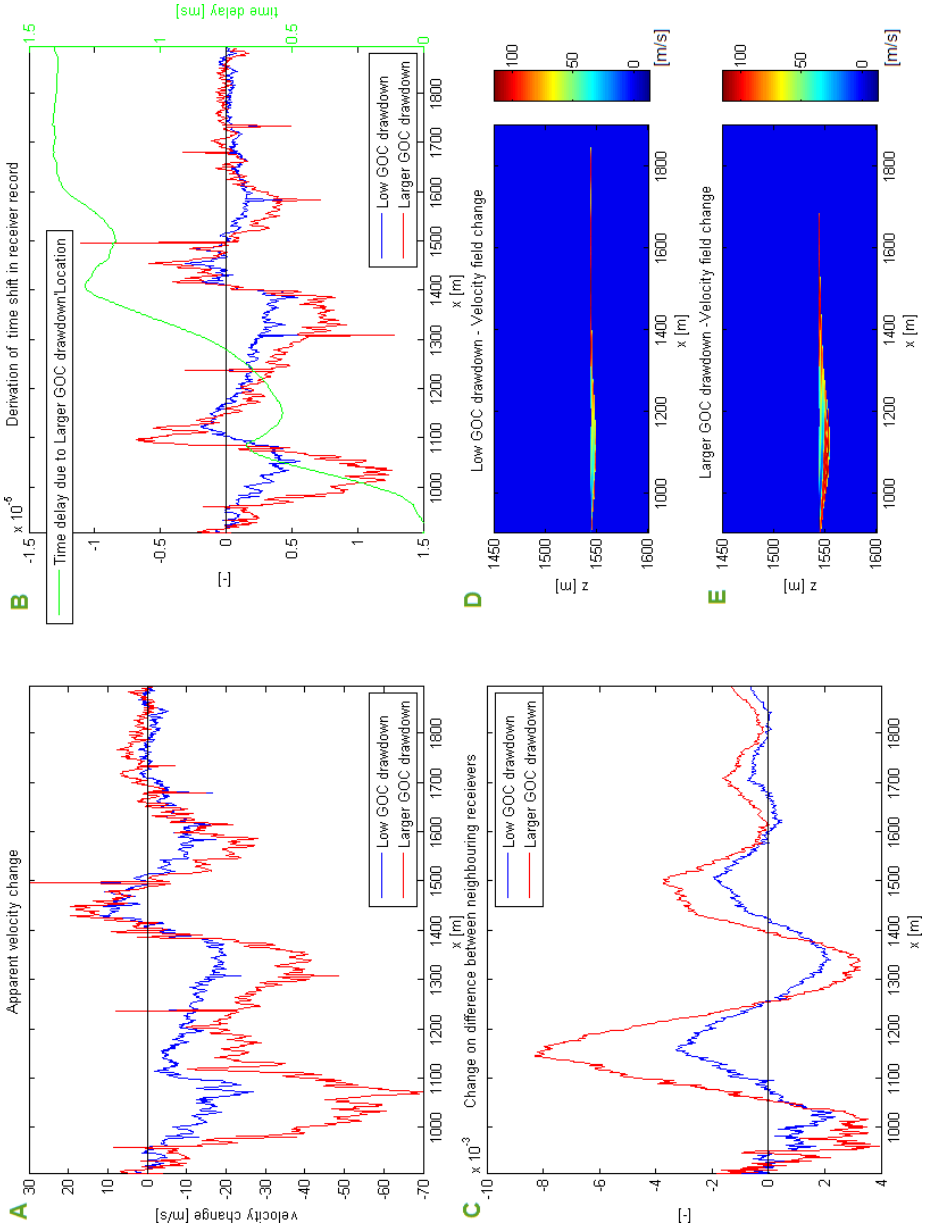

Figure 7.7: **Heel source seismograms analysis.** Blue lines corresponds to results calculated for GOC drawdown velocity changes on D, red lines on E. A - apparent velocity changes due to oil production. B - derivatives of time delay in head wave due to the oil production (here the red line is derivative of the green). Green line - time delay in head wave arrival for the GOC drawdown on E. C - derivative of root E_d of the difference in neighbouring receiver's record.

7.3 Source at Surface: VSP

The differential seismogram for the source at the sea bed was tested in the same manner as the heel source one. 50 Hz provides proportional relation between the differential energy and time shift for whole our model.

The difference of smoother differential energy variation along the profile (Figure 7.8) provides in our case little idea about the GOC.

The differential energy assigned to the middle point (Figure 7.9B) provides general information about the GOC shape, but it is not sensitive to the less drained zones. On the contrary, the root of the differential energy (Figure 7.9C) assigned to the centre between source and corresponding receiver provides generally better shape approximation for the lower GOC drawdown. This is the same type of relations as for the heel source.

A combination of these interpreted GOC shapes might be an initial guess for creating set of various velocity models, if a calibration of the differential energy to drainage is done. Resulting synthetic seismogram would be then compared with the measured one which would lead to the picking the most probable corresponding GOC state in reality.

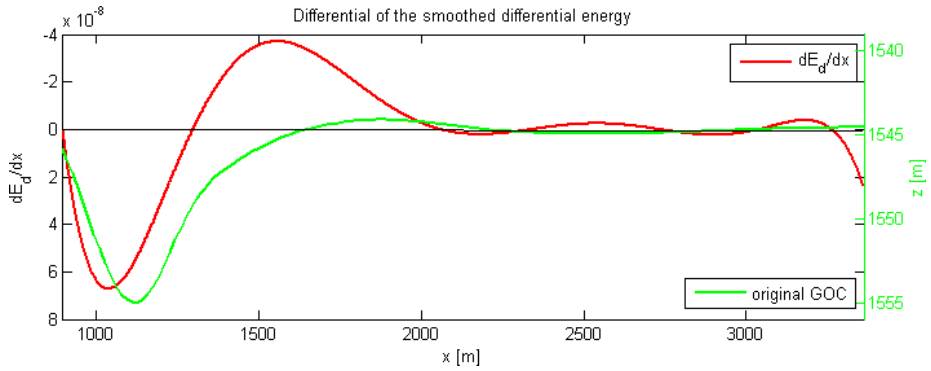

Figure 7.8: Source at surface: **Derivative of differential energy.** E_d smoothed - red line in Figure 7.9A.

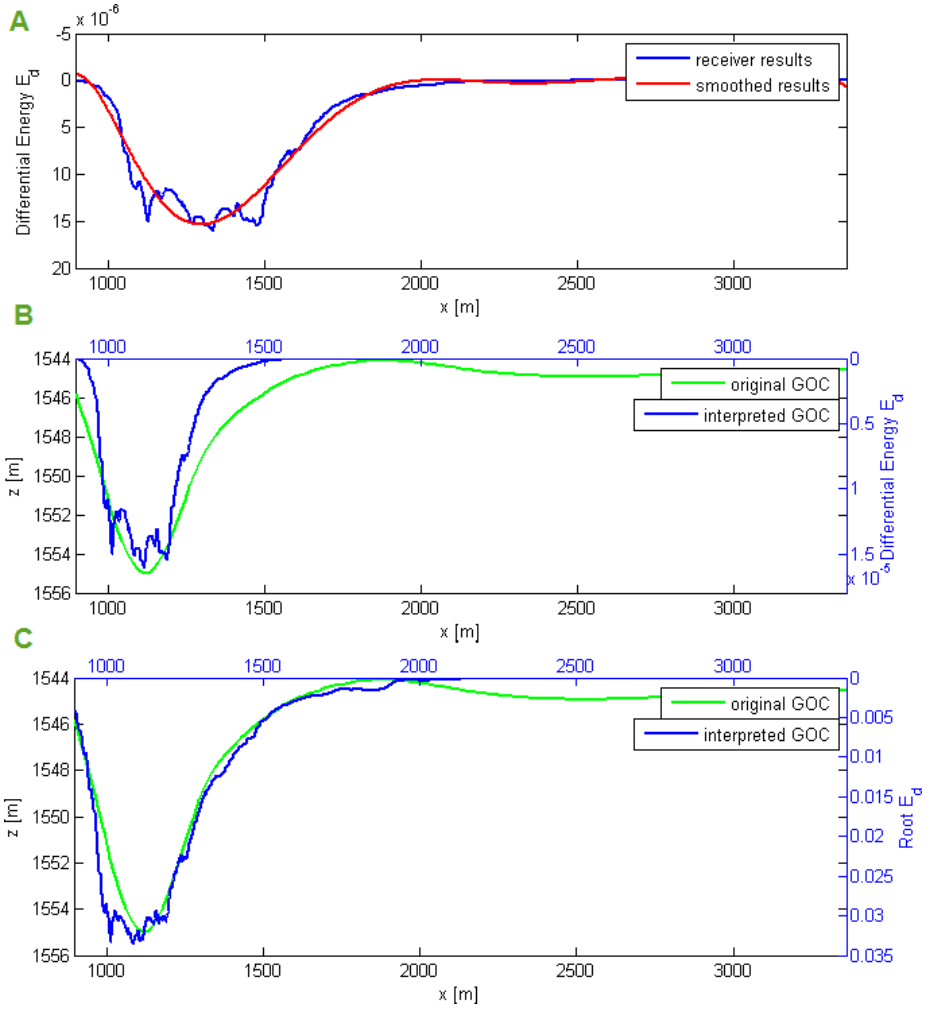

Figure 7.9: Source at surface: **Differential energy** corresponding to the differential seismogram in Figure 6.6C. A - E_d variation along profile; B -E_d assigned to the middle point between source and receiver; C - square root of differential energy assigned to the middle point between source and receiver.

Chapter 8

Effect of Variations in Geological Settings

In previous chapters, the near-to-realistic Troll velocity model represented the Troll reservoir geology as a sequence of continuous, smooth layers with a complex oil drained zone. The goal of this chapter is to learn more about the impact on the GOC monitoring for few variations in the geological setting. The variations are done towards the situations which are more probable in reality.

The effect of geology variations is commented for 1000 Hz multiple sources in the horizontal well and partially also for the 100 Hz source at the well heel.

8.1 Oil-Gas Transient Zone

As it was mentioned previously, the transient zone between oil and gas invaded zone might be a complex function of the reservoir properties. Before the seismograms in previous chapters were calculated with complex transient zone, the effect of few basic transient zones was examined for the 1000 Hz multiple sources in the horizontal well.

The first quick test was done on the basic model by simulating a gradual transition between the oil and gas zone by a system of homogeneous layers with increasing velocity. This setting produces more complex seismograms, but the major GOC indication remains.

The second examination was done on the near-to-realistic model by defining three different residual oil profiles:

1. Constant 10% of residual oil saturation (Figure 8.1B)
2. Linear decrease of residual oil saturation from 50 to 10% (Figure 8.1C)
3. Linear decrease in residual oil saturation is different for c-sand (80-10%) and m-sand (70-40%) (Figure 8.1D)

The original oil saturation is shown in Figure 8.1A.

The first saturation profile - constant 10% residual oil in whole gas invaded zone above the GOC - was assumed in Ona (2006), while interpreting the 4D seismic data utilizing the near-to-realistic Troll model. It might look logical

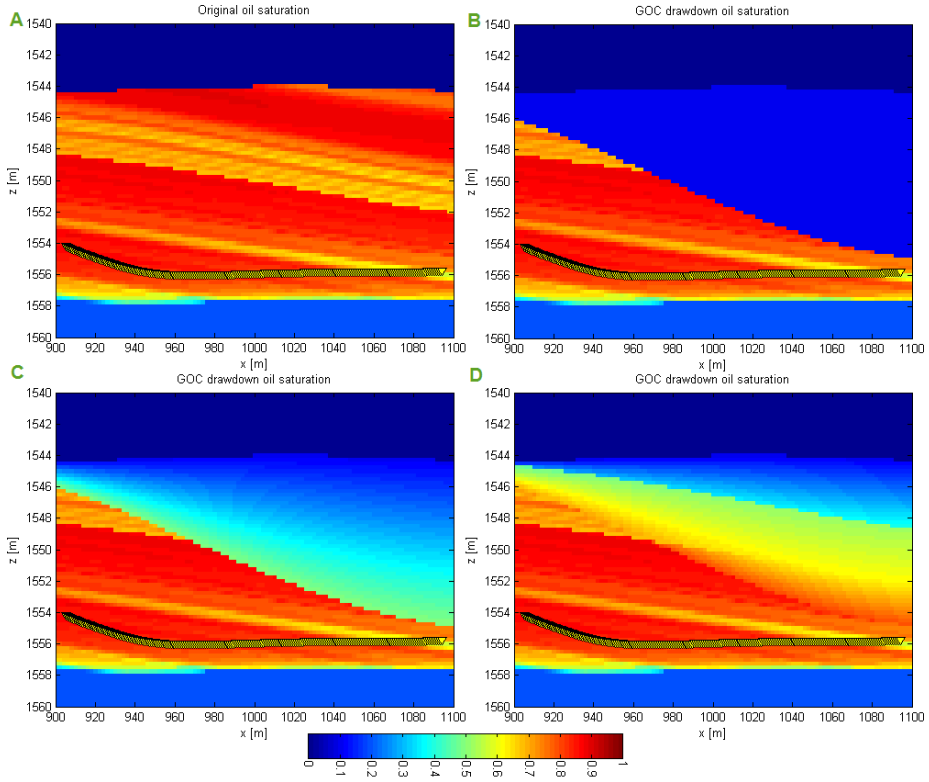

Figure 8.1: **Oil saturation in the transient zone.** A - original oil saturation before oil production. B - constant 10% of residual oil. C - Linear decrease of residual oil from 50 to 10%. D - Linear decrease in residual oil is different for c-sand (80-10%) and m-sand (70-40%).

that higher oil saturation in the drained oil zone could stop some of the GOC indications because of the low velocity contrast. But the gas saturation – P-wave velocity ration in Figure 2.7 shows that 84% gas saturation (10% oil, 6% irreducible water saturation) produces nearly the lowest velocity decrease, which means that up to 90% residual oil saturation the velocity contrast will not be lower than for the 10% oil saturation. That explains why the direct observation stays present on differential seismograms for all tested transient zone variations. Since the third type of transient zone (Figure 8.1D) might be the closest to reality, this transient zone was adopted for all simulations on the near-to-realistic Troll model in chapter 6.

Although the type of transient zone does not influence the direct indication of the GOC for the multiple sources in the horizontal, it would certainly influence the precision of the GOC shape interpretation based on the time delay in reflections from horizons (for sources in the production well) or in the direct wave (for sources in the gas zone).

Different types of oil saturation profiles between oil and gas invaded zone can be implemented while interpreting the heel or VSP data by comparing the synthetic seismograms with the measured ones.

8.2 Calcite-Cemented Layers

As shown in the section 2.1.3, there is a large uncertainty in the shape and continuity of the calcite-cemented layers. Since some of the acquisition scenarios rely on the reflections from reflectors above the GOC (especially for higher source frequencies), the effect of interchanging two smooth, continuous layers (pointed in Figure 4.2) by four types of calcite cemented layers, was examined.

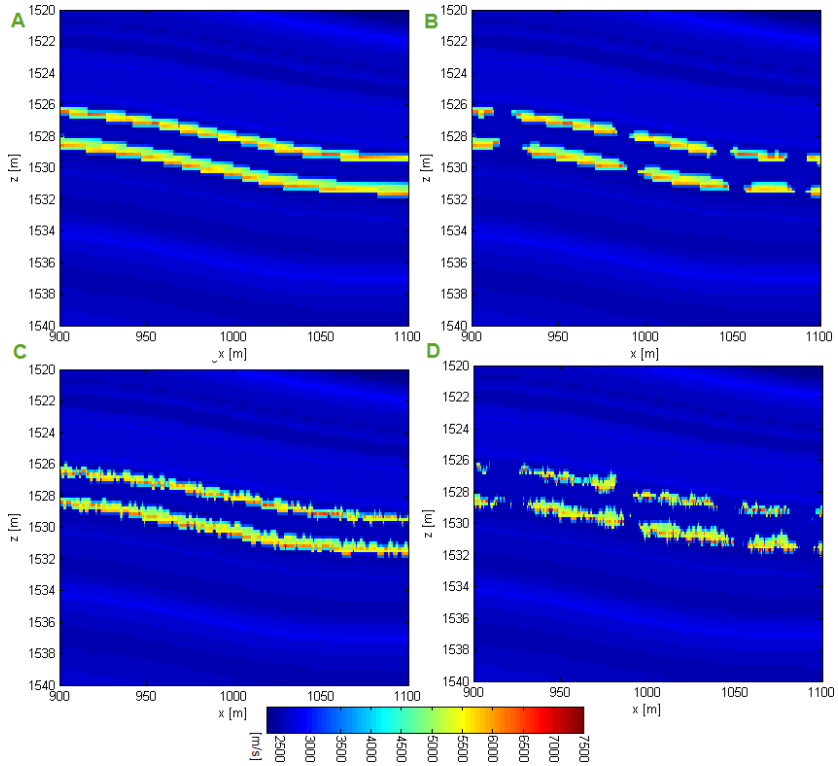

Figure 8.2: **Calcite-cemented layers.** A - Continuous calcite-cemented layers with smooth interface. B - Discontinuous calcite-cemented layers with smooth surface. C - Continuous calcite-cemented layers with irregular interface. D - Discontinuous calcite-cemented layers with irregular interface.

The near-to-realistic Troll velocity model was changed in a way that the original limestone layers at depths 1526 and 1529 m were deleted and new layers were added. The velocity assigned to created calcite-cemented layers is high and is taken from calcite-cemented layers lying below the well[1]. Maximal thickness of each new layer is 1 m, which corresponds to the maximum thickness observed in the core.

Following four calcite-cemented (very high velocity) layers geometries within the layer 4Cc are examined:

[1]Adopting a velocity for the new calcite-cementer layers from below the OWC causes an increase in impedance contrast with respect to the original state. This is done due to an assumption of an artificial limestone velocity decrease due to recalculation to dry properties with a wrong porosity

1. Continuous calcite-cemented layers with smooth interface (Figure 8.2A)
2. Discontinuous calcite-cemented layers with smooth surface (Figure 8.2B)
3. Continuous calcite-cemented layers with irregular interface (Figure 8.2C)
4. Discontinuous calcite-cemented layers with irregular interface (Figure 8.2D)

Multiple sources in horizontal well: Since the calcite layers are above the GOC there is no impact on the direct observation of the GOC shape on the differential seismogram for none of the variation in the shape of calcite cemented layers.

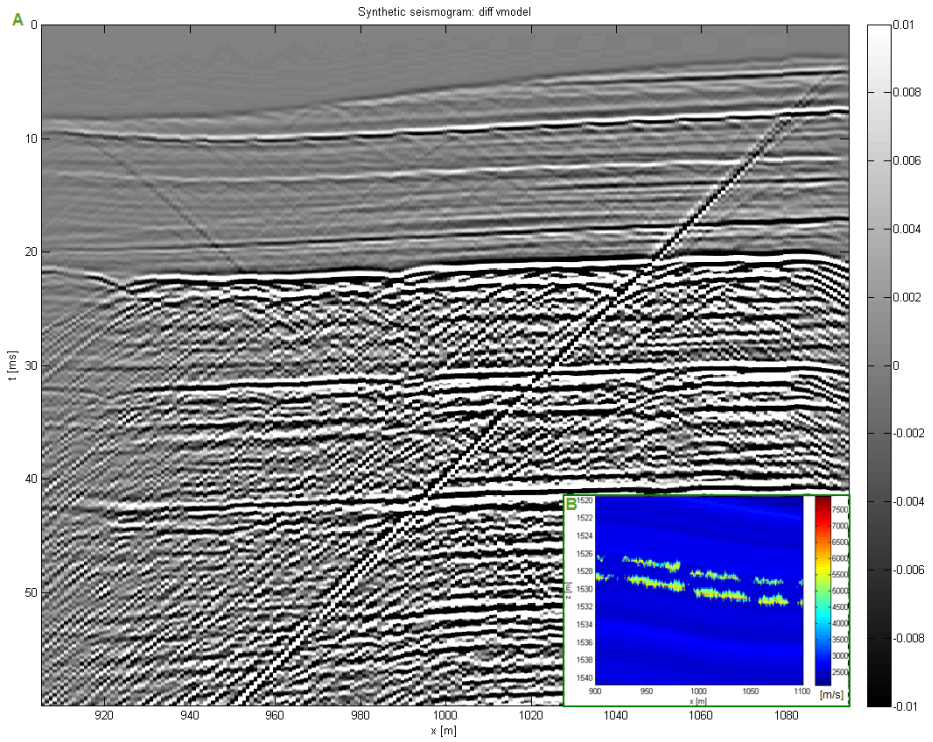

Figure 8.3: **Effect of discontinuous and rough calcite-cemented layers** shown on B. A - differential seismogram for the multiple sources in the production well; dominant frequency of 1000 Hz.

Irregularities on the layer surface are points of the diffraction which distracts the seismic image in later times than the calcite-cemented layers reflections - see the differential seismogram for the discontinuous calcite-cemented layers with irregular interface in Figure 8.3A. Migration based on diffraction hyperbolas collapse would eliminate the diffraction hyperbolas. This distractive effect is nearly eliminated while using lower source frequencies.

Despite the diffraction the main GOC shape can be seen on interpolation of the differential energy variation along the profile, with the same energy decrease at the end of profile as seen for the original limestone.

Source at the well heel: For the low frequency source the shape calcite-cemented layers does not significantly contribute to the GOC indication, therefore the effect of the layers type is negligible.

8.3 OWC Drawdown

Although it would be nice to have all the changes in the velocity field only due to the GOC shift, the OWC is also affected by the production and therefore it will contribute to the time variation in the reservoir. The effect of the OWC shift on the GOC indications was examined on two near-to-realistic Troll models and corresponding velocity changes in the models are displayed in Figure 8.4. The OWC after production adopted for this test is the OWC interpreted from 4D seismic in Ona et al. (2006).

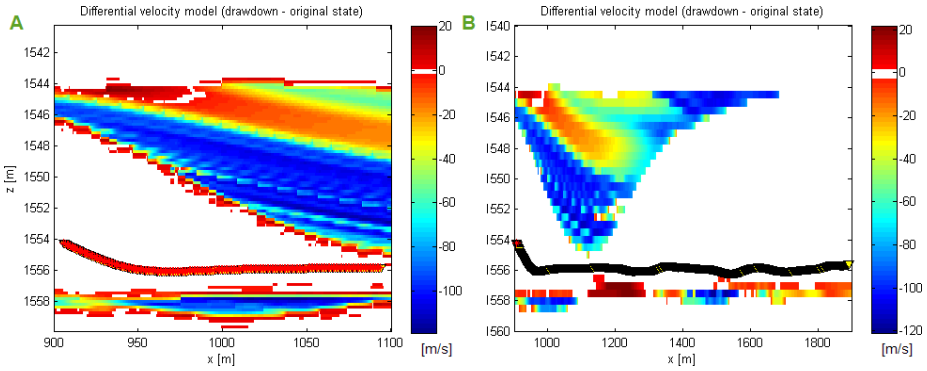

Figure 8.4: **Zoom of differential velocity models with the OWC shift.** A - adopted for 1000 Hz multiple sources in horizontal well. B - adopted for the 100 Hz heel source.

Multiple sources in horizontal well: It is visible on the differential seismogram in Figure 8.5, that even if there is now the OWC which is highlighted the most, the GOC stays visible. Since the differential energy variation along the profile provides for this little model only a general approximation about the GOC shape, influence of this OWC shift is not significant.

Source at the well heel: A refraction wave is spreading through the water layer, therefore the OWC, with corresponding changes, might be derived from the refraction wave arrival in original seismograms. But since the maximum OWC shift is 2 m, the impact on the GOC rough interpretation based on the root of differential energy is negligible, as can be seen in Figure 8.6.

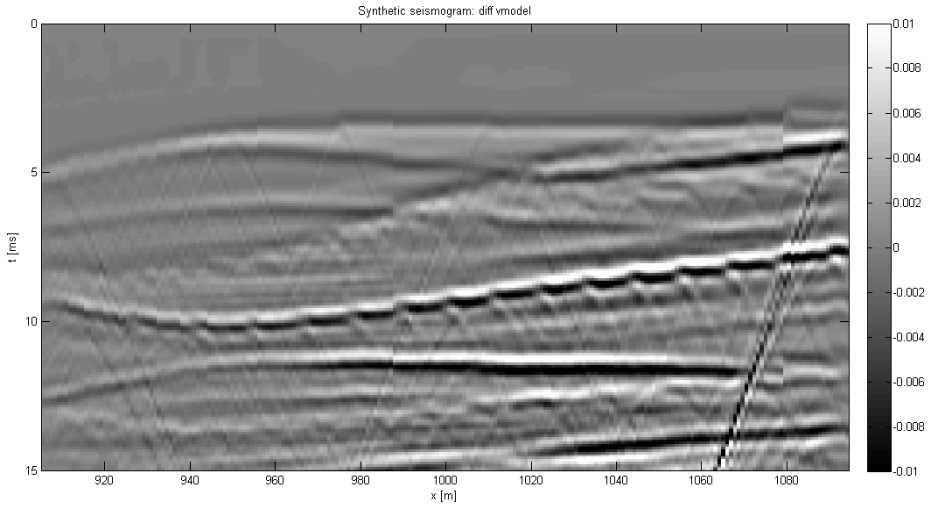

Figure 8.5: **OWC shift effect for multiple sources.** Reflects the velocity changes displayed in Figure 8.4A.

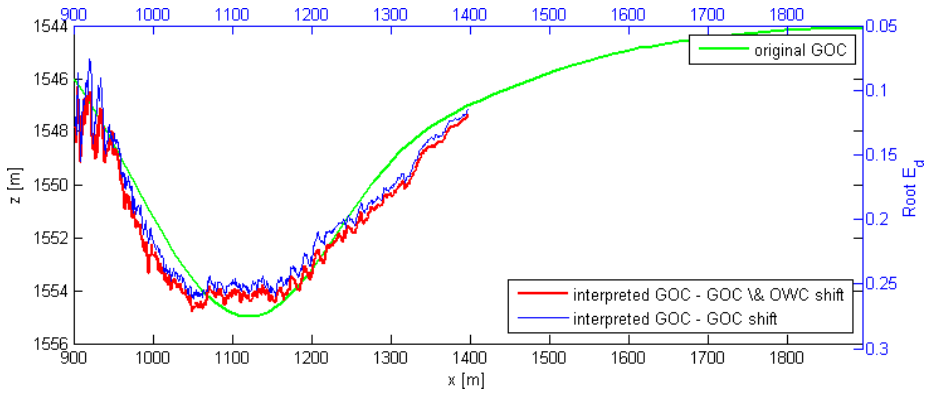

Figure 8.6: **Heel source: effect of the OWC on the root of differential energy.** Red line - reflects the velocity changes displayed in Figure 8.4B. Blue line - for the large model with the GOC shift (Figure 6.6A and B).

Chapter 9

Conclusions & Recommendations

The aim of this thesis was to investigate seismic responses obtained using sensors along horizontal production screeners, especially the application for the gas-oil contact monitoring in reservoir with thin oil column and gas cap. This task was fulfilled by simulating acoustic wave field propagation within 2D models reflecting the situation in the Troll field for source positions and characteristics of the highest potential.

Simulations proved the multiple 1000 Hz sources in the production well as the most beneficial acquisition scenario for delivering precise information about the gas-oil contact by a sequence of seismograms recorded for various stages of the gas-oil contact. For this scenario the information about the gas-oil contact is carried by weak reflections on the gas-oil contact itself and by the time delay in reflections from layers above the gas-oil contact. The oil-water contact shift due to production does not appear to influence the first gas-oil contact indication, but a discontinuity and roughness of high reflective layers might complicate the straight forward interpretation of the gas-oil contact from the horizon reflection.

Despite the clear indication of the gas-oil contact for the multiple sources, it is the low frequency source at the heel of the well and at the sea bed which might be the first installed due to cost issues. Elementary data interpretation for both of these source scenarios shows significant correlation between the gas-oil contact shape and difference in seismograms recorded for different stages of the gas-oil contact. But a calibration to the real gas-oil contact drawdown would be required. Another data analysis for the heel data then indicates a relation to the amount of the gas-oil contact drawdown variation along the well. Since both these interpretations provide only a rough idea about the gas-oil contact, the detailed gas-oil contact estimation would have to be based also on comparison of the synthetic and measured data.

Recommendations:
Full and deepening coverage of the topic is outside the limits of the master thesis. Therefore developing further interpretation of the data would be a logical continuation of this feasibility study. It would be also recommended to test the estimation suggestions for heel and VSP source on more complex gas-oil contact shapes.

If the investigation goes further also in modelling direction, the well could be included in the subsurface models and adopting the elastic simulation (by Thorbecke (2009)) would be more suitable to cover the complexity of tube waves. These simulations might uncover if tube waves introduce such a noise which disables the gas-oil contact monitoring.

Later if the receivers are installed in the production well, it might be of interest to look at the level of noise coming from the production and its possible implication or application for the gas-oil contact monitoring.

Praha, September 2009
Eva Janska .....

References

Bolle, L. 1992. Troll Field: Norway's Giant Offshore Gas Field: Chapter 28. M 54: Giant Oil and Gas Fields of the Decade 1978-1988, 447-458.

Carcione, J. M., 2007. Wave Field in Real Media: Wave Propagation in Anisotropic, Anelastic, Porous and Electromagnetic Media. Elsevier. Chapter 7.

Clayton, R.& Engquist, B., 1977. Absorbing Boundary Conditions for Acoustic and Elastic Wave Equations. Bulletin of the Seismological Society of America, **67**, 1529-1540.

Dreyer, T., Whitaker, M., Dexter, J., Flesche, H. & Larsen, E. 2005. From spit system to tide-dominated delta: integrated reservoir model of the upper Jurassic Sognefjord Formation on the Troll West Field. Petroleum Geology: North-West Europe and Global Perspectives - Proceedings of the 6^{th} Petroleum Geology Conference, Article I.D 093, 1-27.

Elde R. M., Mland, E. & Petersen, S. A., 1992. Technical Requirements for GOC Monitoring in horizontal Wells by Direct-Arrival Trave-Time Inversion. Society of Petroleum Engineers, Formation Evaluation, 47-52.

Lamport, L. 1994. LaTeX: a document preparation system. Addison Wesley.

Lines, L. R., Slawinski, R. & Bording, R. P., 1999. A Recipe for Stability of Finite-Difference Wave-Equation Computations. Geophysics, **64**, 967-969.

Madsen, T. & Abtahi, M. 2005. Handling the Oil Zone on Troll. Offshore Technology Conference. OTC 17109.

Margrave G., F., 2003. Numerical Methods of Exploration Seismology with algorithms in MATLAB. www.crewes.org, draft.

Mikkelsen, J. Kr., Norheim, T. & Sagatun, S.I. 2005. The Troll Story. Offshore Technology Conference. OTC 17108.

Ministry of Petroleum and Energy. 2008. Facts 2008, The Norwegian Petroleum Sector. Norwegian Petroleum Directorate, 151-154.

Oetiker, T., Partl, H., Hyna, I., Schlegl, E., Kocer, M. & Sykora, P., 1998. Ne prilis strucny uvod do systemu LaTeX2e, version CZ-0.9-Beta. Open source book available on internet.

Ona, R., Skjei, N. & Leiknes, S., 2006. Revealing the secrets of the Troll 4D seismic response - Case study using Compound Modelling. 68^{th} EAGE Conference & Technical Exhibition, Expanded Abstracts, E019.

Petersen, S. A., 1999. Compound modelling - A geological approach to the construction of shared earth models, 61^{st} EAGE Conference & Technical Exhibition, Expanded Abstracts, 5-12.

Petersen, S.A., Farrelly, B.A. & Braathen, B.I., 2003. Modeling of fluid effects in Compartmentalized Areas, an Oseberg South Case Study. 65^{th} EAGE Conference & Technical Exhibition, Expanded Abstracts, A25.

Petersen, S. A., 2008. 2D & 3D Compound Modelling: Compound DDr(x) - Manual (version Aug. 2008).

Schlumberger, 2005. Sonic Scanner. Brochure accessible on www.slb.com.

Toxopeus, G., Petersen, S. A., Wapenaar, K., 2003. Improved Geological Modelling and Interpretation by Simulated Migrated Seismic. 65^{th} EAGE Conference & Technical Exhibition, Extended Abstracts, F34.

Thorbecke, J. 2009. 2D Finite Difference Wavefield Modelling. A draft version of the manual of the elastic modelling program fdelmodc.

Vasilevsky, A., Druzhinin, A., Evans, J. R., Murphy, C. A. & Li, X-Y, 2003. Feasibility of Inverting 3-D FTG Data for Reservoir Monitoring. EAGE 65^{th} Conference & Exhibition , Paper Z-99.

Ziegler, P. A., 1975. Geologic Evolution of North Sea and Its Tectonic Framework. American Association of Petroleum Geologists Bulletin,**7**, 1073-1097.

Appendix A

Synthetic Seismograms

This appendix presents some synthetic seismograms acquired while calculating differential seismograms presented in chapter 6. If it is not said opposite, the central frequency of sources is 1000 Hz.

CD: Attached CD contents the pdf version of this master project report, abstract in Czech and results for the subsurface near-to-realistic Troll models in a form of Matlab structures (.mat). The name of Matlab files refers about the source position, central source frequency and grid size. To display the results open required -.mat file and run *plotresult(res)*.

A.1 Source in Heel of Horizontal Well

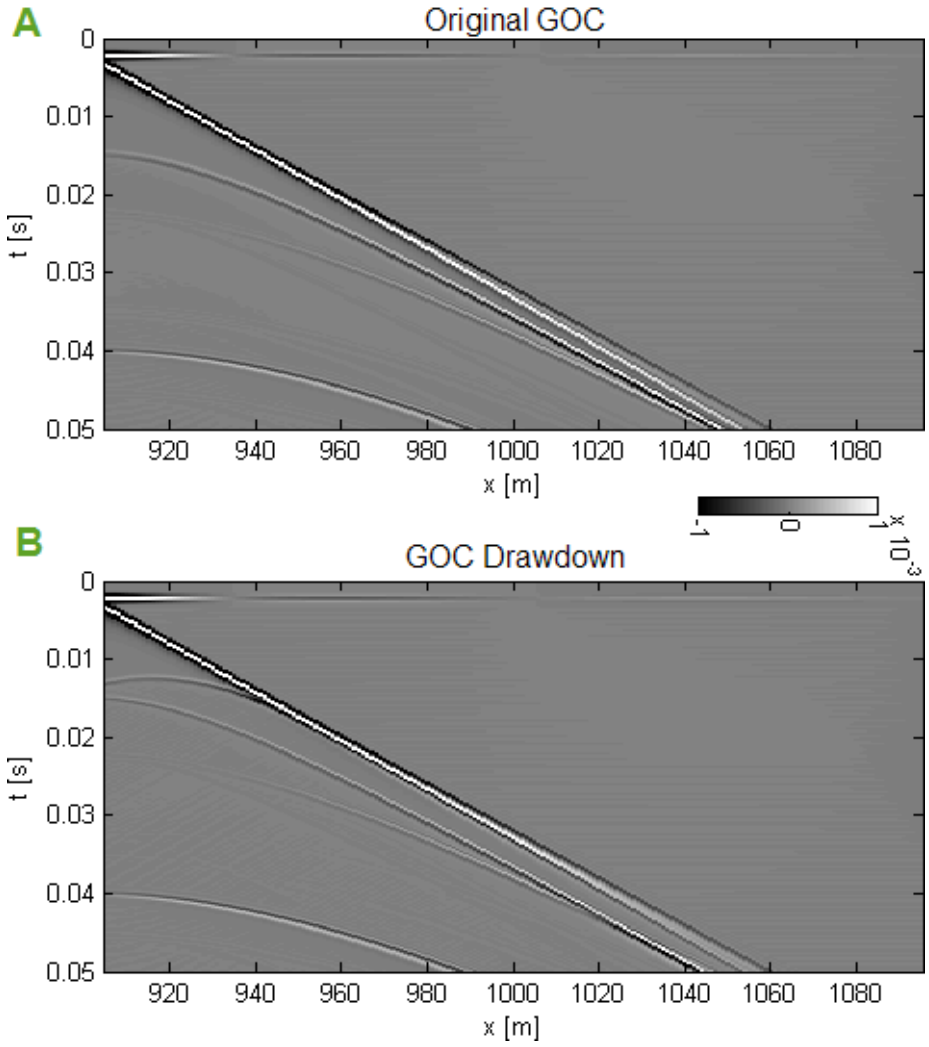

Figure A.1: **Heel source in basic model.**

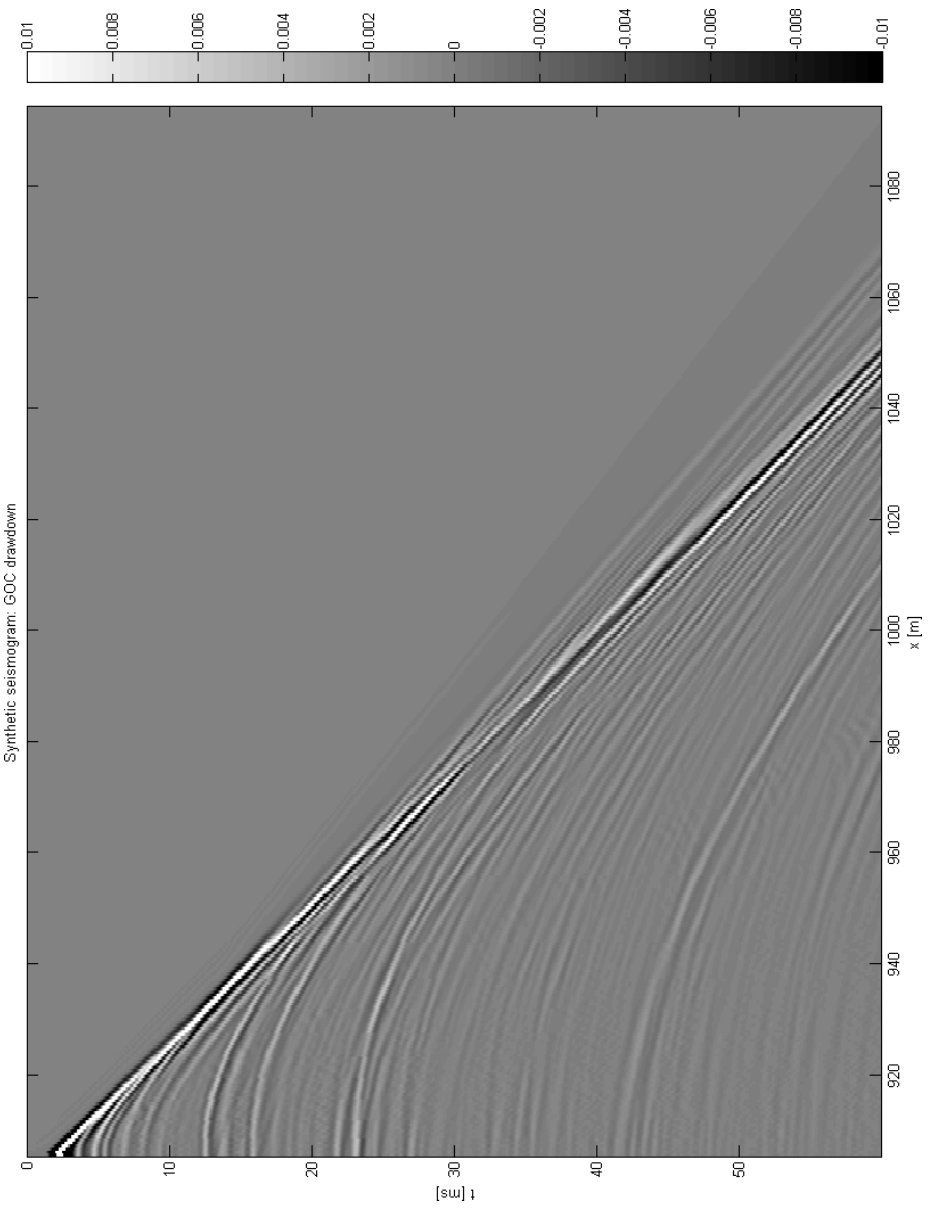

Figure A.2: **Heel source in near-to-realistic Troll model, seismogram for GOC drawdown.**

A.1.1 100 Hz Source and Larger Model Simulation

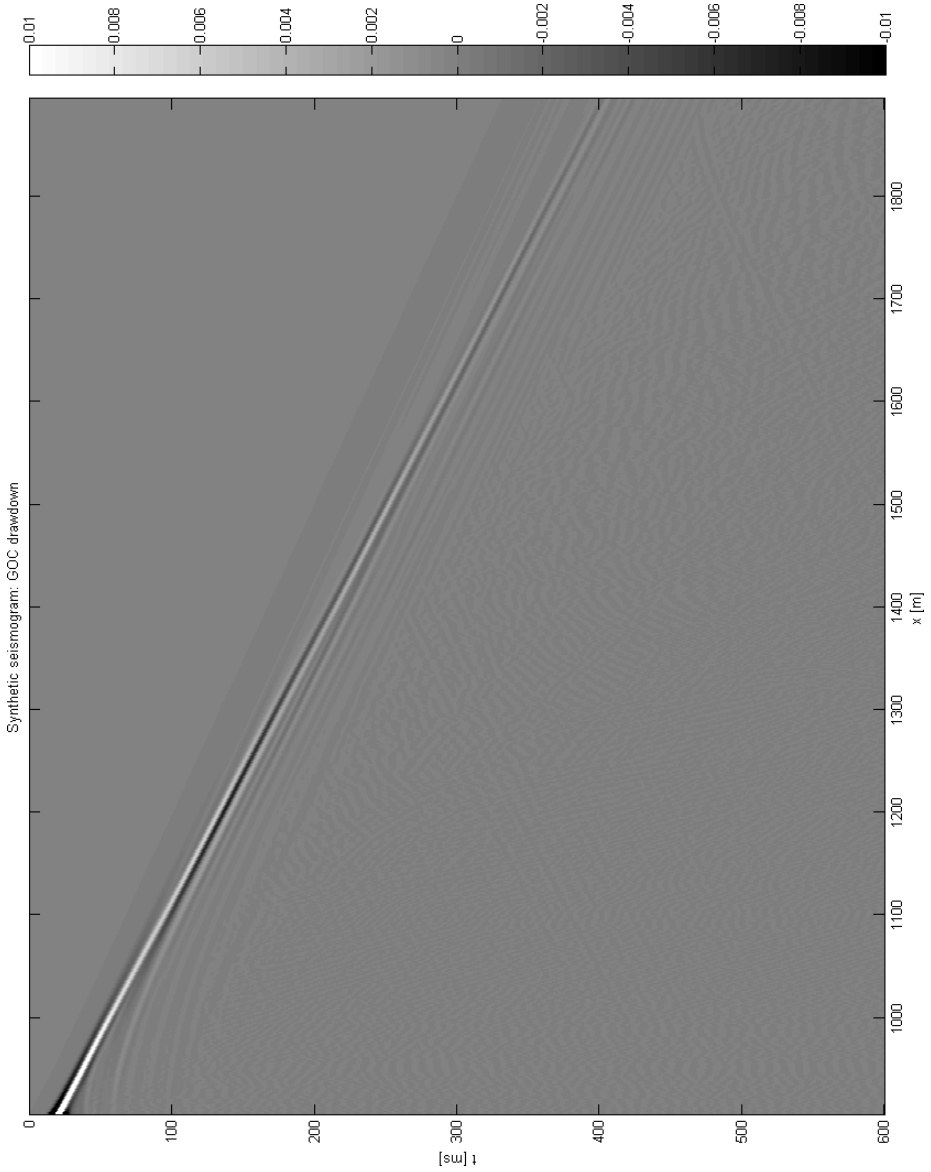

Figure A.3: **Heel source in larger near-to-realistic Troll model, seismogram for GOC drawdown.**

A.2 Source in Centre of Horizontal Well

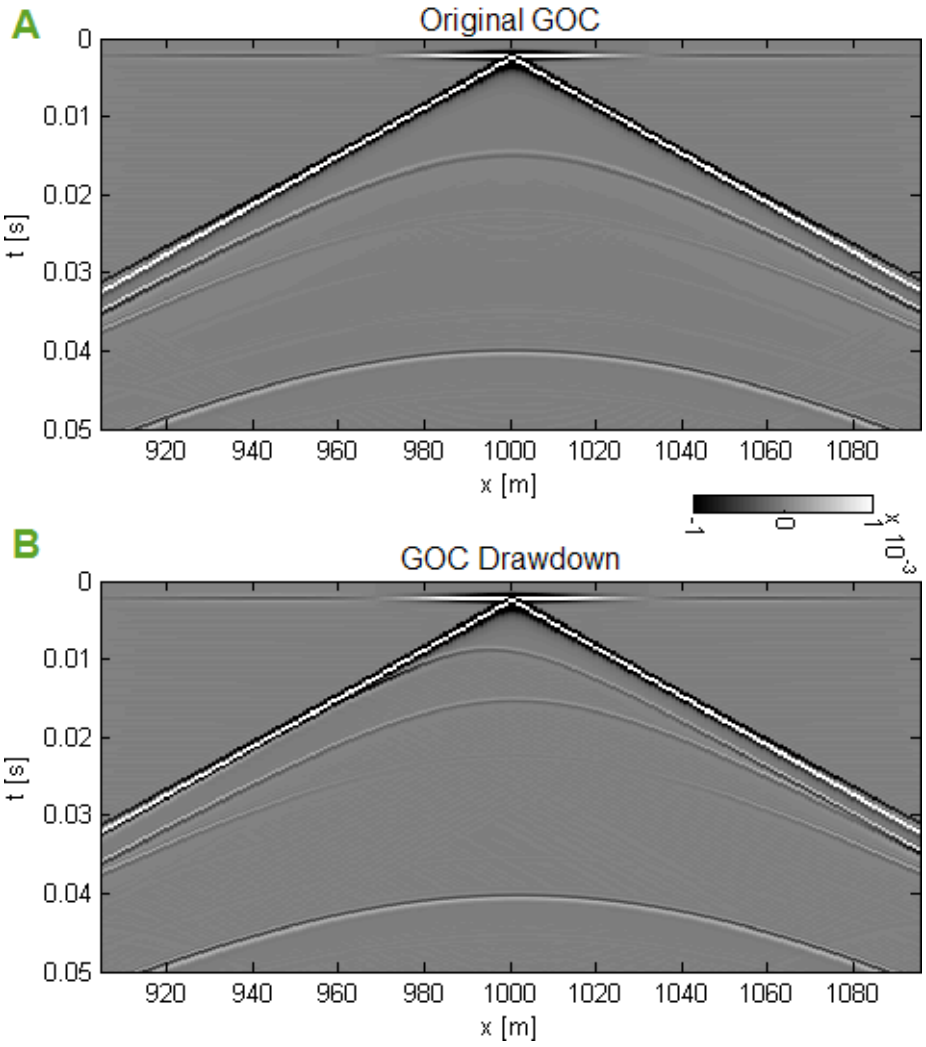

Figure A.4: **Source in centre of horizontal well in basic model.**

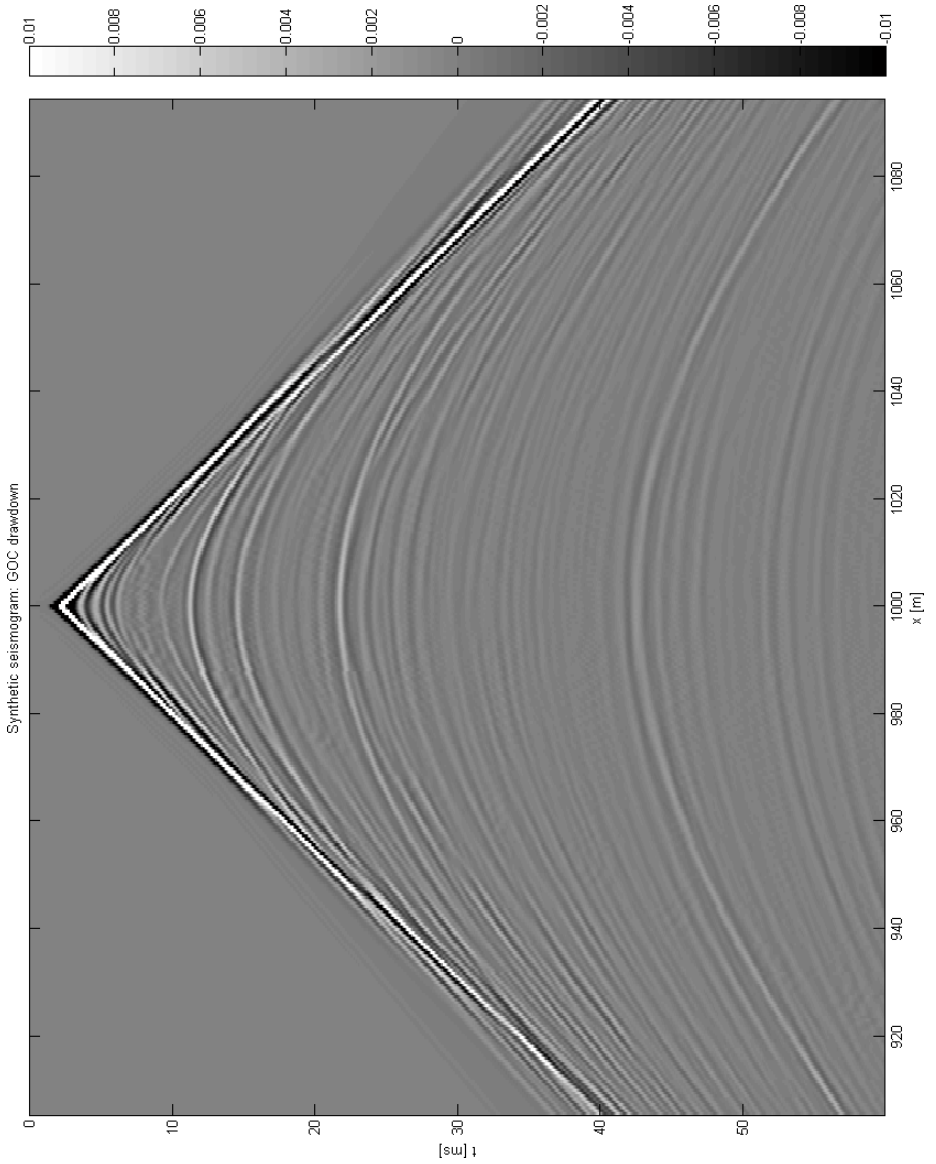

Figure A.5: **Source in centre of horizontal well in near-to-realistic Troll model, seismogram for GOC drawdown.**

A.3 Multiple Sources in Horizontal Well

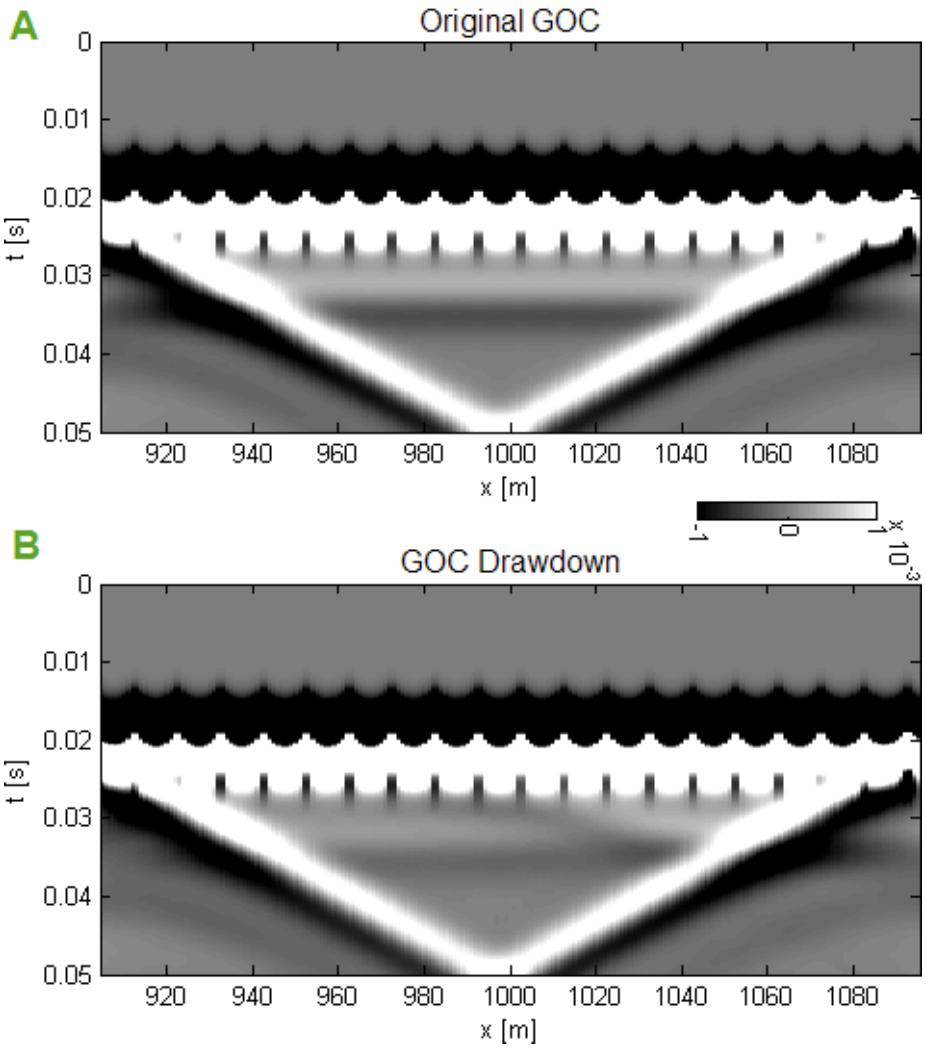

Figure A.6: **Multiple sources in horizontal well in basic model.**

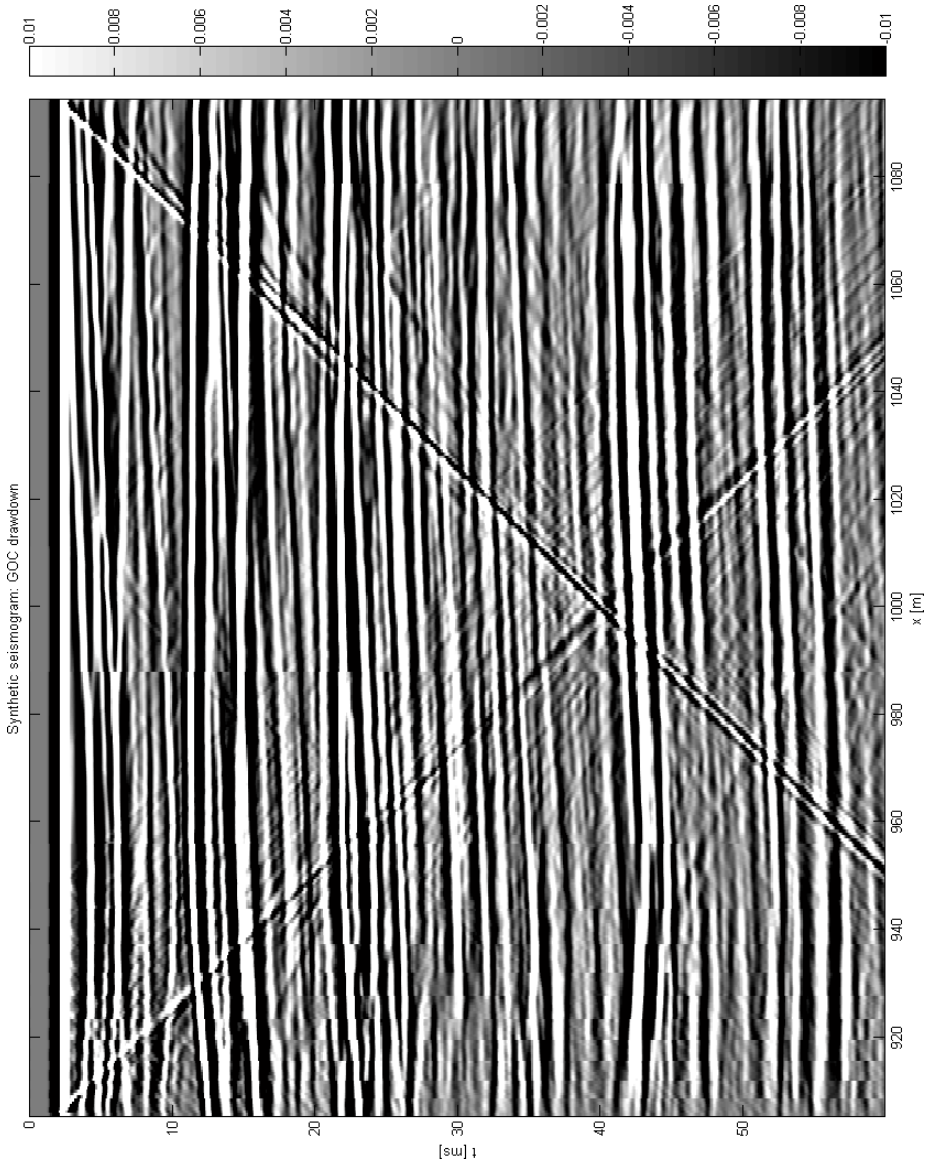

Figure A.7: Multiple sources in horizontal well: **Troll model, seismogram for GOC drawdown.**

A.4 Single Source in Gas Zone

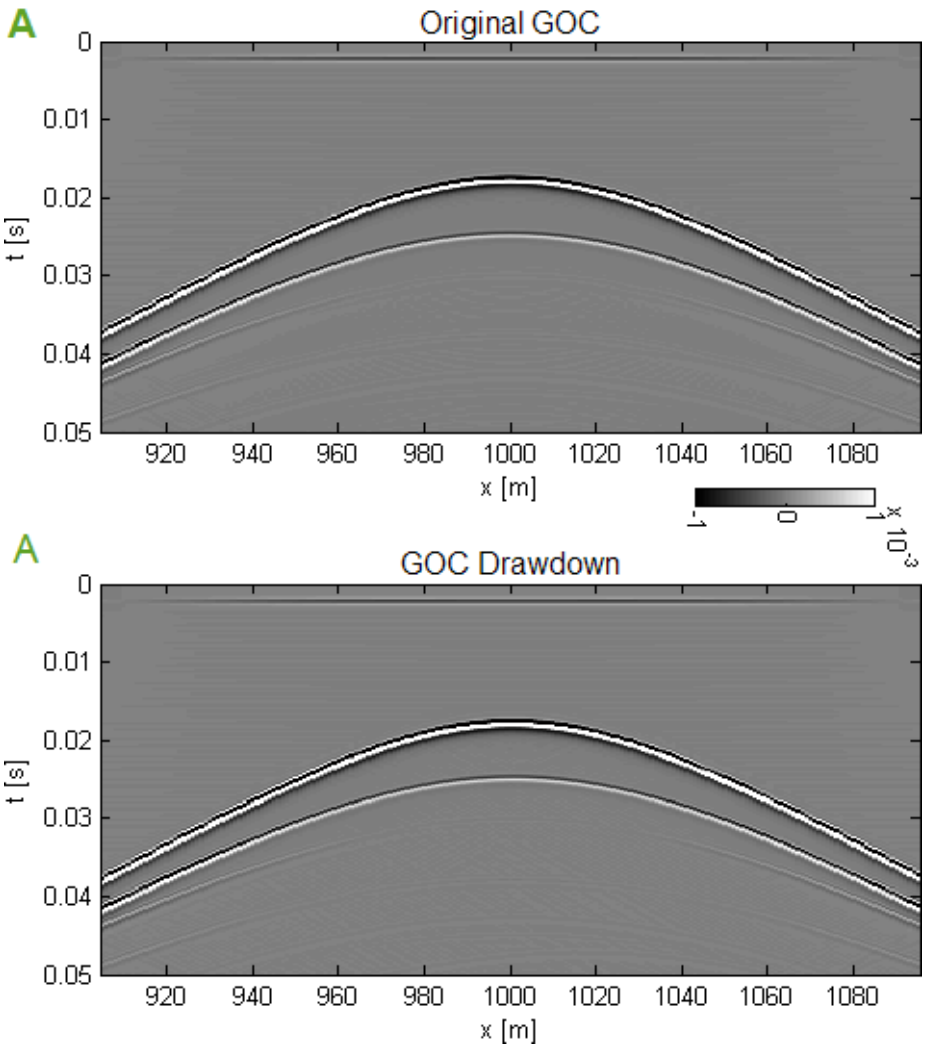

Figure A.8: **Single source in the gas zone in basic model.**

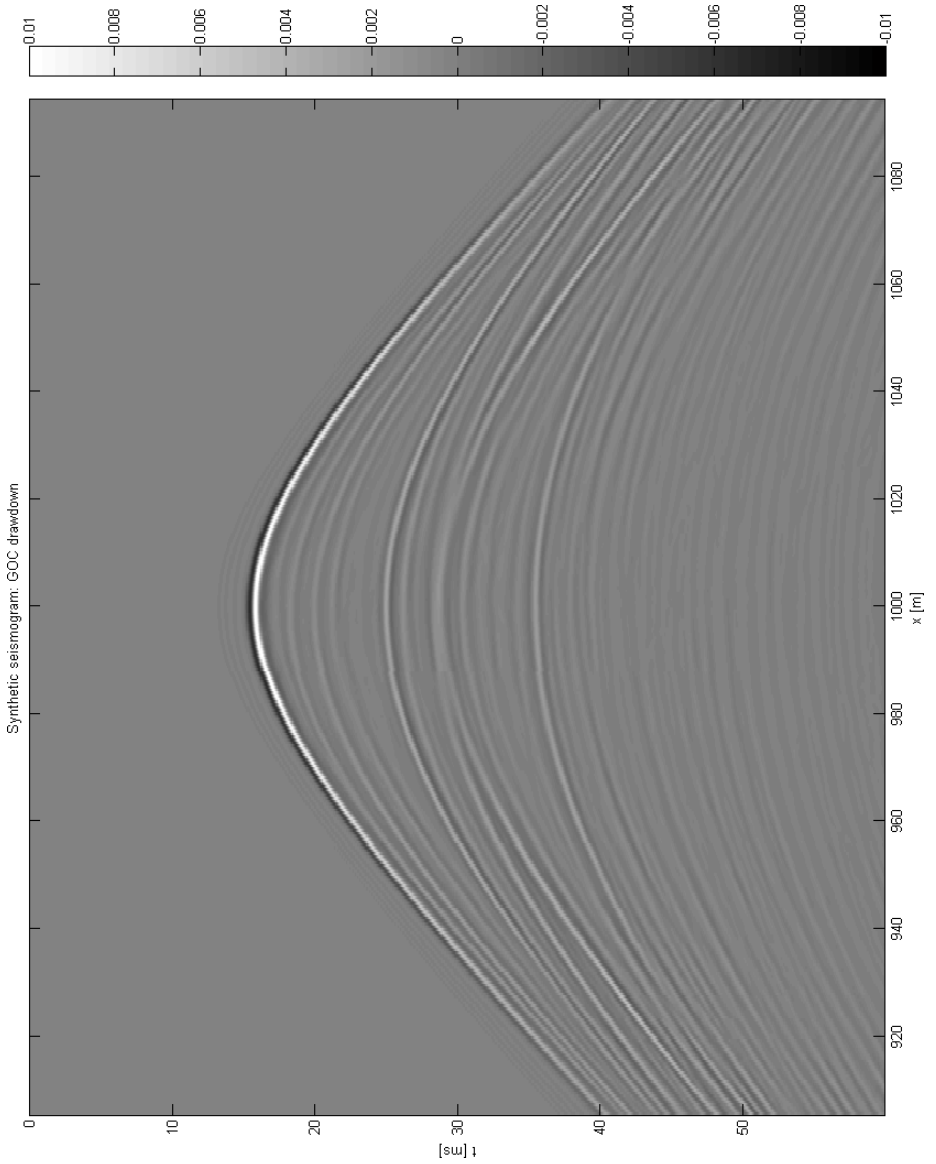

Figure A.9: **Single source in the gas zone in near-to-realistic Troll model, seismogram for GOC drawdown.**

A.5 Multiple Sources in Gas Zone

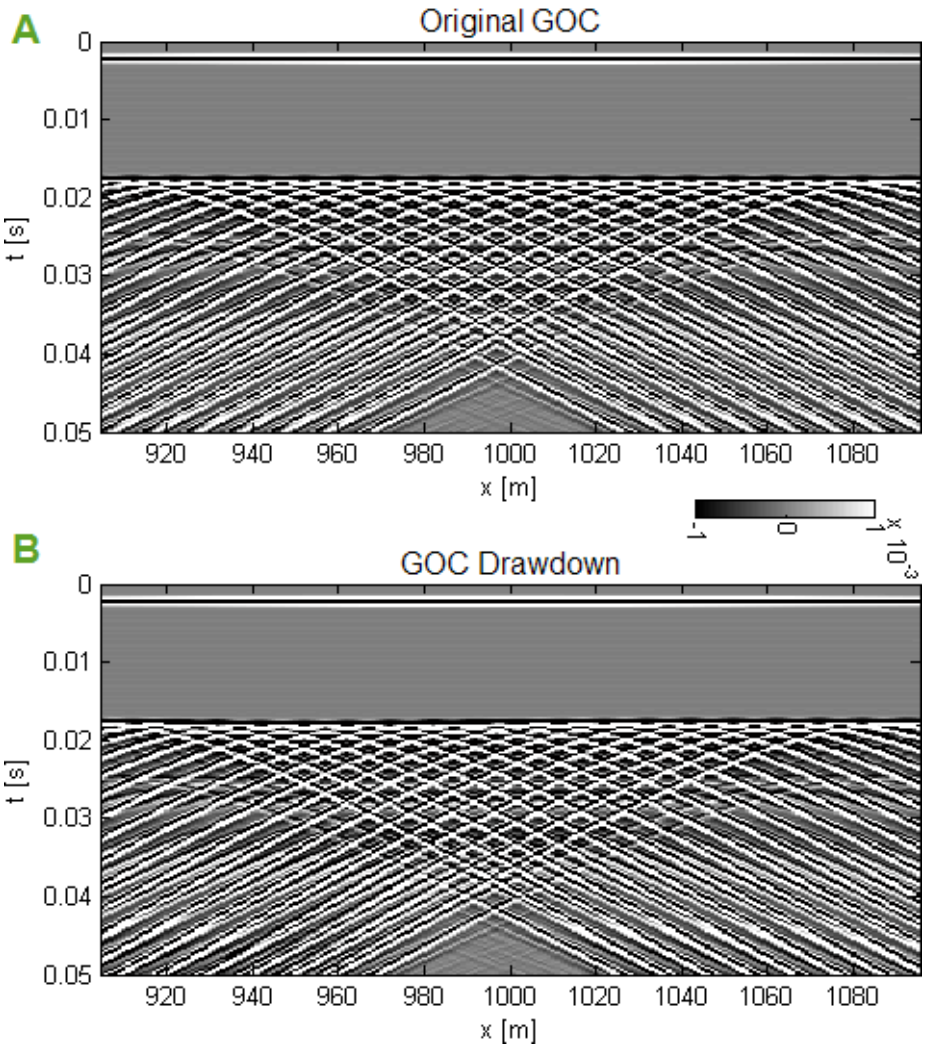

Figure A.10: **Multiple sources in the gas zone: basic model**. The horizontal event at time 2 ms on seismograms is an artefact coming from the way the seismogram calculated with a peak source is convolved with the source wavelet in the CREWES scripts.

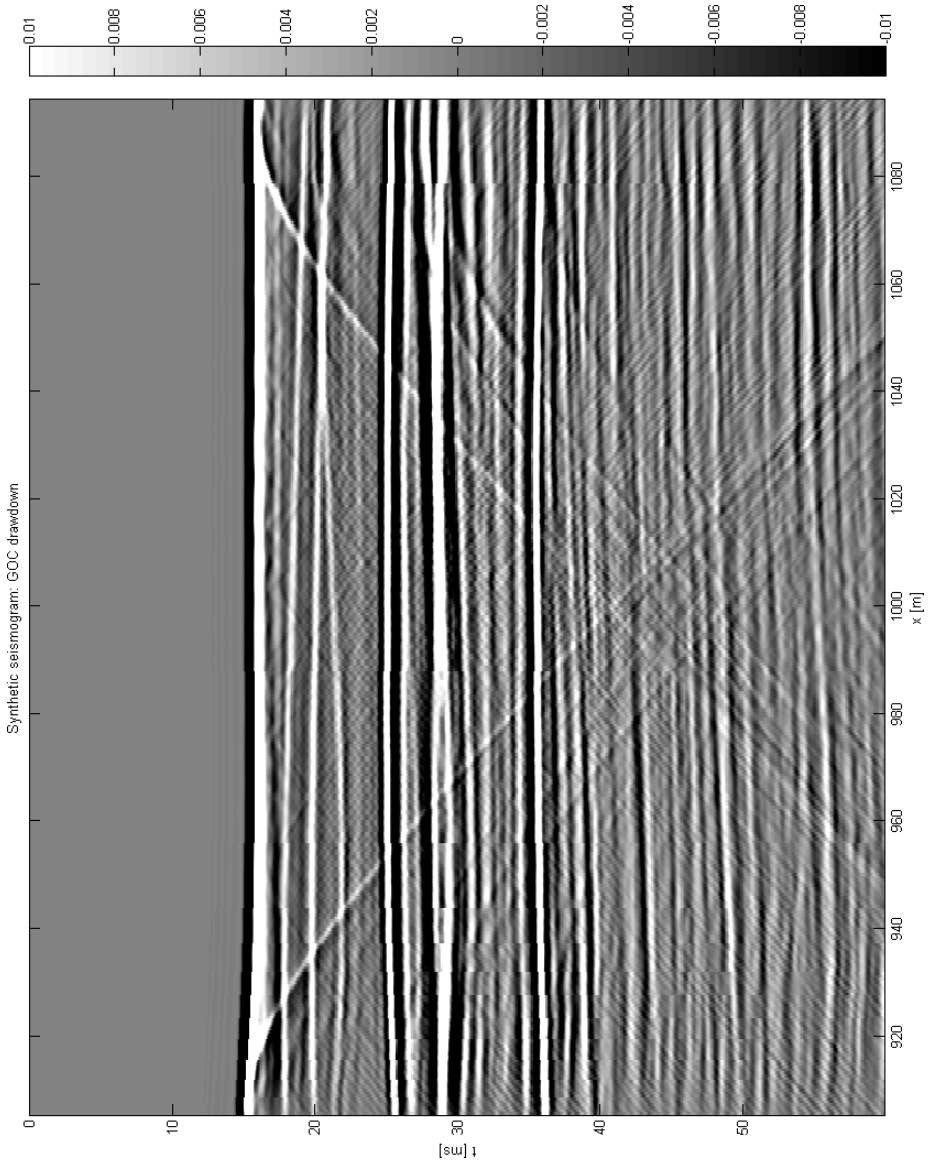

Figure A.11: **Multiple sources in the gas zone in near-to-realistic Troll model, seismogram for GOC drawdown.**

A.6 Source at Surface: VSP

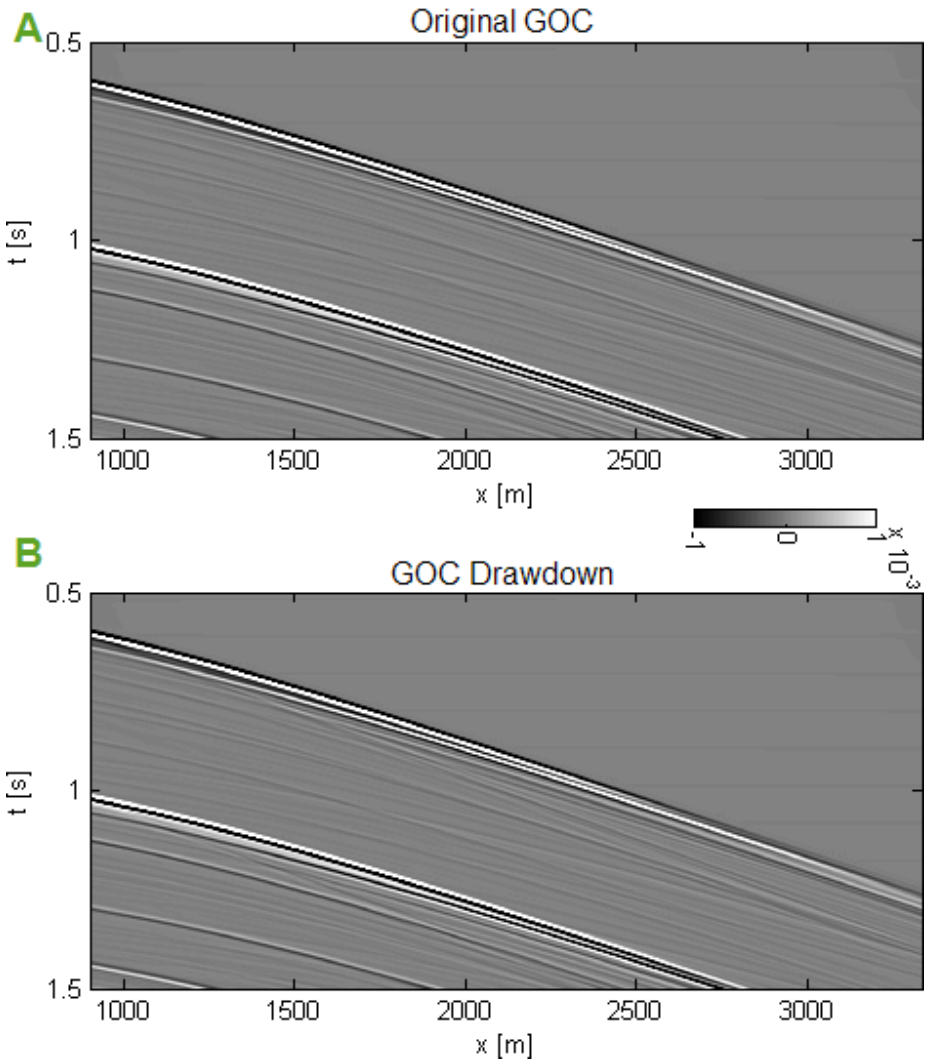

Figure A.12: **Source at surface -VSP in basic model**. A - seismogram for original GOC, B - seismogram for GOC drawdown and C - differential seismogram.

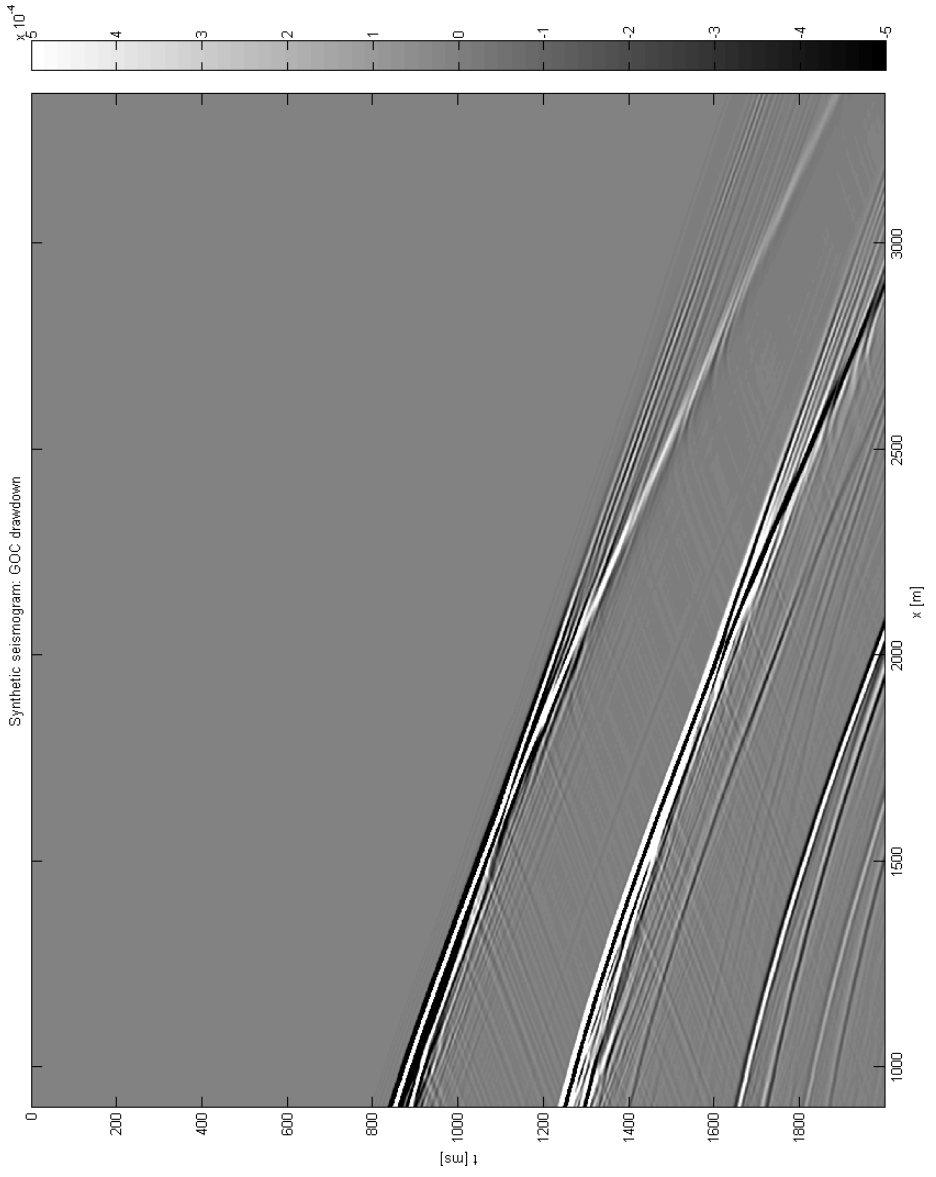

Figure A.13: **VSP Source at surface -VSP in near-to-realistic Troll model, seismogram for GOC drawdown.**